A Geo-Cellular Model of a Multiphase Hydrocarbon Field incorporating Fault-Seal Analysis: Bredasdorp Basin, South Africa

Omar El Saadi

Dissertation presented for the degree of Master of Science in the Department of Geological Sciences
University of Cape Town
February 2015

Supervisor: Mr. George Smith

I know the meaning of plagiarism and declare that all of the work in the dissertation, save for that which is properly acknowledged, is my own.

Signed by candidate

Signature removed

CONTENTS

LIST OF FIGURES

LIST OF TABLES

GLOSSARY OF TERMS

Bscf	Billion standard cubic feet
Mscf	Thousand standard cubic feet
MMscf	Million standard cubic feet
MMbbl	Million barrels
Mbbl	Thousand barrels
Ma	Million years ago
QC	Quality control
GWC	Gas-water contact
OWC	Oil-water contact
FWL	Free water level
mD	Milli Darcy
MMm^3	Million cubic metres
psia	Pounds per square inch area
psig	Pounds per square inch gauge
g/mol	Grams per mole
ppm	Parts per million
g/cc	Grams per centimetre cubed
PVT	Pressure volume temperature (analysis)
API	American Petroleum Institute (A unit of oil density)
RFT	Repeat Formation Test (acquisition of formation pressure data)
Bo	Oil shrinkage factor
Bg	Gas expansion factor
STOIIP	Stock tank oil initially in-place
GIIP	Gas initially in-place
CSF	Clay Smear Factor
SGR	Shale Gouge Ratio
SGS	Sequential Gaussian Simulation
SIS	Sequential Indicator Simulation
TGS	Truncated Gaussian Simulation
PDF	Probability Density Function
Sw	Water saturation
J_Sw	J Function water saturation
NPI	Normalized Porosity Index
RQI	Rock Quality Index
FZI	Flow Zone Indicator
GR	Gamma Ray
VCL	Volume of Clay
USM	Upper Shallow Marine
BUSM	Bottom Upper Shallow Marine
TUSM	Top Upper Shallow Marine
Ht	Height Above Contact
RMS	Roxar Reservoir Management Software
RDR	Rock Deformation Research
AFFZ	Agulhas-Falkland Fracture Zone
CDP	Channel deposit proportion

ACKNOWLEDGEMENTS

I would firstly like to thank my supervisor, Mr. George Smith for his help, patience and encouragement throughout the duration of the project. A special mention must be rendered for my industry mentor and friend, Mr. Gervasio Robles who tirelessly invests his time and knowledge in me. Much of the work of this project was carried out on behalf of PetroSA and all data was used with permission from the company. I would like to extend my thanks to PetroSA for giving me the opportunity to embark on this endeavour and last but not least, I extend my heartfelt gratitude to my understanding wife and companion who has tolerated me with patience during the course of this study.

ABSTRACT

Geological 3D static modelling has become an integral tool during the appraisal and developmental stages of a hydrocarbon field lifecycle. The 3D model becomes the basis upon which reservoir heterogeneity and characterisation are understood, hydrocarbon volumetrics are calculated and field development plans are designed. Reservoir compartmentalisation and fault-seal analysis is also an industry topic which has drawn much interest. Having a 3D model allows for fault-seal analyses to be carried out and evaluated using the statistically distributed reservoir properties. This study incorporates the building of a 3D geo-cellular reservoir model with a fault seal analysis of the E-S field, which is located on the north flank of the Bredasdorp Basin. The reservoir model was built using geostatistical methods to populate the several reservoir parameters into the model to calculate a hydrocarbon volume. In addition, a fault-seal analysis was carried out in order to investigate the phenomenon of having an oil accumulation separated from a gas accumulation either side of a fault. The facies modelling was carried out using the object modelling technique, in order to produce a model which is geologically plausible. Most of the remaining reservoir parameters were modelled using a variogram except in the case of water saturation, which was modelled using a J function equation. The volumetrics were assigned per fault block. Using a recovery factor of 75% for gas and 11% for oil, the calculated total recoverable hydrocarbons were 12.6 Bscf and 1.3 MMbbl respectively. The fault-seal analysis showed that the faults separating two of the fault blocks are not completely sealing. All the calculated fault properties supported this view, with the Shale Gouge Ratio (SGR) and threshold pressure relationship indicating a high likelihood for leakage across parts the faults. Pressure data from Repeat Formation Tests (RFT) however, indicates that the hydrocarbon accumulations in both blocks are isolated from each other. This contradiction has informed the recommendation to drill a highly deviated or short horizontal well which will cross the fault and intersect both blocks, and to complete the well using a sliding sleeve, thus providing the flexibility needed in order to manage multi-phase flow.

1 AIM OF STUDY & HYPOTHESIS

There are two main objectives for this study. The first one was to create a comprehensive geological static model populated with both seismic and well data, and in doing so, obtain a customized workflow which can be re-applied, partly or in whole, to other similar scenarios. The model was also used to calculate the hydrocarbon volumes which were then compared to the results of other authors in order to validate the results obtained in this study.

The second aim was to analyse the fault sealing capabilities of relevant faults to prove whether the current understanding is correct, and also explore the effects on field compartmentalisation. Much of the failure of appraisal wells has been attributed to fault-seal, therefore a fault-seal analysis was carried out to determine the sealing nature of faults and quantify its role in hydrocarbon entrapment and reservoir compartmentalisation.

The result obtained from the fault-seal analysis will have an impact on the possible hydrocarbon recovery and will also determine the subsequent development plan chosen to optimize the recovery. A scenario where critical faults are sealing will cause the recoverable hydrocarbon from a planned producing well to be lower than if the faults were not sealing, and more than one well may be required to drain the field. This is critical when evaluating the economic aspect of this development as too many wells may render it non-profitable.

2 INTRODUCTION

The Bredasdorp Basin is a south-easterly trending basin which formed along with other sub-basins of the larger Outeniqua Basin, during the break-up of Gondwana along the Agulhas-Falkland Fracture Zone. The E-S gas field is located along the north flank of the Bredasdorp Basin approximately 90km from Mossel Bay (Figures 2.1 and 2.2). The field is connected to the E-M pipeline via an 11km tie-in (the E-M pipeline is linked to the F-A platform

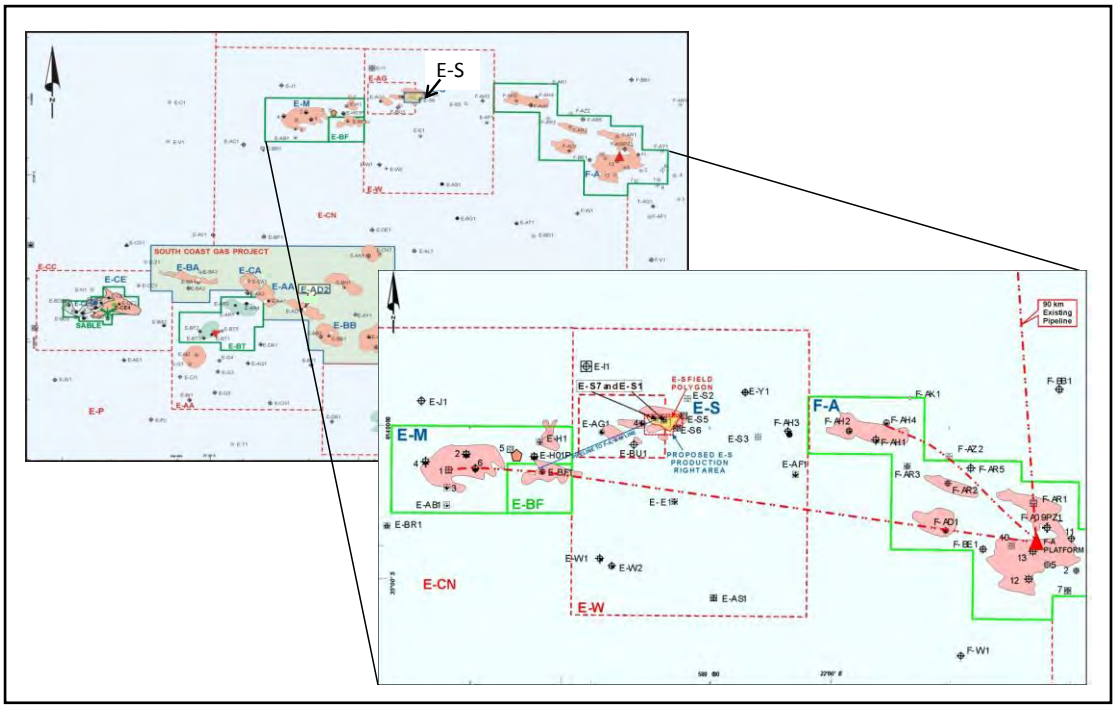

Figure 2.1 Location of the E-S field with respect to neighbouring fields in the Bredasdorp Basin.

where the gas is separated and piped to shore). The E-S field was discovered in 1987 and has tested gas and oil in different faulted blocks. The main reservoir is a shallow marine (shoreface) environment sandstone of Early Cretaceous age called the Upper Shallow Marine unit (USM). The underlying fluvial succession forms the secondary reservoir in the field. Investigating the possibility of producing gas from the field economically has been the main driver of this project. The gas would provide invaluable feedstock to PetroSA's refinery in Mossel Bay and could assist to sustain commercial production in the refinery for the near future.

The E-S field is believed to be fault bound i.e. sealing faults define the limits of the field. The importance of analysing the fault-seal is great, as it is intended to improve our understanding of the so-called fault compartments in the field. These compartments have a direct bearing on the development of the field and in particular, the drilling techniques and production methods. With better understanding of this concept, management decision-making and economic evaluation can be done optimally.

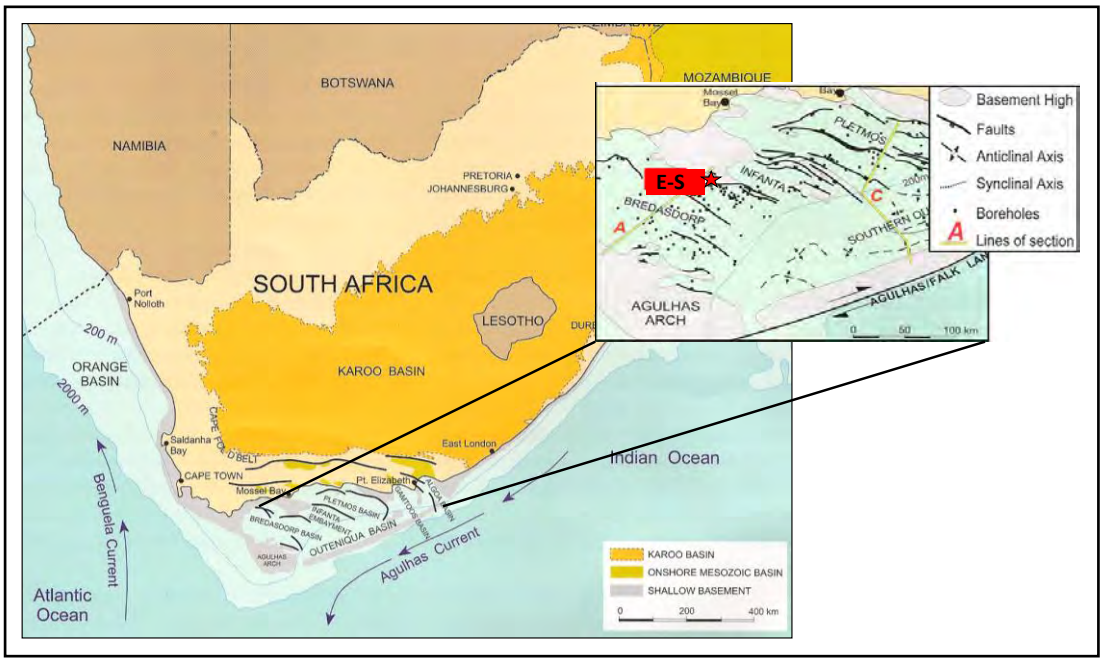

Figure 2.2 Map of Southern Africa showing the offshore basins (after Petroleum Agency, 2000).

2.1 Regional Tectonic Setting

The structural setting of the South African offshore basins is best understood with reference to the plate tectonic development of the southern African plate before, during and after the break-up of Gondwana (Broad et al., 1996). Gondwana break-up commenced on the eastern margin of Africa and this led to the start of the rifting phase in the Middle Jurassic and the formation of the Durban and Zululand Basins (Broad et al., 1996; Petroleum Agency SA, 2000). During the Early to Mid-Cretaceous the Falkland Island Plateau passed the southern coast of Africa along the Agulhas-Falkland Fracture Zone (AFFZ), creating dextral shearing of the South African margin which led

to the formation of the Outeniqua Basin and its sub-basins as a series of oblique half-grabens during the latest Valanginian (121 Ma), marked by the 1At1 unconformity (Broad et al., 1996; Petroleum Agency SA, 2000). After that there were at least three phases of inversion related to continued dextral shearing, which led to the final separation of the Falklands Plateau from Africa in the Mid-Albian which is marked by the 14At1 unconformity which indicates the start of the drift phase (Petroleum Agency SA, 2000).

2.1.1 The Outeniqua Basin

The Northern Outeniqua Basin is composed of a number of en-echelon sub-basins; the Bredasdorp, Pletmos, Gamtoos and Algoa Basins which, together with the smaller Infanta Embayment, converge to the south to form the deeper Southern Outeniqua Basin (Figure 2.2; Broad et al., 1996). The sub-basins are grabens separated by basement arches of Ordovician to Devonian meta-sediments of the Cape Supergroup with its arcuate trend inherited from the structural grain of the orogenic Cape Fold Belt (Broad et al., 1996). Numerous structural characteristics of the Outeniqua sub-basins can be elucidated in terms of strike-slip faulting, and more so in the basins closest to the Agulhas-Falkland Fracture Zone (AFFZ; Broad et al., 1996). In addition it has also been suggested that inversion tectonics due to periodic movement on the AFFZ contributed significantly to the structure of the basins (Broad et al., 1996).

2.1.2 The History of Hydrocarbon Exploration in the Outeniqua Basin

In 1970, the Placid Oil Company drilled the first borehole in the Bredasdorp Basin, F-A1, but only discovered small amounts of gas from the drift succession of the F-A structure (Broad et al., 1996). Ironically, in 1980 Soekor discovered the F-A gas field (in shallow marine synrift sandstones) only three kilometres from the previous well (Broad et al., 1996). During the early 1980's interest was concentrated on the gas fairway along the northern

flank of the Bredasdorp Basin, following the F-A discovery, and resulting in the discovery of its satellite fields (Broad et al., 1996; McMillan et al., 1997). This led to the Mossgas development project with the first gas flowing onshore in March 1992 (Broad et al., 1996; McMillan et al., 1997). In 1987 the first oil field was discovered in the Bredasdorp Basin but it was only in 1997 that the Oribi field began producing the country's first oil (Broad et al., 1996; Petroleum Agency SA, 2000).

2.2 The Bredasdorp Basin: Area of Study

The Bredasdorp Basin is located southwest of Mossel Bay (Figure 2.3) and covers an area of approximately 18 000 km^2 (Brown et al., 1995). The basin is a south-easterly trending basin, about 200 km long and 80 km wide and is bounded by the Agulhas Arch on the west and southwest

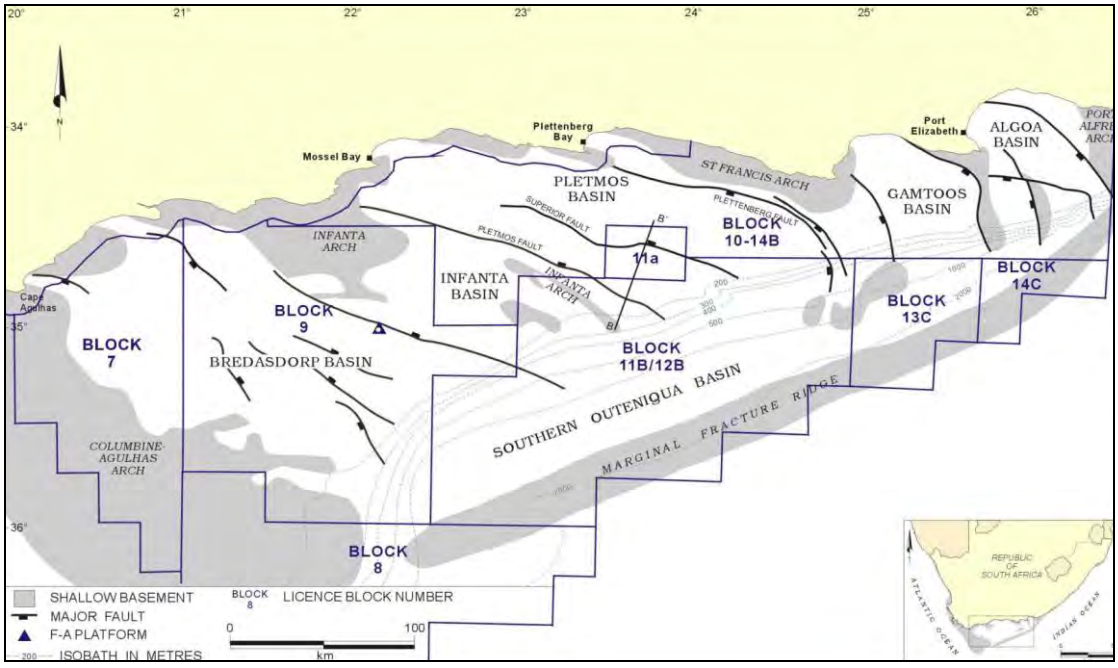

Figure 2.3 Map of South Africa's south coast showing the Outeniqua Basin with its sub-basins.

and by the Infanta Arch on the northeast (Broad et al., 1996; Brown et al., 1995). The Bredasdorp Basin formed due to rifting during the Late Jurassic break-up of Gondwana and the opening of the South Atlantic Ocean. The sequences deposited during this period were also affected by strike-slip

tectonics of the Agulhas-Falkland transform fault. The basement of the basin consists mainly of Devonian-aged Bokkeveld Group black slates but close to the Infanta Embayment, quartzites of the Ordovician-Silurian Table Mountain Group have been observed (Broad et al., 1996; McMillan et al., 1997).

2.2.1 Tectonic Episodes and Related Basin Geology

According to Jungslager (1996) two rifting episodes affected the Bredasdorp Basin, namely the Synrift I and Synrift II (Figure 2.4):

- SYNRIFT I: (Oxfordian – Late Valanginian) refers to the main rifting phase.
- SYNRIFT II: This last tectonic phase started at Late Valanginian (121 Ma) and produced less deformation than the previous one. Sediment deposition mainly occurred during the activation of the Falkland-Agulhas Fractured Zone. This phase ended in the Albian about 103 Ma.

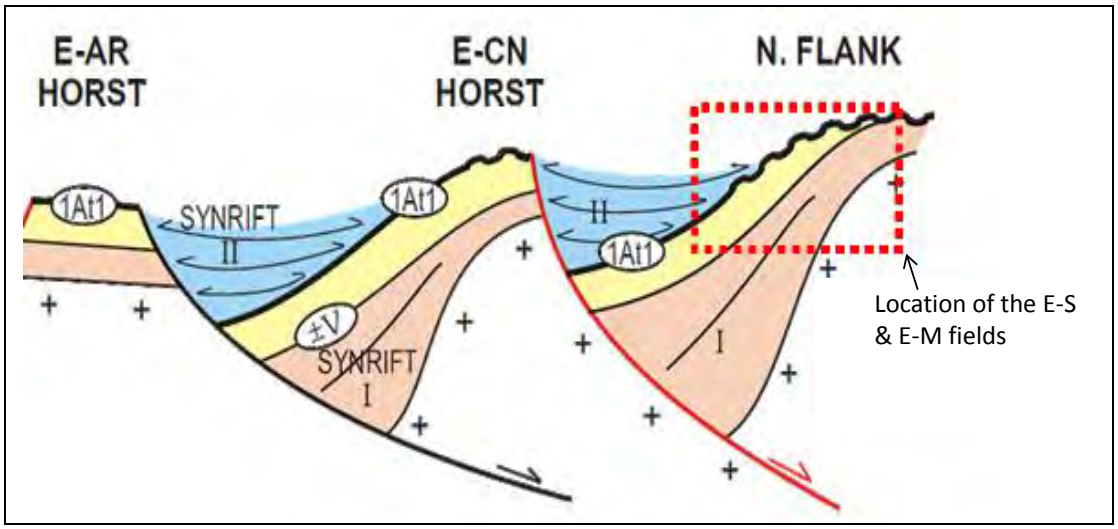

Figure 2.4 Sketch of the Synrift I and Synrift II deposits, the main fault architecture and the 1At1 unconformity in the study area at the end of the Synrift II phase (after Jungslager, 1996).

The start of the Drift succession is marked by the 14At1 unconformity. Figure 2.5 summarises the chronostratigraphy of the Bredasdorp Basin. Further details regarding these tectonic events and their timing are explained below.

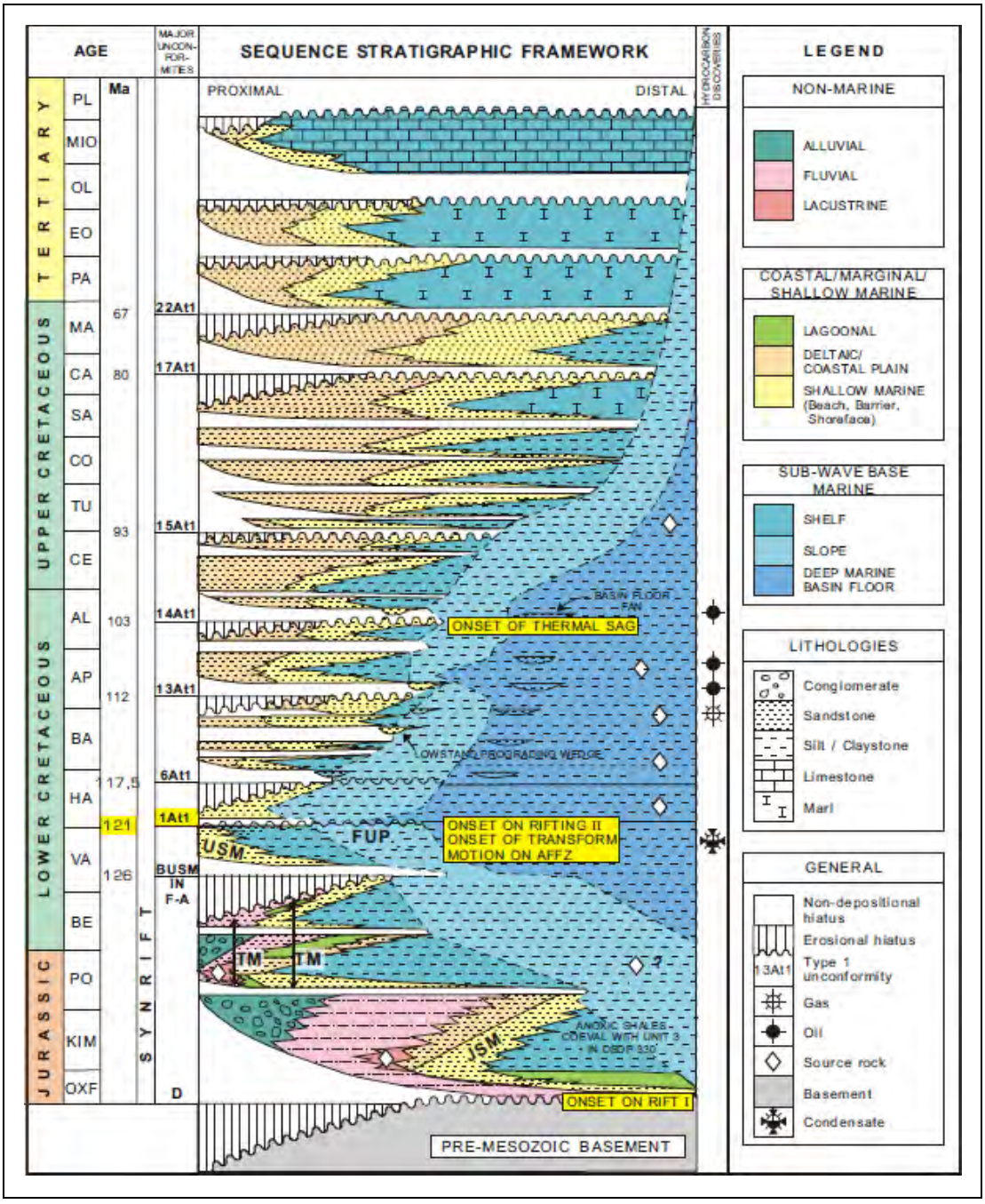

Figure 2.5 Generalised chronostratigraphy of the Bredasdorp Basin (after Jungslager, 1996).

Synrift I

Initial rifting resulted in the development of horsts and grabens in a predominantly extensional regime (Figure 2.3; McMillan et al., 1997). The graben fill was mainly controlled by the boundary faults and mainly included alluvial fanglomerates and braided and meandering fluvial sediments with occasional tuffaceous layers which indicate periods of volcanic activity

(Broad et al., 1996). The thick sedimentary successions are the result of major marine transgressive and regressive cycles chiefly produced by syndepositional normal faulting events (McMillan et al., 1997). Marine sandstones within the synrift sequence represent a thick shallow marine coastal complex and form the main hydrocarbon reservoirs on the northern margin of the basin e.g. the F-A, E-S and E-M fields (Broad et al., 1996). The end of most of the active rifting sedimentation is represented by the 1At1 unconformity which records significant uplift, and which in some areas cuts deeply into the sandstone reservoirs (Broad et al., 1996; McMillan et al., 1997). Tectonic processes during the rift and rift-drift transition were characterised by re-activated faulting and inversion that yielded potential traps for hydrocarbon accumulations (Broad et al., 1996; McMillan et al., 1997). The synrift source rocks are mature over large parts of the basin (Petroleum Agency SA, 2000).

Synrift II

From the Valanginian, permanent marine conditions prevailed with sedimentation occurring in deep marine, poorly oxygenated conditions (McMillan et al., 1997). Sedimentation was characterised by repeated phases of progradational and aggradational deposition with frequent deposition of hydrocarbon source shales during highstands and basin-floor reservoir sandstones during lowstands leading to the formation of numerous petroleum systems, the most significant ones being those occurring in the 13A and 14A sequences (Broad et al., 1996).

The 13A sequence, which overlies the Mid-Aptian 13At1 unconformity represents a time of restricted circulation in the basin, resulting in the formation of high-quality, organic-rich source rock shales (Broad et al., 1996). These shales entered the oil window in the Late Cretaceous and large areas are thermally mature for oil generation (Broad et al., 1996). Interbedded with these source shales, porous and permeable deep marine turbidite sandstones were deposited (Broad et al., 1996).

Drift

The overlying 14A interval typically contains similar turbidite successions (Broad et al., 1996). The Late Cretaceous and Cenozoic successions are thin and characterised by aggradational deposition and very slow sedimentation rates under stable shelf conditions (Broad et al., 1996; McMillan et al., 1997).

2.3 The E-S Field: The Field under Analysis

2.3.1 Exploration and Production History

The E-S field was discovered by the E-S1 well in 1983. Based on the 2D seismic available at that time, the trap was identified as a southerly dipping tilted fault block with fault and dip closure. E-S1 intersected 133m of shallow marine sandstone, of which the upper 27m is gas-bearing, and also intersected the underlying fluvial section. The well was tested in both the Upper Shallow Marine and fluvial sections, and flowed with a combined rate of 57.5 MMscf/d gas and 856 bbl/d condensate (PGS, 2000). Later in 1983, both the E-S2 and E-S3 wells were drilled and did not encounter any hydrocarbons. E-S2 intersected reservoir-quality rock but was water-wet, while the reservoir in E-S3 is interpreted to be eroded (PGS, 2000). Thereafter E-S4 was primarily drilled in order to test the fluvial section and although the fluvial section was found to be gas bearing, the well also encountered a significant oil (35° API) column that flowed at 2523 bbl/d (Willis et al., 1987). E-S5 and E-S6 were drilled down dip of E-S1 and found to be water-wet at both the Upper Shallow Marine and fluvial levels. The E-S7 well was drilled and completed as a gas producer in 2007. Although the well did encounter gas, the top of the shallow marine reservoir came in 95m deeper than expected thus reducing the expected pay zone of 102 m to just 10 m (Fedderson et al., 2007). The well was perforated and tested in the Upper Shallow Marine and fluvial zones flowing 5.6 MMscf/ gas and 16.4 bbl/d condensate, and 7.3 MMscf/d gas and 125 bbl/d condensate respectively.

The well was producing from only the fluvial zone up until late 2012, when production from the Upper Shallow Marine interval was also opened (PetroSA Operations, pers. comm.). Figure 2.6a, 2.6b and 2.6c show the structural configuration between the different hydrocarbon accumulations and the across-fault fluid relationships by means of a schematic cross section and structural maps.

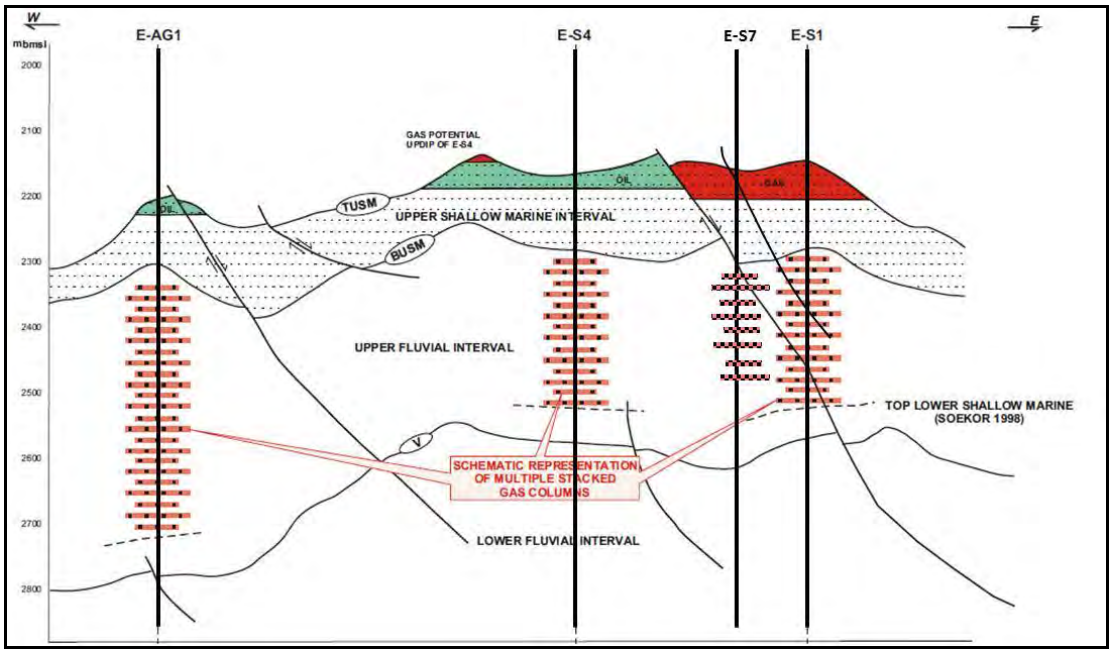

Figure 2.6a Schematic cross-section showing the structural configuration of the hydrocarbon accumulations together with across-fault fluid relationships. E-S7 is superimposed on the original figure (adapted after Frewin et al., 2001).

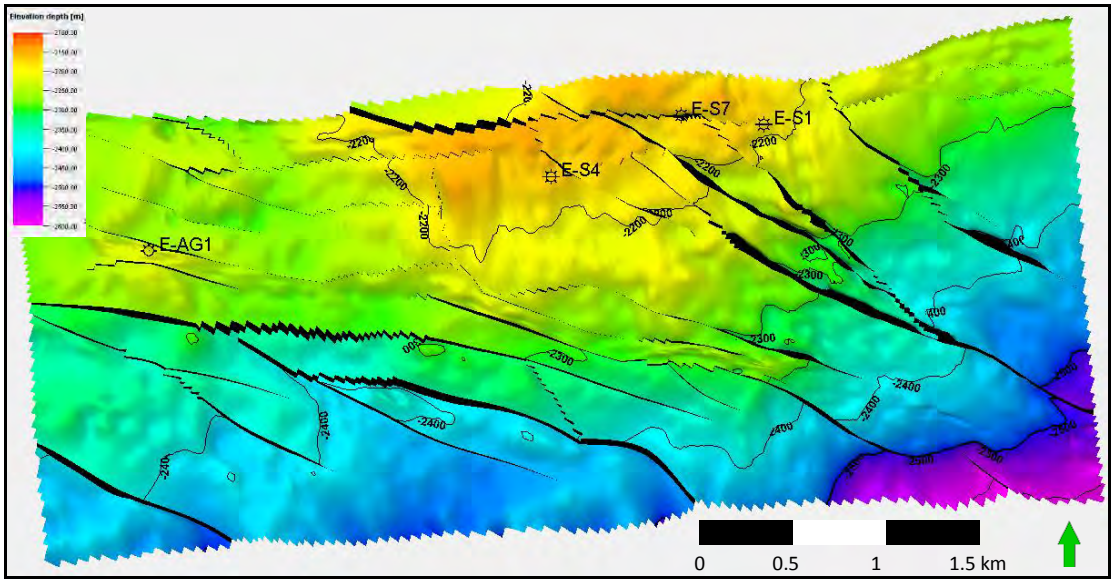

Figure 2.6b 1At1 Structural Map of the E-S and E-AG fields.

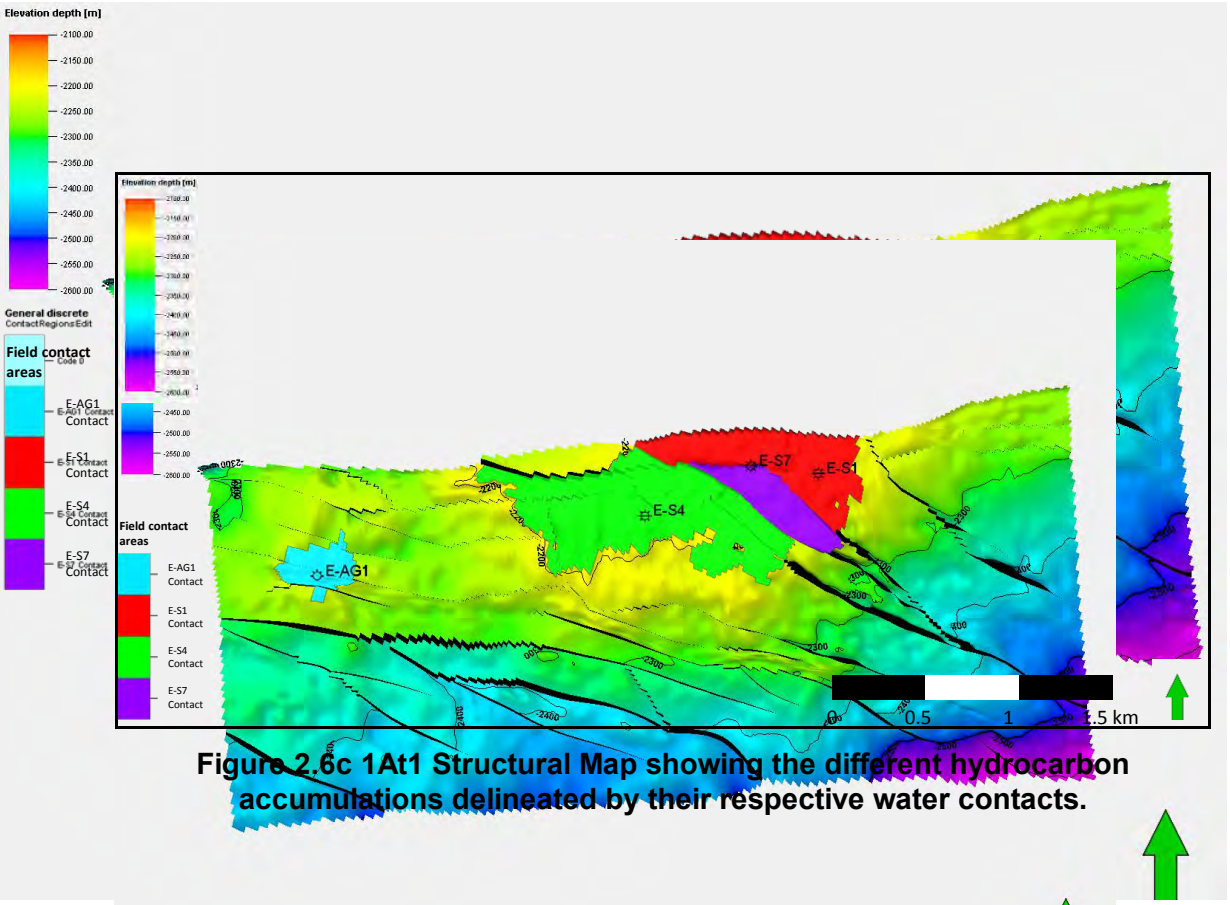

Figure 2.6c 1At1 Structural Map showing the different hydrocarbon accumulations delineated by their respective water contacts.

2.3.2 Reservoir Geology

Hydrocarbons are reservoired within the Upper Shallow Marine and the older fluvial intervals of the synrift succession. The synrift succession on the Bredasdorp Basin's north flank consists of regressive fluvial red bed lithologies punctuated by two transgressive shallow marine intervals. The Shallow Marine intervals were deposited in an upper shore face, high energy marine environment that resulted in thick, relatively clean sandstones with good petrophysical properties. The underlying fluvial section consists of thick claystones of overbank inter-channel floodplain origin, cut by anastomosing fine-grained channel sandstones (Frewin, 2005).

2.3.3 Structural Style and Setting

The E-S field is characterized by two main normal fault trends: a main E-W trend which exhibits a bigger structural relief and a WNW-ESE trend of smaller en-echelon faults. This arrangement produces ridges (*horst and graben*) which strike ~25°-30° obliquely with respect to the main trend (Antonio Ravaglia, Pers. Comm). Moreover, the structural style seems to repeat itself at different scales; the same structural style and orientation of

the fault sets are evident from regional scale to basin scale down to field scale (Figure 2.7).

The basal contact of the Synrift II deposits correlates to the 1At1 reflector, which is an erosional truncation on uplifted areas like the E-S field, and a correlative conformity basinwards (Figure 2.4). The internal layer architecture of the Synrift II sequence, particularly in this area, looks like a post-rift sequence rather than a synrift one as mentioned above, and is sometimes referred to as the drift sequence. There are no clear growth strata, only evidence of onlapping geometries and differential-compaction-induced deformation features (Jungslager, 1996).

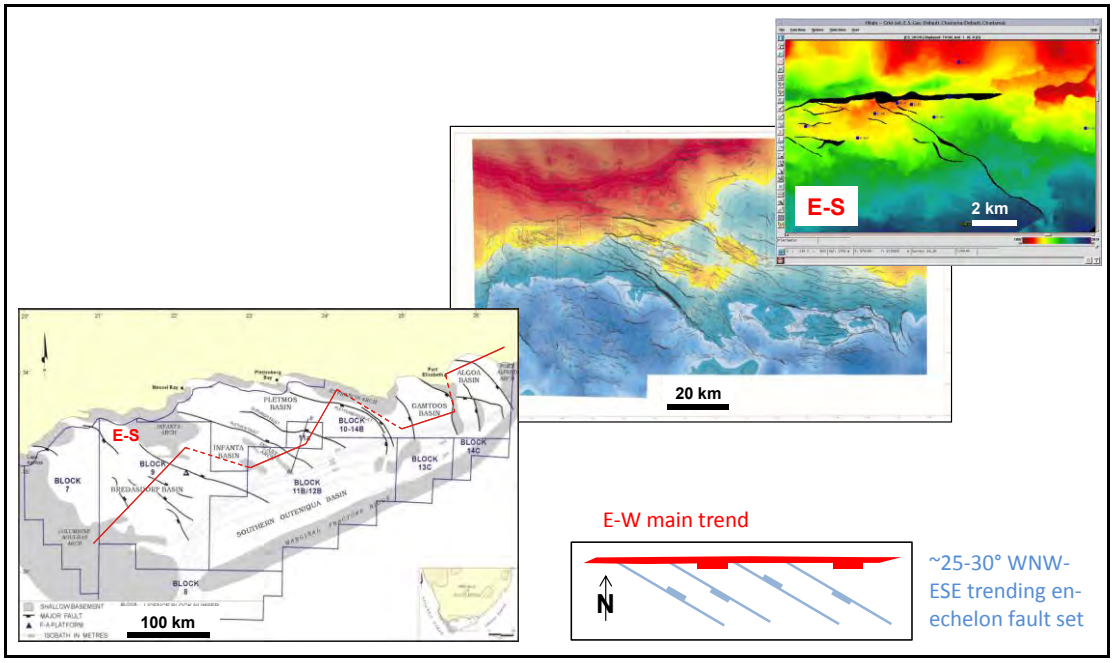

Figure 2.7 The structural style seen on the field scale can be traced back to the structural style seen on the basin scale (Antonio Ravaglia, Pers. Comm).

The accommodation faults, which developed during the rifting phase, affected the synrift deposits and to some extent the pre-rift deposits, and are almost always truncated by 1At1. Very few faults on the north flank show activity which post-date and offset 1At1. Tectonic inversion is claimed to have occurred in the area between Synrift I and II (Jungslager, 1996). Tectonic inversion might have been the mechanism which uplifted the topography and produced the later eroded relief (1At1). There is no evidence of reverse

faults and of inverted synrift basins in the E-S area, however tectonic inversion can be very irregular from place to place.

In the study area, some conjugate structures are present. Cross-cutting faults are common in normal fault systems and and can occur on a range of scales and in a variety of tectonic settings (Antonio Ravaglia, Pers. Comm).

2.4 Regional Stratigraphy

The lithostratigraphy of the E-S and E-W fields can be extrapolated from the E-M field. Figure 2.8 shows a merged log from wells in the E-S and E-M fields representing the stratigraphy which records the tectonic processes recorded above.

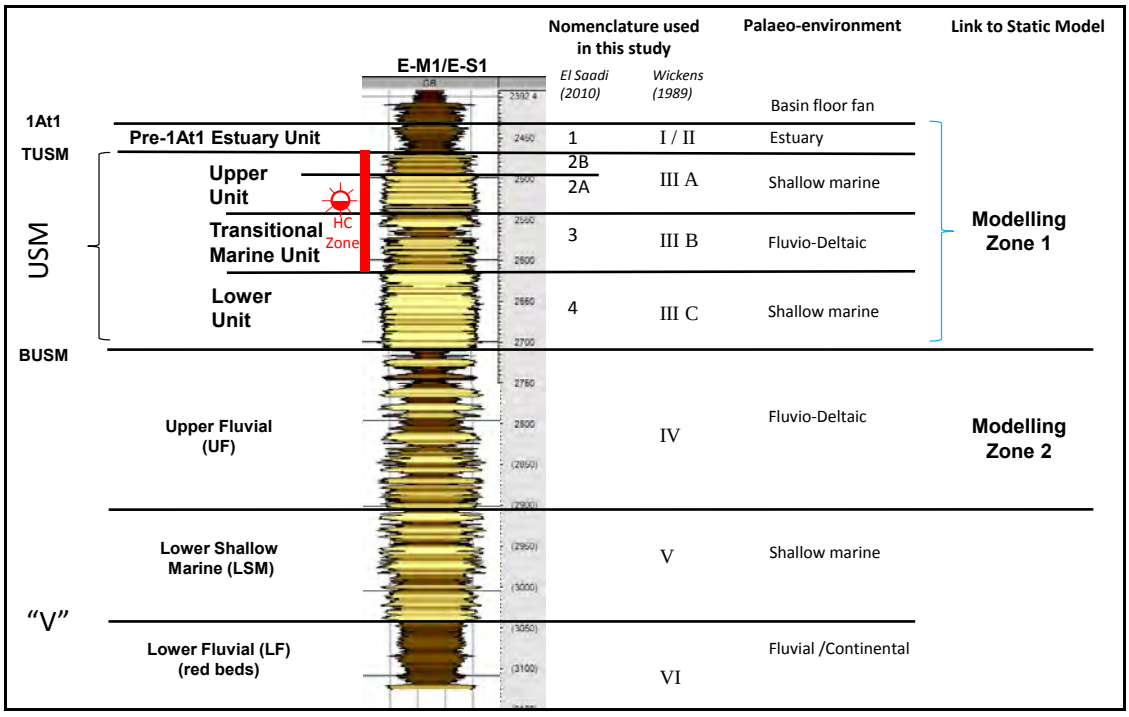

Figure 2.8 Lithostratigraphic units represented on an idealized well using a merged log: E-M1 for Pre-1At1 Estuary Unit and Upper Shallow Marine, and E-S1 for Upper Fluvial, Lower Shallow Marine and Lower Fluvial.

In Summary, non-marine (fluvial) sediments overlie the basement rocks of the basin. The top of this Lower Fluvial (LF) sequence is known as Horizon V and marks the interface between marine dominated processes and the underlying continental red beds. The Lower Shallow Marine (LSM) sandstone was deposited unconformably on the Lower Fluvial during a shallow marine

transgression. A marine regression, followed by a second shallow marine transgression resulted in the deposition of the Upper Fluvial (UF) sediments and the Upper Shallow Marine (USM) sandstone respectively. An additional period of significant regression and eventual subaerial exposure resulted in the deposition of the Pre-1At1 Estuary Unit followed by a period of major erosion represented by the 1At1 unconformity. Thereafter, a new relative sea level rise caused flooding of the northern flank of the Bredasdorp Basin.

2.5 Sedimentology and Depositional Environment of the Reservoir Sequences

The stratigraphy and sedimentology of the synrift sequences (1At1 to Horizon V) were studied by Wickens (1989) and El Saadi (2010) whose criteria were adopted in this thesis and form the basis of the sedimentological review hereunder. Some information from Dubost et al. (2009) was also considered. Table 1 correlates the zones from both studies to the conventional stratigraphic units.

2.5.1 Sedimentological Description for each Stratigraphic Sequence

Wickens Zone VI: Lower Fluvials (LF)

The Lower Fluvial sequence was not penetrated by any E-M or E-W field wells but has been intersected by most of the E-S wells. The sequence overlies the region's basement rocks, which are Table Mountain Group quartzites, and consists predominantly of red and green coloured shales, red siltstone and sandstone. The red lithologies are a strong indicator of an oxidizing depositional environment, probably terrestrial. The sandstones are fine to medium grained and well sorted, becoming coarse to gravelly in places. The weakly defined upward-fining cycles seen from gamma ray logs in the E-S wells together with the presence of pebbly sandstones in the cores have indicated a distal alluvial fan environment dominated by braided channel and interchannel mud flats.

According to Wickens (1989) coalescing alluvial fan systems with transverse and longitudinal gravel and sandbars, coupled by vertically accreted overbank or floodplain muds were indicative of the Early Mesozoic depositional regime in the Bredasdorp Basin.

Conventional Stratigraphy	E-M/E-S Field Zones – El Saadi (2010)	Sedimentological Zones - Wickens (1989)
Pre-1At1-Conglomeratic Facies	1	I
Pre-1At1		II
Upper Unit (USM)	2A & 2B	III (A)
Transitional Marine or Fluvio Deltaic (USM)	3	III (B)
Lower Unit (USM)	4	III (C)
Upper Fluvial	Not considered.	IV
Lower Shallow Marine	Not considered.	V
Lower Fluvial	Not considered.	VI

Table 1: Comparison between conventional stratigraphy and sedimentological zones.

Wickens Zone V: Lower Shallow Marine (LSM)

The Lower Shallow Marine has been cored in E-S4 and has an average thickness of 100m and an erosive base. It contains glauconite, shell fragments and oolites coupled with sedimentary structures that indicate deposition during a marine transgression. These features evidence high energy levels which removed finer sediments offshore while coarser sediments were pushed towards the shore. The frequent occurrence of glauconite together with reasonably good sorting indicates a marine environment although the glauconite grains could have been derived from reworked offshore deposits. Bioturbation and shell debris are present in the upper and lower parts of the sequence respectively but are otherwise very rare.

The lower part of this succession is interpreted to have been deposited in a subtidal to intertidal environment characterised by flaser and lenticular laminated sandstone with some calcareous interbeds. The upper part of this succession exhibits sedimentary features indicative of a regressive deltaic system. From the bottom upwards, the environment can be interpreted to have evolved from a high energy tidal-dominated system characterised by progradational coarsening upward patterns (from the gamma ray logs) to a lower energy fluvio-deltaic setting characterised by upward fining patterns probably due to channel abandonment and filling.

Wickens Zone IV: Upper Fluvials (UF)

The upper part of the underlying Lower Shallow Marine succession grades into the sub-aerially deposited sediments of the Upper Fluvial zone. The average thickness of this zone in the E-S area is around 170m, reaching a maximum of approximately 275m in some wells. In fact, interest in this succession was aroused due to the discovery of gas-bearing sand channels in the E-S region. The only core that has been cut in the upper fluvial zone is from the E-S4 well.

The Upper Fluvial zone is composed of red and green overbank or inter-channel floodplain claystones alternating with fine-grained channel sandstones. Once again, the red and green lithologies suggest a more terrestrial influence during deposition, and upward fining log patterns further support the process of meandering channel incision, followed by filling of sand and eventual channel-fill abandonment.

Wickens (1989) describes the sandstones in this zone as tabular, forming channels which are vertically offset from each other and being totally encased by surrounding overbank deposits. However, modelling data together with inferences from production data and well tests evidence a much smaller, isolated system where the channel sands are more pod-like rather than tabular in nature. Crevassing phenomena (break-up of levees during flooding) could also be responsible for the apparent tabular nature of the

sands. In addition, mixed palynofacies occurrences could indicate a more fluvio-deltaic setting in most of the E-M and E-S field wells.

Wickens Zone III: Upper Shallow Marine (USM)

The Upper Shallow Marine sandstones represent the main reservoir unit for most of the gas fields in the Bredasdorp Basin. The USM unconformably overlies the Upper Fluvial zone while its top is differentially eroded (in places) by the basin-wide 1At1 erosional event. It has an average thickness of 250m when it is fully preserved but this is considerably reduced by the 1At1 unconformity. The package consists of two distinct sand units (El Saadi Zones 2 and 4) separated by the fluvio-deltaic, Transitional Marine unit.

The USM sequence was clearly deposited in the near shore zone incorporating an important fluvial input of gravel and abundant plant material. The USM sediments are a mixture of fine and medium sandstones, interbedded with thin and generally discontinuous conglomerates transported to the marine environment by river systems. Once in the marine environment, the waves and currents rework the available grain population so that the textural variation becomes a highly significant parameter determining the nature of the bed-forms, sedimentary structures and sequences.

El Saadi Zone 4: Lower Unit (part of the USM)

Zone 4 is only cored in the E-M3 well. The lithology consists primarily of glauconitic sandstone and the gamma ray log signature displays an aggradational sequence comprising of sandstone beds with a predominant fining upward character, separated by beds of mudstone generally <1m thick. The thickness of this zone ranges from around 100m in the E-M field to between 40-85m in the E-S field. The contact with the fluvial succession below is unconformable, representing a transgressive surface where marine sandstones directly overlie terrestrial sediments. The sandstone is generally fine to medium to pebbly grained, well sorted and is clear to light greenish grey in colour with variable amounts of glauconite. Some facies characteristics in parts of this zone display resemblance to those of Wickens

Zone V so that similar shoreface wave and storm dominated environments can be proposed.

The environment of Zone 4 and Zone 2 share many similarities and the interpretation that follows applies equally to both zones. The environment was certainly not conducive to either accumulation or preservation of substantial thicknesses of fine muddy sediment. Bioturbation structures and shell debris are very rare. It could be interpreted that energy levels were very high and fine mud was effectively removed offshore whilst coarser sediment was pushed towards the shore. The common occurrences of glauconite together with the sedimentary structures present, favour a shallow marine setting. Reworked sands from the Lower Fluvial system were deposited in a near shore environment and could be interpreted to represent a barrier bar complex formed under regressive conditions.

El Saadi Zone 3: Transitional Marine Unit (part of the USM)

Zone 3 comprises a stack of thin and thick fining upward sandstone sequences separated by thin mudstone beds. Usually medium grained sands fine upwards to very fine sand, siltstone or thin grey-green mudstone. Occasionally, fine sands occur with some in-situ plant roots structures, and fine to very coarse lignitic laminae or woody structured driftwood is present (Dubost et al., 2009). Sedimentary structures include trough to planar cross bedding, planar horizontal lamination and occasional ripple cross lamination. Bioturbation structures, shell debris and glauconite are absent implying a non-marine environment. Based on the prevalence of fining upwards sequences, abundant carbonaceous debris and conglomeratic lags, this interval can be interpreted as fluvial, dominated by channel sand sedimentation (Dubost et al., 2009). Jungslager (1996) did a palaeo-geographic reconstruction where the fluvial source was a major river flowing in the northwest part of the basin from the Infanta Arch downslope. Being synrift, the channels directions may have been locally influenced by fault scarp palaeotopography.

The depositional environment was non-marine with strong fluvial influences indicated by meandering channel-fill and floodplain deposits (core and gamma ray log data). Although some authors have proposed deposition in a fluvial or lacustrine setting (Field Appraisal Team, 1984; Selley, 1985; Selley, 1986), Wickens (1989) supports marine deposition and attributes any ambiguity in the data to the influence of a shallow water fluvial-dominated deltaic environment.

El Saadi Zone 2: Upper Unit (part of the USM)

Zone 2 reaches up to 50-60m in thickness where it is not subjected to 1At1 erosion and can be easily distinguished from the zone below by the difference in log shape and increased content of glauconite. The sandstone is clear to light greenish grey in colour, and is well sorted with variable amounts of glauconite. Sedimentary structures and features include rip-up clasts, gravel lag deposits, heavy mineral laminations, scour and fill features, erosive bases, absence of any bioturbation and claystone; all of them clearly evidence a high energy environment. Course conglomerates derived from landward fluvial systems and later reworked and redistributed by wave dominated marine processes further support a high energy environment controlled by rapid deposition of sediment over short distances. Wickens has appropriately described Zone 2 as being representative of a “destructive, wave-influenced deltaic phase with deposition mainly confined to the lower shoreface to foreshore sub-environments” (Wickens, 1989; p19).

El Saadi (2010; like Dubost et al., 2009) divided Zone 2 into two subzones, A and B. These subzones can be distinguished on gamma ray logs (Figure 2.8).

Zone 2A provides the best reservoir facies comprising lithic-feldspathic sandstones with glauconite, moderate to good sorting and moderate to locally very good intergranular porosity. The dominance of medium grained, well sorted sands and moderate quartz cementation, results in good permeability shown by repeated intervals of up to 2m thick (Dubost et al., 2009). The zone is dominated by massive to indistinctly planar cross bedded, locally trough

cross bedded, quartzose lithic sandstones, that are predominantly medium grained and show moderate to good sorting. Remarkably few fine grained, thin laminated sandstone intervals occur, in contrast with the abundance of this lithofacies within the overlying Zone 2B sequence. The resultant interpretation is a stack of sheet-like sand-dominated depositional packages, each about 15m thick and which are internally heterogeneous (Dubost et al., 2009).

Zone 2B is characterized by inter-bedded massive sands and fine grained planar laminated sands, more or less in equal proportions with varying bed thicknesses. Towards the top of the zone, discontinuous mudstone beds are present, ranging in thickness up to 2m. Core logging and petrophysical logs have demonstrated that Zone 2B displays a higher proportion of fine grained laminated sandstone facies than Zone 2A. The former is dominated by very fine to fine grained sandstone, with occasional claystone intervals.

In general, facies characteristics of Zone 2 are similar to those of Zone 4 and therefore a similar depositional environment can be inferred. The different mixing of facies proportions between Zone 2B and 2A can be related to a more offshore location for Zone 2B where the abundance of plane bedded sandstone is a likely indicator of a further offshore location for Zone 2B with respect to Zone 2A. This shifted location may be related to a change from an aggradational to progradational regime in Zone 2A, perhaps related to the rifting onset; to a more transgressive regime in Zone 2B, prior to the transgression of the Upper Shallow Marine shelf and deposition of the muddy sediments of Zone 1 (Dubost et al., 2009). In general, Zone 2 displays large scale cyclicity of stacked sandstone beds, with both coarsening upwards and fining upwards units. It, together with the prograding deltaic deposits of Zone 3, forms part of an upward coarsening megacycle.

El Saadi Zone 1: Pre-1At1 Estuary Unit

Zone 1 in the E-W wells is different from Zone 1 in the E-M or E-S wells. This is why Wickens (1989) chose to differentiate two different sedimentological zones in his study (Table 1). The geophysical logs of the E-W wells show a

sand body embedded in the muddy sediments of Zone 1 whereas this sand body is absent in the E-M or E-S area. The thick sequence of nearshore sandstones (i.e. the USM sandstones) is overlain by estuarine or marine muds and by thinner channelised debris flow sands and conglomerates. The upper sandstone in Zone 1 has a limited lateral extent as inferred from its depletion during testing (there is however some contention regarding the depleting nature of the sand). The lateral seal could have been produced by erosive truncation by the 1At1 horizon or by parallel faults.

2.5.2 Depositional Palaeo-environment Summary

As the Upper Shallow Marine sediments were deposited during a synrift phase in the margin of the basin, their sediment features and thicknesses were controlled by the basin subsidence, accommodation (the space available for sedimentation), erosion and sediment supply.

The marine Zone 4 of the USM was deposited in a prograding nearshore area with a fluvio-deltaic input of abundant coarse sediment and plant material during a highstand stage. Conversely, Zone 3 was interpreted as deposits of a fluvial-dominated delta on the north flank of the basin. In the E-W area, Zone 3 shows a more open marine nature (occurrence of in-situ glauconite). The coarsening-upward cycles reflect a sediment supply higher than basin subsidence.

Zones 2A and 2B were deposited below the wave base, with similar characteristics to those of Zone 4. A wave dominated (destructive) delta was interpreted for Zone 2, with the deposition mainly confined to the shoreface (Zone 2B) and foreshore (Zone 2A) in a rapidly transgressing shallow marine shelf. Zone 1 records a wave dominated estuary or island bar – lagoon system where the muddy marginal marine facies could have played a role as a good seal for hydrocarbons (Dalrymple et al., 1992). This could also explain pressure differences in adjacent hydrocarbon reservoirs i.e. Upper Shallow Marine vs Pre-1At1 Estuary Unit sands (Dubost et al., 2009).

The entire region was subjected to intermittent faulting during and after deposition, and finally it was locally eroded as the 1At1 unconformity reflects. For this reason the good quality reservoir intervals of the USM in the study area have only been partially preserved.

3 METHODOLOGY

3.1 Data Collection and Preparation

Following are the main data sets used in this study.

- The E-S field is covered by a 3D seismic survey acquired in 1995 which spans 160km^2.
- The main wells used in this study were E-S1, E-S4, E-S7 and E-AG1. An entire suite of geophysical logs was available and used for each of the wells. This included Gamma Ray (GR), Resistivity (ILD, LLS, LLD, MSFL), Sonic (DT), Neutron (NPHI), Density (RHOB) and Checkshot data.
- Additional wells were included for the purpose of well-seismic tie. These were E-S2, E-S3, E-S5, E-S6, and E-BU1.
- Furthermore, E-M1 and E-M5 were incorporated for structural well correlation.
- Well Markers observed in the wells were tied to the seismic data. The interpreted surfaces used in this study are:
    - 1At1
    - BUSM (Bottom Upper Shallow Marine)
    - Horizon V (Top of the Lower Fluvial section)
- Petrophysical data derived from conventional core analysis was also incorporated. Data included core porosity, core permeability-air and core permeability-Klinkenberg. Other petrophysical data was processed from log data and will be discussed later.
- Well Recommendation and Well Completion reports were used to gather and analyse general data about the wells.

3.1.1 Log Correlations and Cross-Sections

The E-S1, E-S4, E-S7 and E-AG1 wells were chosen as being the more important wells in the E-S field owing to them encountering hydrocarbons and therefore they were analysed in detail (Figure 3.1). Log correlations were

made for 1At1, Bottom Upper Shallow Marine, and Horizon V. A number of stratigraphic cross-sections across the area between the E-M and E-S fields were created in order to correlate the stratigraphy (Figure 3.2 and 3.3). The 13At1 marker horizon was chosen as the stratigraphic datum upon which the cross-sections were hung because of its continuity across the north flank and its strong log character. Once correlations were completed and the stratigraphy was pinned down with reasonable confidence, relevant structural cross-sections were created and analysed (Figure 3.4 and 3.5).

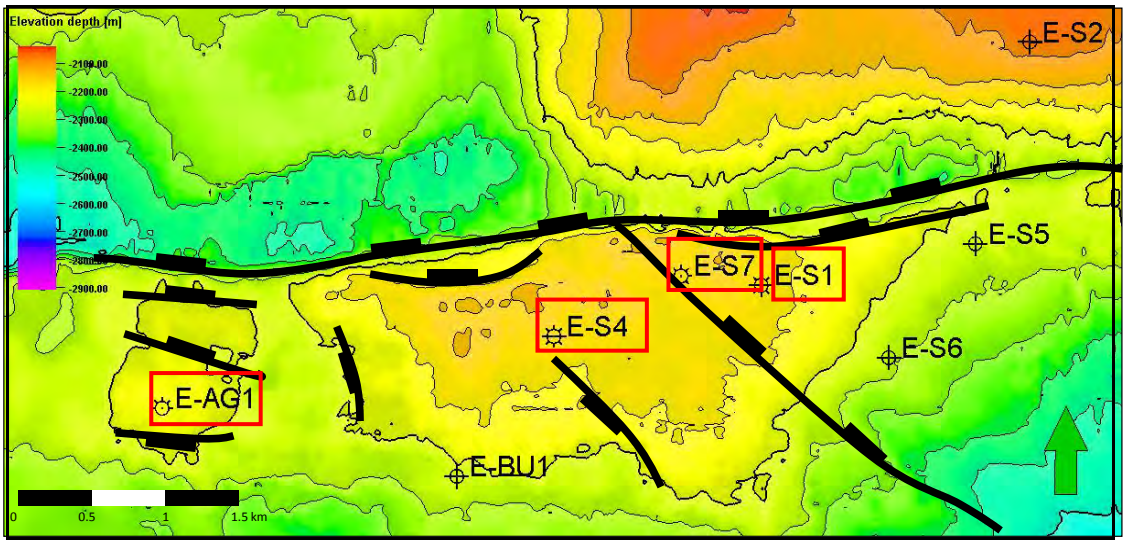

Figure 3.1 Structural map of the 1At1 surface (regional interpretation) with the main faults showing the location of the E-S and surrounding wells.

In the main E-M field, the presence of a complete Synrift I section is apparent. Erosion increases in an easterly direction and on reaching the E-AG1 well, the 1At1 erosional surface has already cut into the Upper Shallow Marine sandstone (USM). The full section present in E-M1 is significantly reduced, leaving the E-S wells having a lesser USM thickness. The E-S field is also structurally higher than the E-M field, and this could be a contributing factor to the more pronounced erosion in that area.

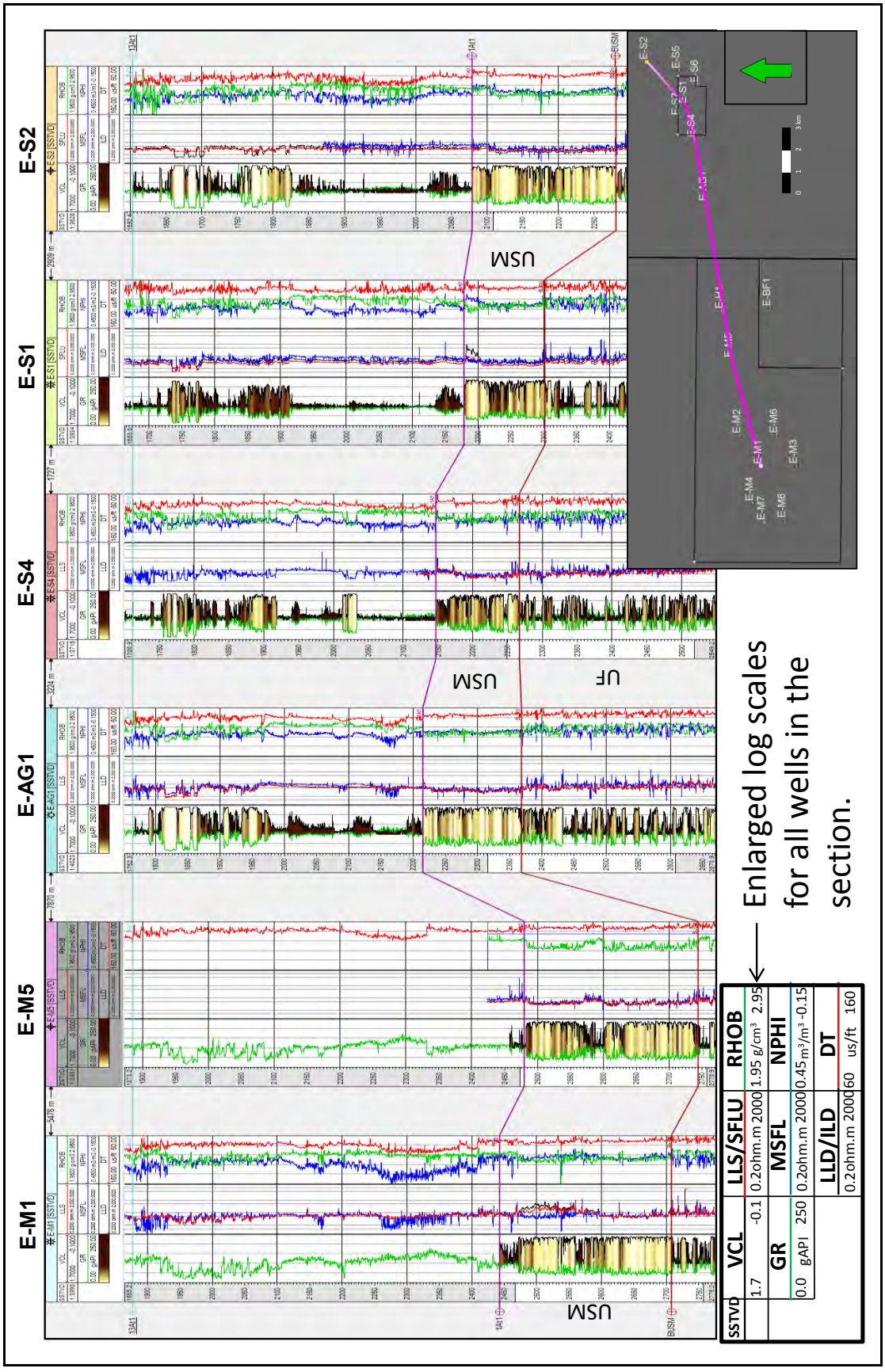

Figure 3.2 Regional stratigraphic cross-section from west to east flattened on the 13At1 horizon.

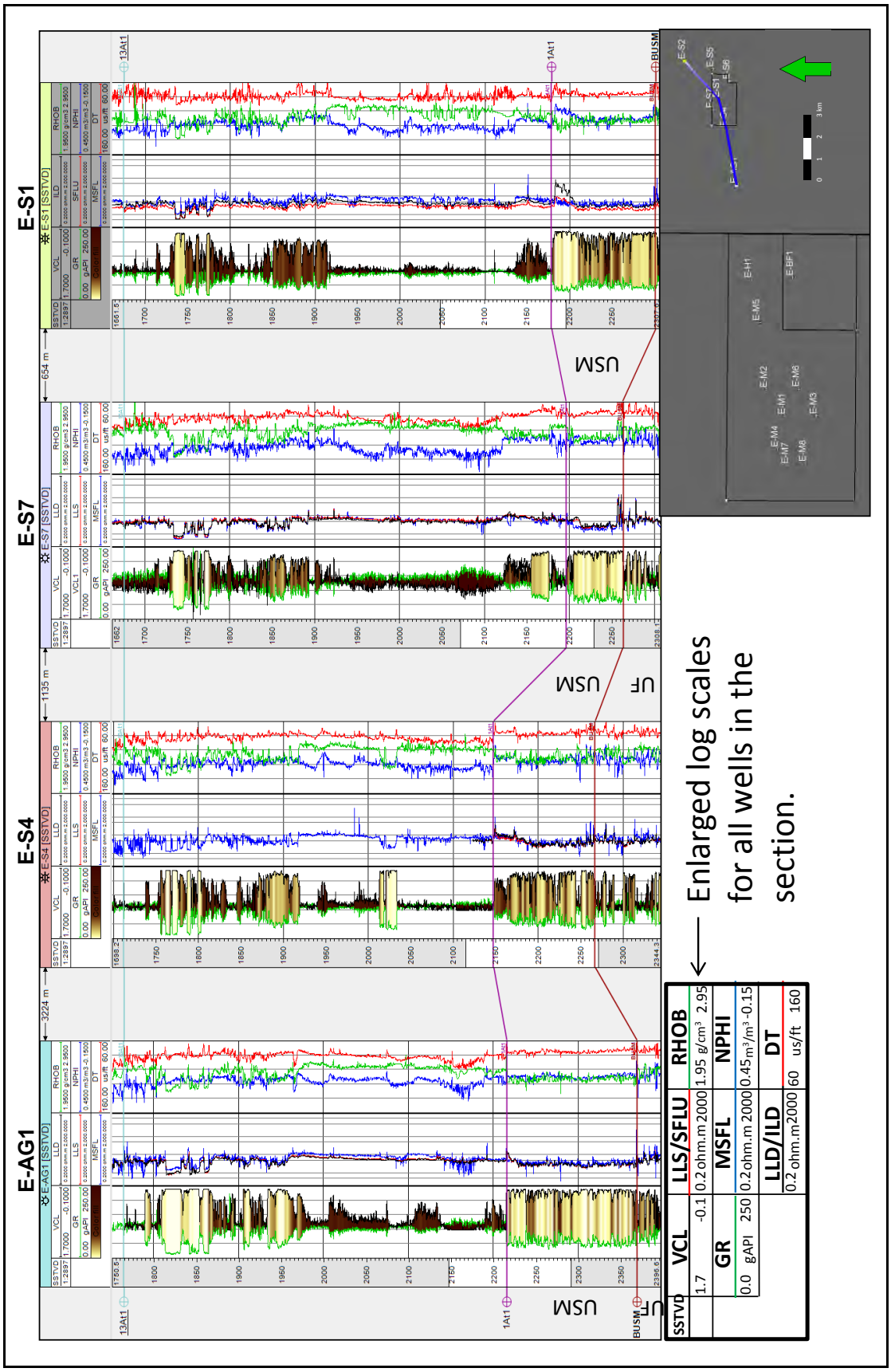

Figure 3.3 Stratigraphic cross-section from west to east flattened on the 13At1 horizon, incorporating the main wells of the study.

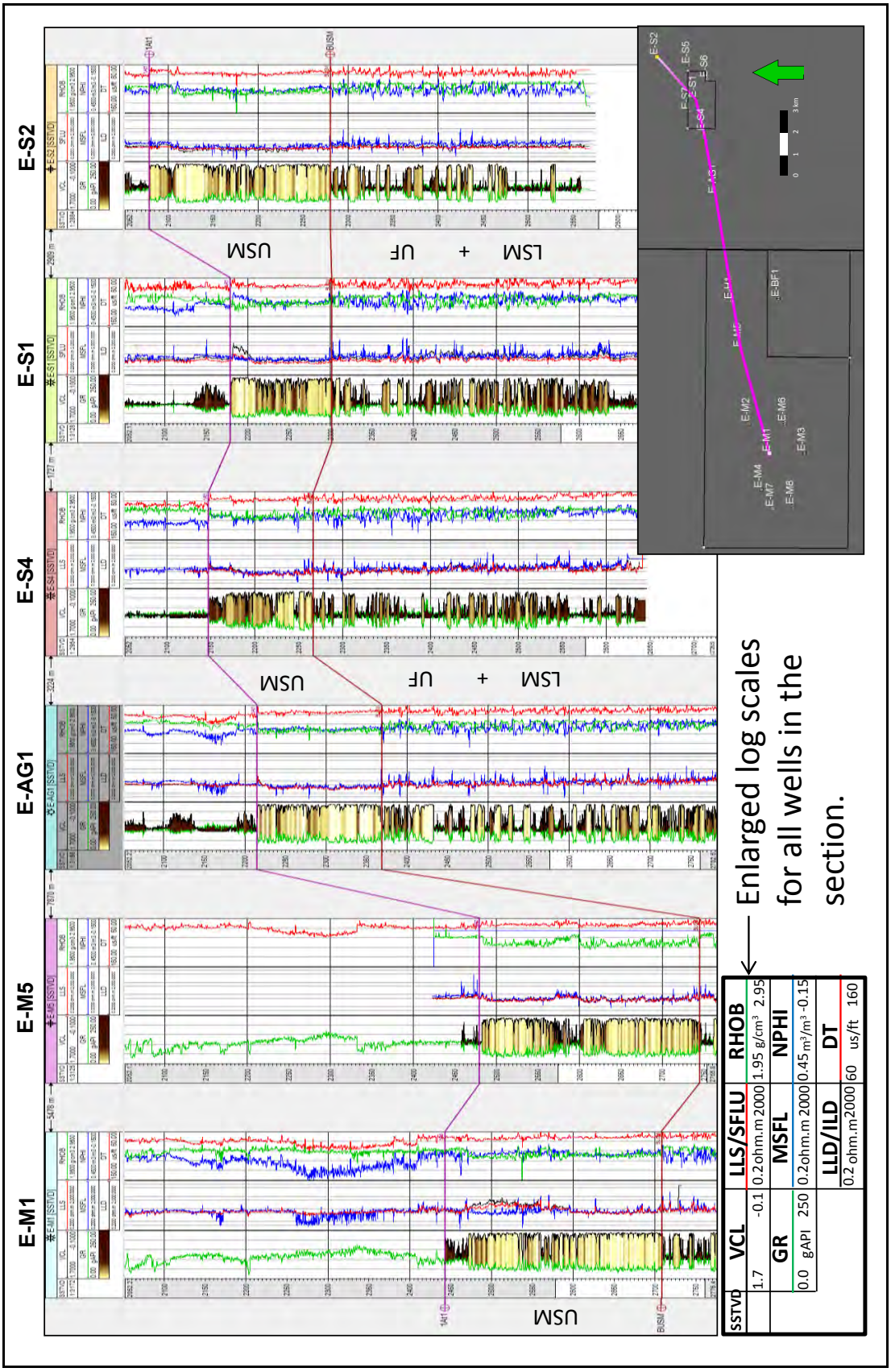

Figure 3.4 Regional structural cross-section from west to east.

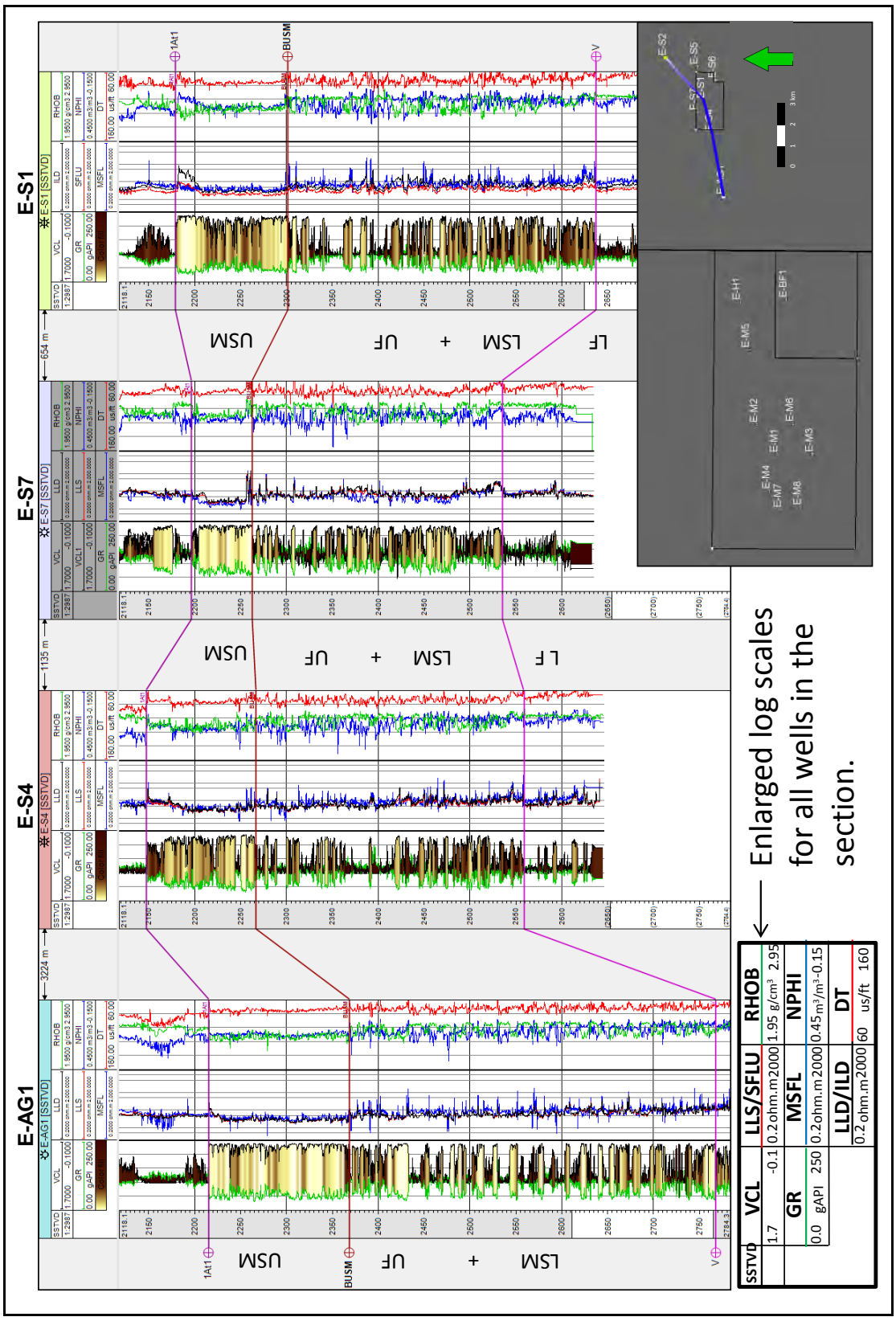

Figure 3.5 Structural cross-section from west to east incorporating the main wells of the study.

3.1.2 Seismic

Five (5) key horizons have been identified and interpreted in a 3D seismic cube covering the E-S Area (Figure 3.6):

a) Sea Floor
b) 13At1
c) 1At1
d) Bottom Upper Shallow Marine (BUSM)
e) Horizon V

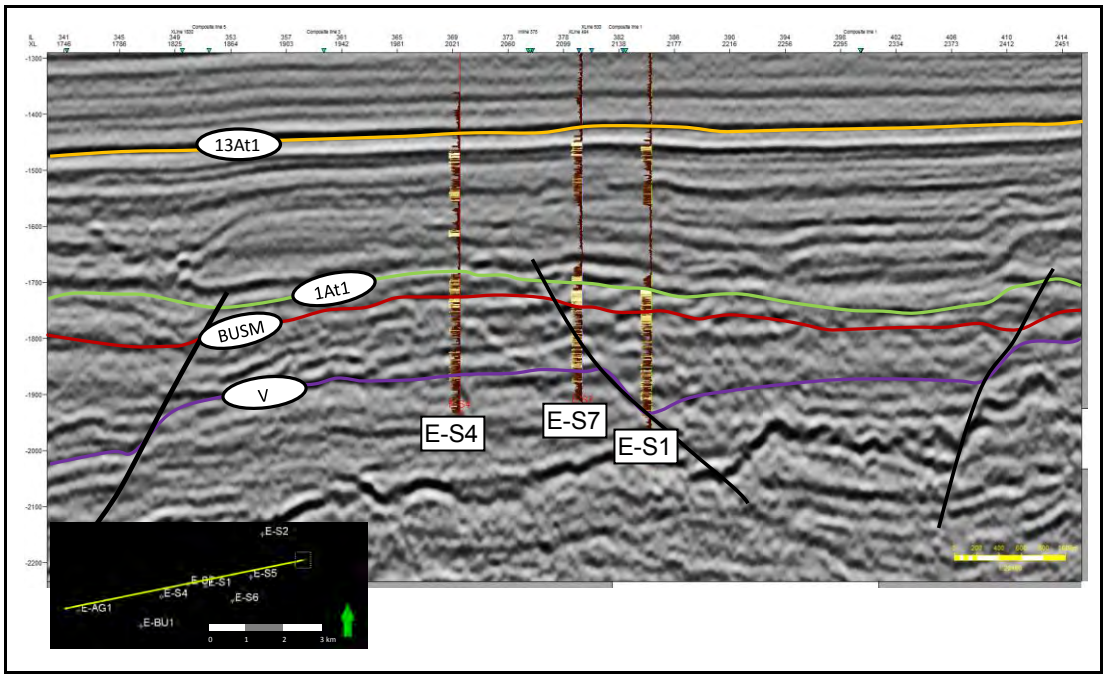

Figure 3.6 Seismic section through the E-S field showing some interpreted surfaces and main faults.

The horizons have been selected owing to their importance in defining the reservoir at the sequence level. The seafloor and 13At1 reflector assisted in constraining the velocity model needed to create a depth conversion model (details discussed later). The Bottom Upper Shallow Marine marker is difficult to pick due to its weak seismic signal. Therefore, the more continuous Horizon V marker was used to guide the interpretation together with the faulting style and geometry prevalent in the study area which resulted in a better understanding of the entire reservoir setting. The interpreted seismic reflections associated with the geological markers were tied with the use of

synthetic seismograms at the well locations (Figure 3.6). Once the time-depth conversion process converted the surfaces to depth, these surfaces were also used to create isopach maps of the reservoir zone which were later used in the modelling process.

3.2 Data Management and Workflow

Since this study is focussed around the creation of a static geo-cellular model, some of the data was received in already edited form e.g. well logs. All data was loaded into the PETREL software in order to create the geo-cellular model. The Rock Deformation Research (RDR) module was also added to PETREL to carry out the fault-seal analysis workflow.

3.2.1 Summary of Workflow

The flowchart below (Figure 3.7) summarises the workflow undertaken during this study.

- All relevant data was collected and prepared. This includes well data and well correlations together with interpreted seismic horizons.
- A velocity model was created to convert time interpretation to depth (T/D). From this point on, all work was done in the depth domain.
- Building the geocellular model began by defining and modelling the faults in order to produce a structural model.
- A stratigraphic model was built based on Horizon and Zone definition. This together with the structural model formed the container into which reservoir properties were populated.
- A facies model was defined using geostatistical (two-point statistics) and object modelling methods.
- All reservoir properties including Volume of Clay (VCL), porosity (φ), net/gross and water saturation (Sw) were created and populated accordingly into the respective facies designations.
- Hydrocarbon volumetrics were calculated for both gas and oil accumulations in the field and were compared to previous studies.

- A fault-seal analysis was carried out in order to evaluate the effect of compartmentalisation on reservoir connectivity and production (simulation phase).
- A number of fault properties were generated in order to quantitatively evaluate the fault seal. These included Volume of Clay, Clay Content prediction and Column Height and Contact Depth prediction.
- Although the workflow has been represented as being linear, many of the steps involve multiple iterations before their outcomes are finalised.
- A detailed account of the static model building and fault seal analysis processes can be seen in Section 5 and Section 6.2 respectively.

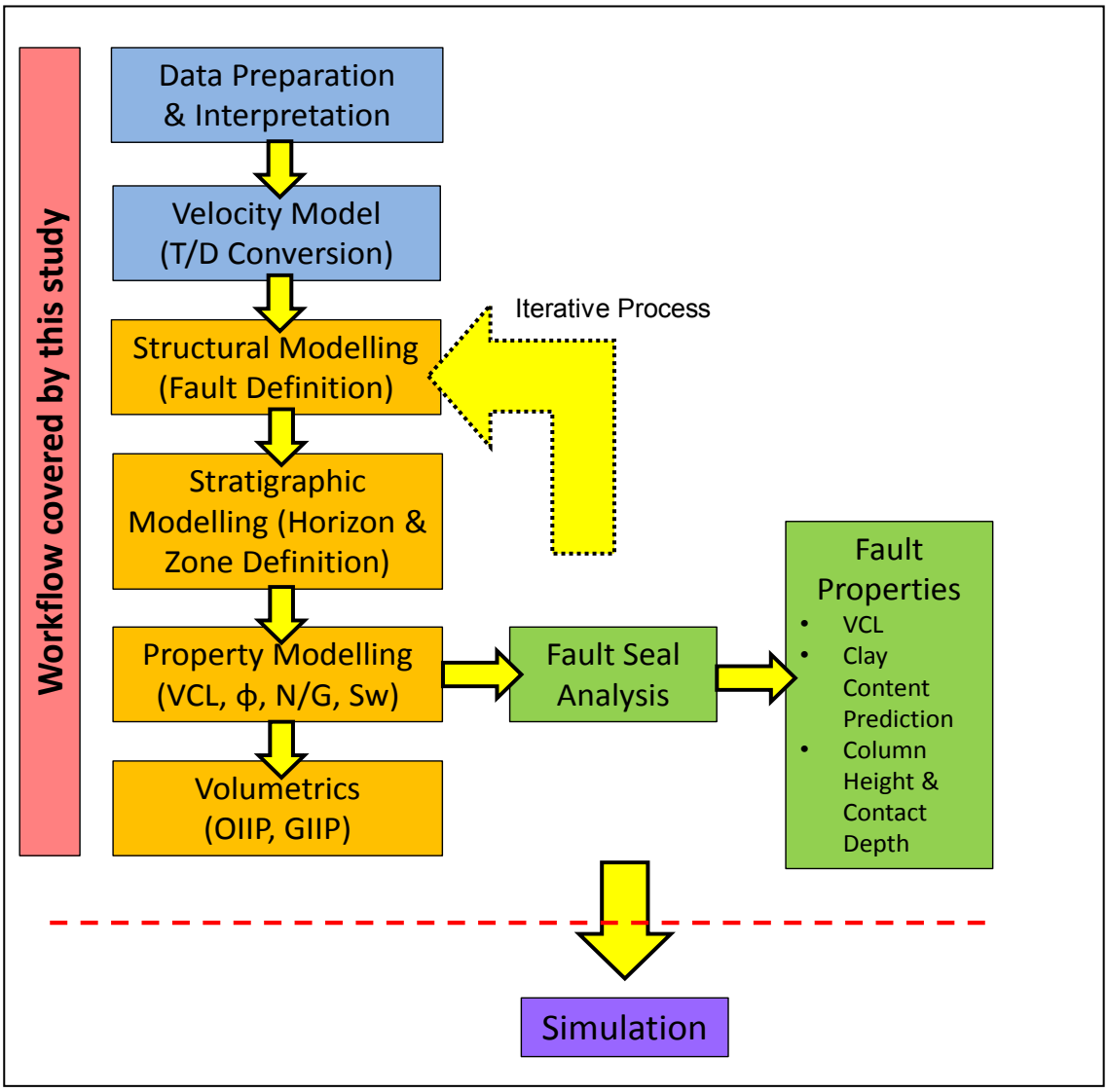

Figure 3.7 Summary of workflow used in this study.

4 THE GEO-CELLULAR MODEL

4.1 Introduction to 3D Geo-cellular Modelling

Geologists traditionally use 2D well correlation panels, fence diagrams and maps to build a geological story. To convert these geological ideas into usable inputs for processes like dynamic reservoir simulation, they should ideally be in 3D. The problem with the 2D models is that they do not solve the issues pertaining to reservoir connectivity, often causing a disconnect between the geological model and the reservoir simulation model (Dubrule, 1998). The result is that the simulation model does not contain the level of geological detail entrenched in the geologist's 2D model (Dubrule, 1998). In addition, the 2D geological model is deterministic and does not account for any uncertainty pertaining to different interpretations or possibilities emerging from the same dataset. Stochastic 3D geo-cellular models built using geostatistics allows for uncertainty to be quantified through an *nth* number of different realisations (or scenarios) while maintaining a realistic representation of heterogeneity (Dubrule, 1998). Some of the main benefits of using geostatistics in the model building process are that it supports multidisciplinary data integration, it allows for reservoir heterogeneity to be modelled (using Conditional Simulation algorithms) and it provides a robust basis for uncertainty to be quantified. The concept of geo-cellular 3D modelling is a fairly new addition to the sphere of applied petroleum geology, and has rapidly become a regular part of standard workflows in the production and development side of the oil and gas industry. Zakrevsky (2011) has attributed this rapid implementation of 3D modelling to the development of key mathematical principles and algorithms that form the basis of the model building process, together with the emergence (and continuous progression) of ultra-high computing power coupled with specialised modelling software packages.

The most effective 3D geo-cellular models are built towards satisfying certain goals. They support the accurate assessment or calculation of hydrocarbon reserves, and provide a platform upon which wells can be designed and development plans ratified. Such a model also serves as a powerful tool during

geosteering drilling where changes in the well path can be effected and viewed in real time. The stochastic nature of 3D modelling also lends itself to being an integral part of any risk and uncertainty assessment. Dubrule (1998; p7) aptly summarises the model as being “a conceptual representation of the architecture of genetic bodies (e.g. fluvial channels, floodplain shales) within which petrophysical variations can be distributed”. The economic implications of these representations can be better understood through optimally choosing in-fill well locations or through results from reservoir simulation exercises and ultimately the type of development strategy chosen (Dubrule, 1998).

A static geo-cellular model or 3D grid consists of a network of numerous cells, the size of which is defined by the user, and which can be populated with different reservoir/geological properties based on user-defined parameters using geostatistics (the variogram, Kriging & Conditional Simulation). This grid forms the structure within which all the stages of geological modelling occurs (Zakrevsky, 2011). Grids can be both structured and non-structured with the latter allowing for more flexibility and thus better definition of complex geological geometries (Zakrevsky, 2011). However, the objective of building a model is most often not restricted to just being purely a geological tool but the results of the model are frequently used by reservoir engineers to simulate the flow dynamics of the reservoir. The process of dynamic modelling requires that the geological static model is built with a structured grid to reduce computing time and calculation complexities associated with a non-structured grid. In general, the simpler the grid the easier it is to compute the dynamic simulation (Zakrevsky, 2011).
The use of this type of model helps to capture the complexity present in the subsurface and attempts to bridge the gap between reality and our understanding. It is obviously a somewhat simplified representation of reality, but it serves to best characterise both visually (through the 3D model itself) and statistically (through property population) what could be encountered deep in the subsurface.

4.2 Uncertainty in 3D modelling

The model of any practitioner is only a representation of reality based on the available data together with the resultant decisions made to guide the data to a geologically defendable and plausible end result. Subsurface data is never enough, leading to a high dependency on the interpreter to “fill in the gaps”, using geological knowledge and creativity in order to understand the subsurface heterogeneity. One aim or purpose of 3D modelling is to create multiple alternative 3D numerical models, each capturing the geophysical, geological and reservoir engineering properties of the subsurface (Caers, 2005), whilst respecting the data-set at hand. An interpreter will use all the data available, even though it may be subjective, to create a number of equiprobable scenarios taking into account knowledge regarding geological continuity (trends between data points inferred from different types of data e.g. seismic, geological conceptual model, petrophysical log analysis etc.) while taking care to not over-bias one type of data. To understand this better, if one were to use only seismic data to guide a geological trend e.g. porosity, the low resolution of the seismic would lead to a result which is too smooth resulting in an improbably homogeneous model. By creating multiple models or realisations using a geostatistical approach, the interpreter attempts to encompass the entire range of geological possibilities or scenarios that the data could represent while maintaining any interpreted geological variability (Caers, 2005). This allows decision makers to understand the risk and uncertainty present in the subsurface and places them in the best position to make informed decisions using the entire range of possible outcomes at their disposal.

4.3 Spatial Correlation: The Experimental Variogram, Using Variogram Models, Kriging and Conditional Simulation

Geological data can be described as being “non-random”. This means that data values which are closer together are more likely to be more similar than those that are a further distance apart (Caers, 2005). Geostatistics plays an

integral part in applying this concept in 3D space using the usually less than adequate data-set available to the interpreter or modeller. Most geostatistical methods, in one way or the other, use variography or more specifically the variogram as the main tool to estimate and model spatial variability. The role of the experimental variogram is to quantitatively measure and describe the continuity or spatial correlation of reservoir properties, like porosity and permeability (Caers, 2005). In theory, the variogram measures the average square difference between two points a certain distance apart, in a particular azimuth (Caers, 2005; Pyrcz and Deutsch, 2014). Pyrcz and Deutsch (2014; p87) have aptly described the variogram as: “A chart of geological variability versus direction and Euclidean distance”. In general terms, the difference between data values is likely to increase as a function of distance. Although not common, differences could begin to decrease after having displayed a trend of continued increase which could indicate periodicity or cyclicity in the data – termed the *hole effect* in geostatistics.

The **experimental** variogram refers to the plot of squared differences versus distance using the **actual** data points. It is not practical to use the experimental variogram for processes such as Kriging (or subsequent Conditional Simulation). These processes/methods require that conditional positive definiteness is maintained and that the purely statistical variability of the data should be removed. In addition, the behaviour of the variogram from the origin to the first data point needs to be quantified. These criteria are met by using different (though applicable) mathematical variograms to fit the experimental variogram. What is important here is that the experimental variogram informs the choice of variogram model. The variogram models will change with different study areas and so the experimental variogram is computed in order to constrain the choice of variogram model. The variogram model is therefore based on the experimental data (observed data) which is used to create the experimental variogram. The variogram model is dependent on the observations and their spatial structure together with the judgment of the

modeller. The use of variogram models also helps to simplify and standardise the way the algorithms are calculated.

The shape of the variogram changes depending on the direction along which it is calculated as geological continuity in most cases is likely to exhibit some degree of variation and is rarely isotropic (Caers, 2005; Pyrcz and Deutsch, 2014). Generally, due to the lack of dense data-sets, the most common practice in petroleum reservoir modelling is that the main trend controls the anisotropy along a single major and minor axis of horizontal (bed-parallel) continuity (Caers, 2005; Pyrcz and Deutsch, 2014). The vertical direction is taken perpendicular to the horizontal directions mentioned above (Pyrcz and Deutsch, 2014). The final directions chosen for the major and minor axes of the variogram will be based on the geological understanding of the interpreter which should conform to the strongest trend (average major and minor trend) displayed by the property being modelled.

Kriging is an interpolation method/process which uses variograms as its main input. Kriging is said to be the best linear unbiased estimator (Dubrule, 2014). The ultimate aim of most Kriging methods is to limit the difference between the estimated value and the true (unknown) value. The final output of the Kriging algorithm is a series of weights for each of the neighbouring points so that the estimate is essentially a weighted average of the control points. If one were to expand this mathematically one would find that one can express the difference between the observed and estimated values as a system of linear equations relating the mutual variances between controls i.e. pairs of data, and the mutual variances between controls and the unknown point i.e. data point and target point. Therefore, if we have variances for all the pairs of points concerned then we can input these into such a system of equations and solve for the weights (Cathy Dillon, Pers. Comm.).

As mentioned before, data in the petroleum industry is usually sparse, and coupled with the fact that variograms look at the relationship between pairs of points, using a variogram alone to build a model produces a result that lacks realistic geological shapes and heterogeneity (Caers, 2005). Kriging tries to

minimise possible error and therefore produces results which are too smooth especially in the case where the property exhibits high degrees of variability. This is the main constraint of modelling only by Ordinary Kriging and is a point of caution to avoid producing results which are too synthetic or homogeneous. However its main strength is that it takes into account the configuration of the data and the location of each data point with respect to the target points.

4.3.1 Collocated Co-Kriging – A Kriging Variant

Collocated Co-kriging is a variant of Kriging which applies the Kriging algorithm to two sets of data; one known at the wells and the other known between the wells. This method is highly effective when the primary variable is relatively under-sampled with respect to the secondary variable. The correlation coefficient or co-variance between the variables is used to guide the interpolation of the primary variable with the assistance of the more densely populated secondary data. Collocated Co-kriging was used during the building of the static model to relate a modelled property to another already modelled property.

4.3.2 Morphology of the Variogram

The variogram is described with specific terminology related to its morphology (Figure 4.1). It begins from the origin (or sometimes from a value above the origin: this is termed the *nugget effect* and is discussed later) and reaches a point where it is interpreted to plateau. The characteristic of reaching the plateau, which is known as stationarity, is dependent on the type of theoretical variogram that is chosen. Certain types of variograms do not exhibit stationarity e.g. the power variogram. The behaviour of the variogram at the origin is most important and is the key indicator of the manner in which the data varies spatially over short distances i.e. whether change occurs rapidly at very small distances or changes are smooth and occur over larger distances.

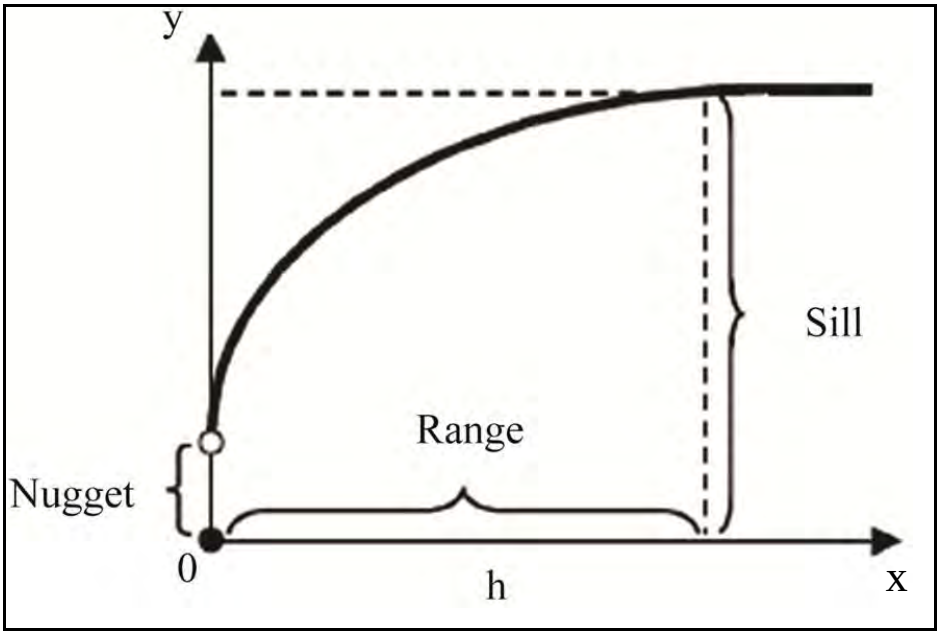

Figure 4.1 The morphology of a theoretical variogram (after Meilianda et al., 2012).

The distance from the origin to the point it intersects the plateau (on the x axis) or the point at which it becomes stationary is called the *range.* The value of the range represents the average distance of continuity or correlation for a specific property in the chosen direction (Caers, 2005). When the variogram is stationary (it has reached the range) i.e. it has reached the point at which differences measured between data pairs of a particular variable is said to be constant or it is outside the sphere of influence. At this point, the mean is relatively constant and interpolated data varies around this constant mean. No more correlation can be made between data pairs beyond the value of the range. Kriging will tend to produce “bull’s-eyes” around widely-spaced data points as the algorithm tries to go towards the mean value further away. The result is that low and high areas on the map are centred around measured data points.

The horizontal range is usually much greater than the vertical range due to the greater continuity of lateral distances driven by depositional processes and can sometimes appear to be infinite (Pyrcz and Deutsch, 2014), but this depends on the geological environment and related reservoir properties. In addition, the vertical variogram is usually sampled directly from log data along

the wells and would therefore have a much smaller range due to the faster rate of change when compared to the more continuous nature of geological data in the horizontal direction.

The value at which the variogram plateaus is termed the *sill* (on the y-axis). The sill represents the overall statistical variance of the property or variable (Caers, 2005). It however does not contribute to providing geological information in the way that the range does. Changes in the sill do not affect Kriging weights or the kriged values but they do change the Kriging standard deviation.

The *nugget effect* occurs when there is an apparent discontinuity at the origin (Caers, 2005; Pyrcz and Deutsch, 2014). While the variogram can be described as a measure of the random variable plus the random error; the nugget is in one way, a measure of the variance of the random error. This type of nugget could be interpreted as being representative of “noise” in the data. If a data type is expected to be distributed smoothly in space, but instead shows unexpected variations over very short distances, it is an indication of experimental error and a nugget should be applied to the variogram to remove this effect (Figure 4.2). Seismic velocities generally exhibit a smooth gradational trend and any rapid changes of this kind would most probably be spurious values i.e. noise in the data.
Alternatively, a nugget can also be used to reflect the behaviour and account for the geological variability at distances smaller than the shortest distance between any pair of samples in the data-set (Caers, 2005; Pyrcz and Deutsch, 2014). The use of this type of nugget should however be treated cautiously with petroleum data, as sedimentary processes and their resultant properties are usually continuous and gradational resulting in the absence of or a very small nugget.

Kriging incorporating a pure nugget effect (i.e. total randomness) results in a map that represents the mean within the search area. With decreasing nugget,

maps of decreasing degrees of smoothness are achieved until the nugget is zero, where the Kriging algorithm produces a map, honouring all data points.

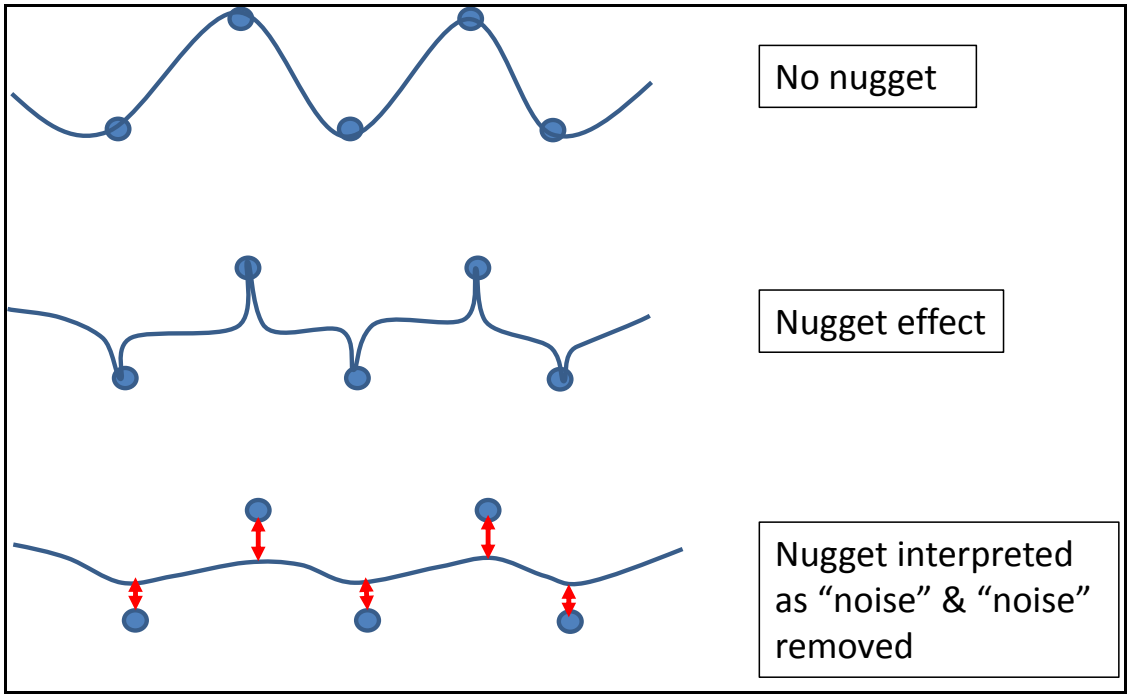

Figure 4.2 The nugget: when it is used to indicate random error in the data (Adapted from Dubrule, 2014).

4.3.3 Types of Variogram Models and their Applications

Appropriate variogram models are chosen on the basis of the experimental variogram and as explained previously, are used for quantifying the spatial variability of rock properties and other variables. The types of variogram models frequently used in geostatistics are Spherical, Exponential, and Gaussian (Figure 4.3; some other types are Linear, Power or Cubic Models).
The Spherical variogram represents the highest mathematical stability because it is basically a function which is linear at the origin. For this reason, it is the most widely used variogram model (Leonardo Santana, Pers. Comm.).

The Exponential model behaves exponentially at the origin while the Gaussian model is parabolic close to the origin; both do not reach the sill (in theory they reach the sill at infinity). When these models reach their "effective range", they do so asymptotically reaching approximately 90-95% of the value of the sill defined by the user in the model (Leonardo Santana, Pers. Comm.). If you

have a variable which exhibits a high degree of variation within the range, the exponential variogram is most suited to fitting the experimental variogram. The exponential and the spherical models produce very similar results with the exponential model yielding slightly more variable distributions.

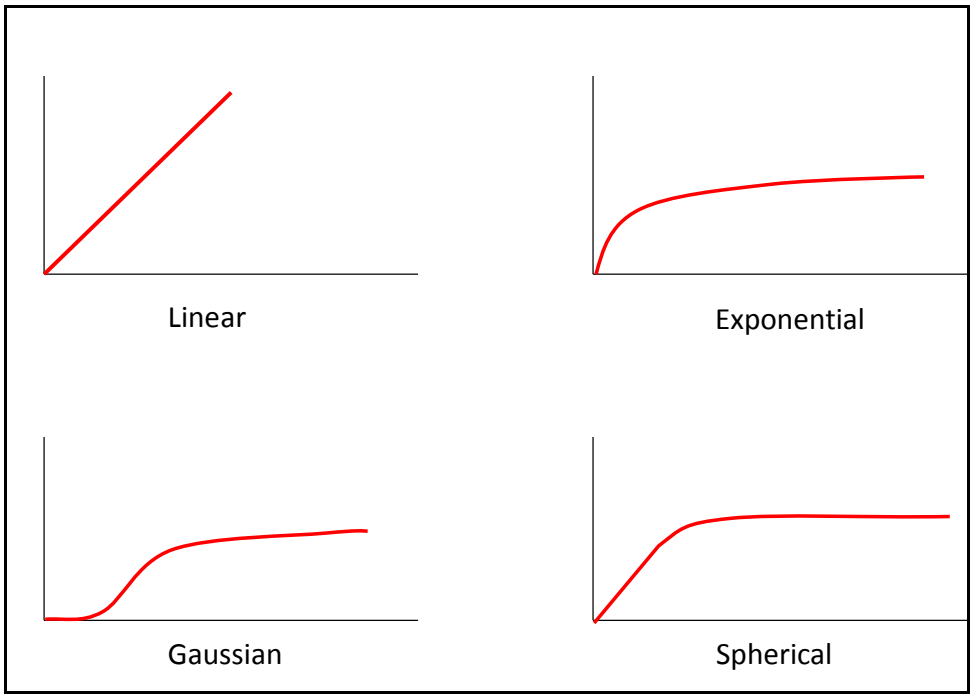

Figure 4.3 Main types of theoretical or mathematical variograms.

The Gaussian model displays the highest smoothness. It causes interpolation to be smoothed, sometimes resulting in unrealistic results. If the variability of the data is quite "gentle" (horizons or surfaces are good examples because high variations over short distances are not usual, unless the surface is highly faulted), the use of a Gaussian model is most appropriate. (If the software that you are using has the option to choose a Cubic model, it may be better to use instead of the Gaussian. Both shapes are similar, but the Gaussian model is much smoother at the origin than the Cubic model; Leonardo Santana, Pers. Comm.). When the variable contains very rapid changes at small distances, a Gaussian model is not recommended and one should use a model that has a steeper behaviour close to the origin e.g., the Exponential model.

The decision regarding the choice of variogram model is an individual one; however the choice should best reproduce the geological model that the

practitioner has in mind while also reflecting the variability revealed by the data. The choice cannot be made without discerning the purpose of the model, whether it is for mapping or simulation coupled with the type of property that is being modelled. There is also an element of “trial and error” in choosing the best model and it would definitely be helpful to check which model performs better or which one reduces the estimation error. It is here that time can be spent tuning the variogram and histogram parameters in order to reduce the Kriging estimation error. This tuning can range from choosing Exponential instead of Spherical models, a de-clustered histogram rather than raw histogram, a map correlation coefficient rather than constant correlation coefficient, nested structures rather than a single structure or anisotropy rather than isotropy. Ideally, one should integrate and calibrate data from different sources using several algorithms as tests and the one which performs best should be retained (Oliver Torres, Pers. Comm.). One way to test and compare different approaches is by using a blind test. This involves removing one of the wells in the data set one-by-one and testing the different parameters in order to establish which parameter produces a result which is generally closest to the well data at all the well locations.

There are many ideas expounded by experts and experience plays a great role in the choices a user will make, but it must be borne in mind to always try and keep the model as simple as possible.

4.3.4 Conditional Simulation

As discussed earlier, Kriging is an interpolation technique which is designed to minimise error in interpolation and as a result tends toward the mean value far away from measured data points. Therefore, Kriging on its own generally will not produce the correct heterogeneity implied by the variogram. In addition, Kriging uses a single variogram and is hence, in a way, deterministic. Kriging though, is an intermediate step towards Conditional Simulation. Conditional Simulation algorithms are able to quantify heterogeneity and are capable of producing multiple realisations using the same variogram. This means that the

mean of all the realisations will be equivalent to the kriged scenario. While Kriging would most often underestimate the variability of a mapped parameter relative to reality, Conditional Simulation will try and mimic the natural variability of the parameter. Even though this will not be the truth, the result will be more realistic than that generated by Kriging. The behaviour of the variogram in these methods brings about another important difference; with Kriging, the results away from data points become smoother as the variogram displays more randomness (shorter range). While with Conditional Simulation, more randomness in the variogram produces results which are also more random.

There are a number of Conditional Simulation algorithms. The most commonly used one is Sequential Gaussian Simulation (SGS). It is a conditional type of simulation, meaning it forces the simulation to match the well data. Sequential Gaussian Simulation works using an iterative process of sampling and populating of grid positions one point at a time. A random point in the grid is chosen and a kriged value and standard deviation for the location is calculated. This allows for a Gaussian histogram or Probability Density Function (PDF) to be generated, from which a random value is taken and assigned to the location. When estimating the value at the next random location, all values simulated so far are included in the simulation until all locations have been populated. This loop can be done an *nth* number of times, each time producing a different realisation using a single variogram and maintaining the same distribution in the Probability Density Function and therefore preserving the mean.

Simulations generate realistic and plausible, equiprobable realisations and are the best way to understand and quantify heterogeneities in a reservoir.

5 MODELLING WORKFLOW

The 3D model is constructed in a multi-stage process involving structural modelling (building the framework of the model), stratigraphic modelling (by means of horizons), zones and layers, 3D grid construction, facies modelling, petrophysical modelling and volumetric analysis (Figure 5.1).

In order to confirm the structural and stratigraphic modelling processes, a thorough well-section correlation must be completed and tied to the reference seismic surfaces that were interpreted. Boundaries are defined to confine the model and a suitable grid cell size is chosen. This decision to choose a certain grid cell size culminates from accounting for the various scales of each data set and ultimately should be an average grid cell size (Caers, 2005). The chosen grid cell dimension is termed the model resolution (Caers, 2005). An example of very high resolution data is core or log data. These data from existing boreholes within the model are rescaled or upscaled by applying an averaging algorithm to the grid cells intersected along the length of the boreholes. The well data together with any seismic trend parameters (optional if available), are used to calculate the property volumes in the inter-well grid cells (Zakrevsky, 2011). The lithological property, facies, is calculated first, followed by the continuous properties of porosity, permeability and water saturation. These then form the basis upon which hydrocarbon reserve assessments are done. It is important to note that the validity of the 3D geo-cellular model is based on a robust geological conceptual model where sound geological ideas and processes guide the fundamentals of the model building procedure. The 3D grid also has its own reference system, the ijk system, which is different from the XYZ coordinate system. It references each cell to each other rather than a geographic location. This designation and differentiation is important as geological phenomena, like faults, can be made to coincide with 3D cell boundaries. Also adjacent cells in ijk space may be laterally separated in XYZ space if a fault between them exhibits appreciable dip.

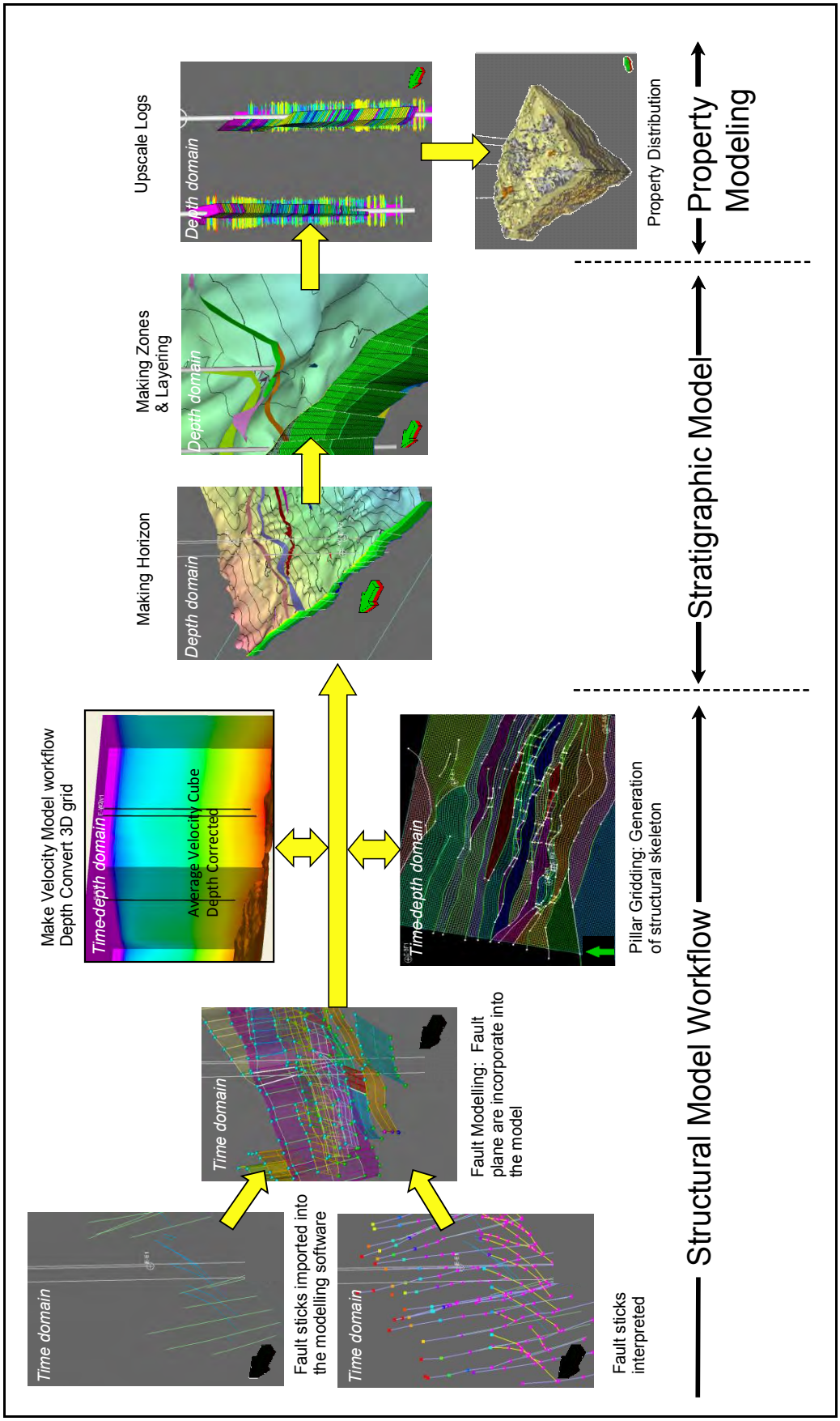

Figure 5.1 A simplified 3D geo-cellular model workflow.

The model exists in the depth domain and therefore all input into the model, specifically fault and tops interpretation must be depth converted using a suitable velocity model. The depth conversion process can be implemented before or after the creation of the fault model. In this particular study, the faults were converted to depth before input into the model. This was done in order to prevent additional editing once the faults were completely modelled.

5.1 Velocity Model

The starting point for most static modelling studies is an interpreted seismic dataset consisting of both surfaces and faults and this interpretation is usually done in the time domain (Dubule, 1998). A velocity model is needed in order to convert any interpretation done in time to depth while ensuring the best fit between the geological markers that were obtained from logs and the seismic interpretation.

Since the fault and surface interpretation provided by the geophysicist comes directly from the seismic it is in time and therefore must be depth converted. A step preceding the building of the velocity model involves the tying of the wells to seismic. The checkshot-calibrated sonic and density logs of the 9 wells used were convolved with an extracted wavelet from seismic in a window of interest to build a synthetic seismogram. Overall, the synthetics showed a good correlation with the seismic at the well location. The velocity logs generated in the above-mentioned step was used as an input into the 3D velocity model.

The 3D velocity model is based on the same fundamentals as conventional 2D methodologies but this alternative solution seeks to take advantage of working in a 3D environment. Figure 5.2 illustrates the workflow used in order to facilitate the depth-conversion process. This process was adapted from a workflow suggested by Mr. Jorge Adrian (Pers. Comm.) and is described below:

Data: All wells used in this process, except E-S7, have checkshot data. The sonic and density logs were conditioned, to remove spikes,

prior to the well-seismic tie. The interpreted surfaces were also used as input into the process as a lateral constraint.

Building a 3D Time Grid: A 3D framework was then created using the interpreted surfaces. The vertical resolution of the grid is a function of the velocity's vertical variability and should be similar to the resolution of the seismic data.

Quality Control and Velocity Adjustments: Since interval velocities naturally display gradational variability, it is quick and easy to apply quality controls. Outlier samples can be identified in the time vs velocity cross-plot and also visualised in 3D.

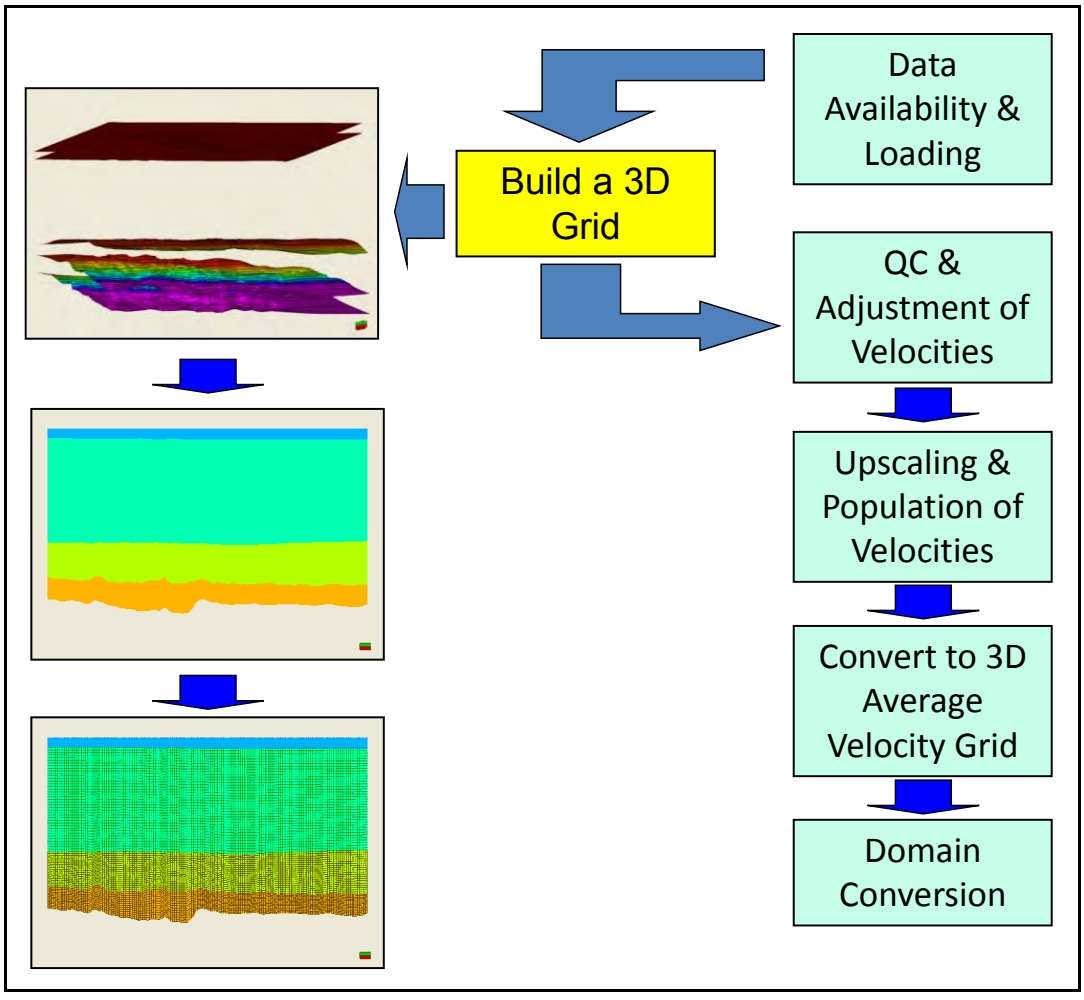

Figure 5.2 A simplified depth conversion workflow.

Upscaling and Population of Velocities: Once the data was upscaled, it was subjected to a series of Data Analysis/quality control processes involving analysis of velocity distribution, spatial trends and spatial variability (using a variogram). All settings applied to the model are zone specific. The interval velocity was then populated using Convergent Interpolation, which is a deterministic gridding method, thus producing a single estimated result rather than multiple realisations.

Calculating 3D average velocities: The interval velocity grid was converted to average velocity using the average velocity equation:

$$\mathrm{Vavg} = \frac{\Sigma\ \mathrm{ti\ Vi}}{\Sigma\ \mathrm{ti}} \quad \ldots\ldots\ldots\ldots\ldots\ldots\ldots\ldots\ldots\ldots\ldots\ldots \ (1)$$

Where:

Vavg = average velocity

ti = interval time

Vi = interval velocity

The interval velocity (Vi) was generated based on checkshot data from wells (Figure 5.3). The interval time (ti) was calculated by creating a cell height property in the model. This property, as the name suggests, measures the height of each cell. This property was then multiplied by the interval velocity and summed vertically. Thereafter Σ Viti (as a property in the model) was divided by the total time Σti to calculate the average velocity (Figure 5.4). This average velocity forms the velocity model with which the depth conversion is run.

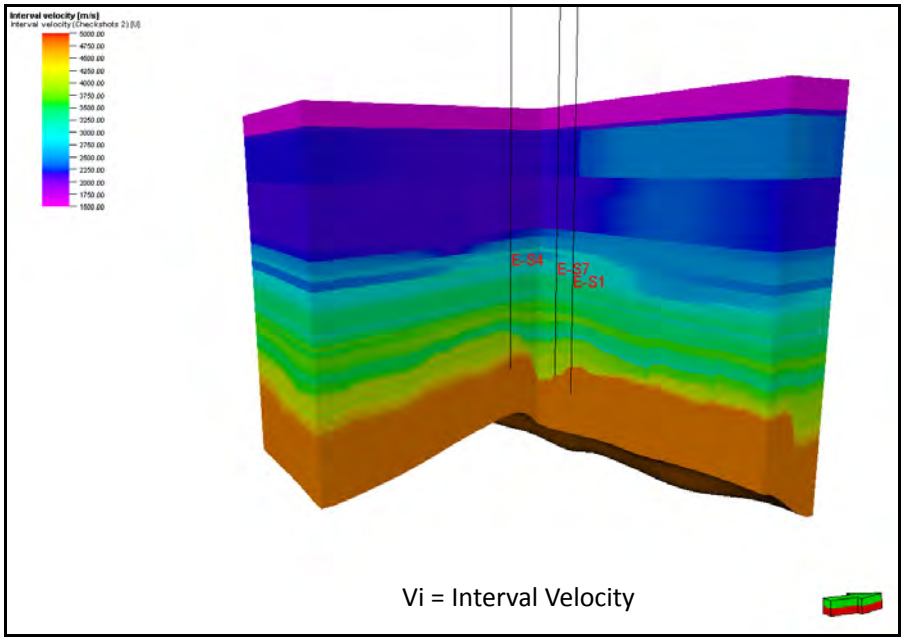

Figure 5.3 Well Interval velocities populated in the 3D grid.

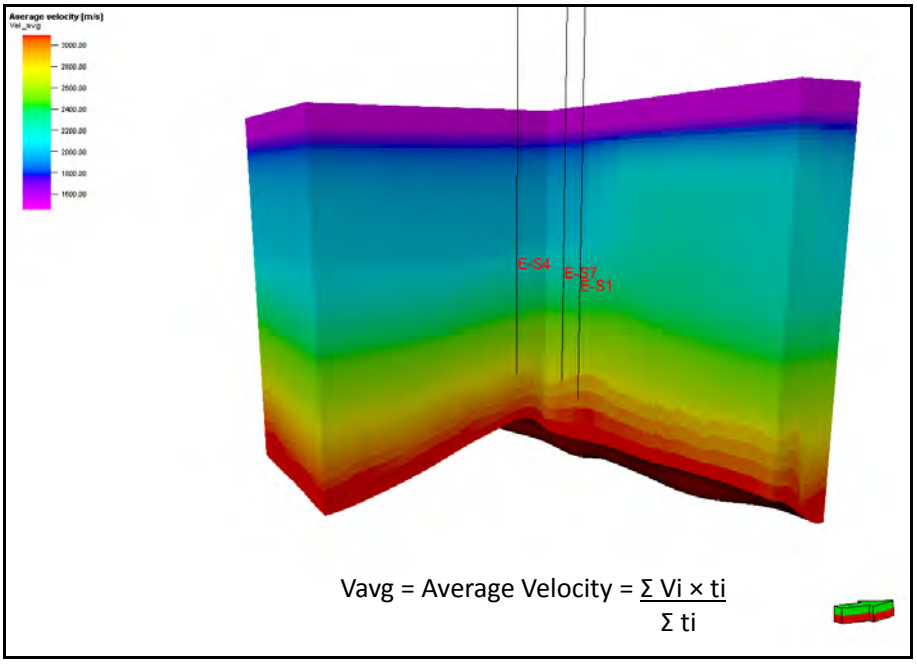

Figure 5.4 An average velocity cube calculated via an interval velocity cube operation.

Domain Conversion: The depth conversion process converts the grid on a node-by-node basis. The velocity model was calibrated by using the well tops (Figure 5.5). This forces the velocity layers, and therefore the interpreted surfaces in depth to intersect the wells at the interpreted well markers.

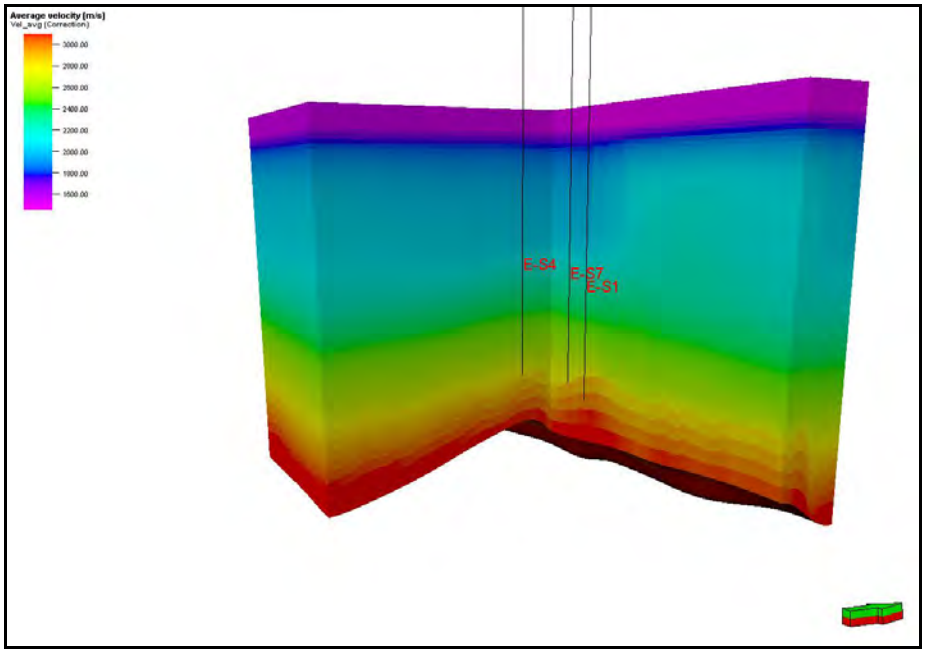

Figure 5.5 The average velocity cube adjusted by the well markers, i.e. depth corrected.

5.2 Structural/Fault Modelling

The structural model is an integral part of the geo-cellular model as it forms the framework of the model and thus controls the geometric integrity of the cells, which are the building blocks of the model itself. It may not be necessary to include all interpreted faults into the model, as the number of faults controls the complexity and thus the computing time associated with the 3D grid. In an area where the number of interpreted faults is excessive, Zakrevsky (2011) recommends following a hierarchy of importance when choosing the faults to model. He places emphasis on incorporating faults which separate blocks with different hydrocarbon-water contacts, faults with the largest length and throw, faults with throws of more than half a layers thickness and faults whose presence is confirmed with other data (e.g. production test analyses or well interference testing).

Building the structural model is based on the positioning of the fault “pillars”. The geophysicist provided the interpretation of the faults as fault sticks (fault points, surfaces or polygons can also be used) which were loaded into the modelling software. All the faults, as fault sticks, were then converted to

depth (using the velocity model described in the previous section) before any fault modelling was done, so as to prevent any fault movement after the editing phase.

Once in depth, the fault sticks were converted to modelled faults. This process uses the fault interpretation to provide a set of “pillars” (the number and spacing between pillars is user-defined) for each fault which the user can manipulate in order to model/edit the faults (Figure 5.6).

Defined depths for the fault planes were set using 1At1 and Horizon V as controls for the top and base respectively. Another control on the modelled fault planes is the local adjustment of the top and base reservoir surfaces. Both the top and base reservoir surfaces* were adjusted (it is better to make a copy of the surfaces before doing this) a certain distance away from each other so as to provide upper and lower limits for fault propagation. The faults were truncated using a set surface limits process (Figure 5.7). Smoothing of the surfaces before the truncation helps to produce a better result. Minor adjustments to the fault pillars may be needed after the truncation process is complete.

Cross-cutting faults are usually avoided in the modelling process in order to simplify the model due to algorithm and computing limitations in the fault modelling process.

*Note on semantics: Stratigraphic/seismic surfaces are brought into the modelling software as interpretation. The interpretation is then gridded and thereafter referred to as “surfaces”. These surfaces are used as input into the model resulting in modelled surfaces, referred to as “horizons”. Surfaces and horizons used in this context are seismic and modelling terms respectively and should not be confused.

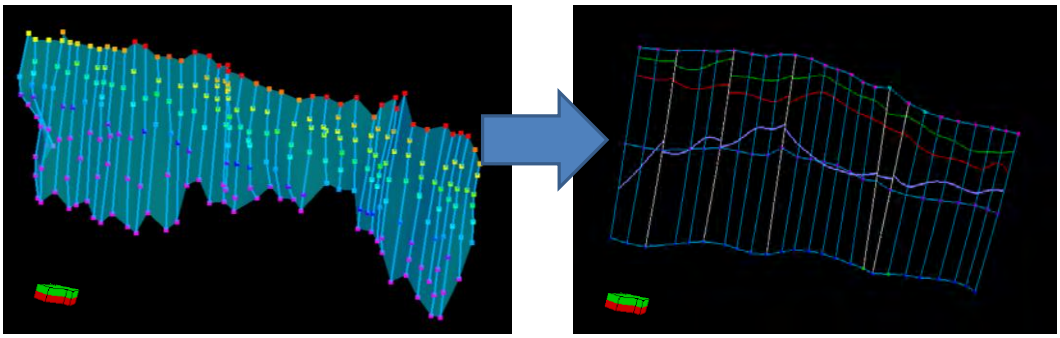

Figure 5.6 An example of converting fault sticks to a modelled fault.

5.2.1 Pillar Gridding: Generation of the Structural Skeleton

The final step in the structural modelling phase was to carry out the gridding process in the fault model, known as pillar gridding. The areal extent of the model or model boundary is defined in this space together with the model increment (resolution) or average cell size, which in this model was set as 40x40m. The process produces a skeleton grid with 3 surfaces which serves as a guide/framework for the distribution of the rest of the cells in the model (Figure 5.8). The grid is usually aligned parallel to the main fault trend to induce structural grid trends parallel (I-direction) and perpendicular (J-direction) to the main trend in order to maintain, as far as possible, cells which remain orthogonal with respect to the faults. This is the ideal situation and never really materialises fully due to geometrical limitations. Certain fault elements in the grid must be set without a trend in order to produce a workable result. In this model only an I-direction trend was used due to a lack of faults present in the J-direction (Figure 5.9). Having orthogonal cells eases the simulation process during dynamic modelling while triangular cells adjacent to faults pose calculation complexities. Fault segments are also defined by the fault connectivity in the grid and fault trends can be extended to the model boundary for segment delineation (Figure 5.10).

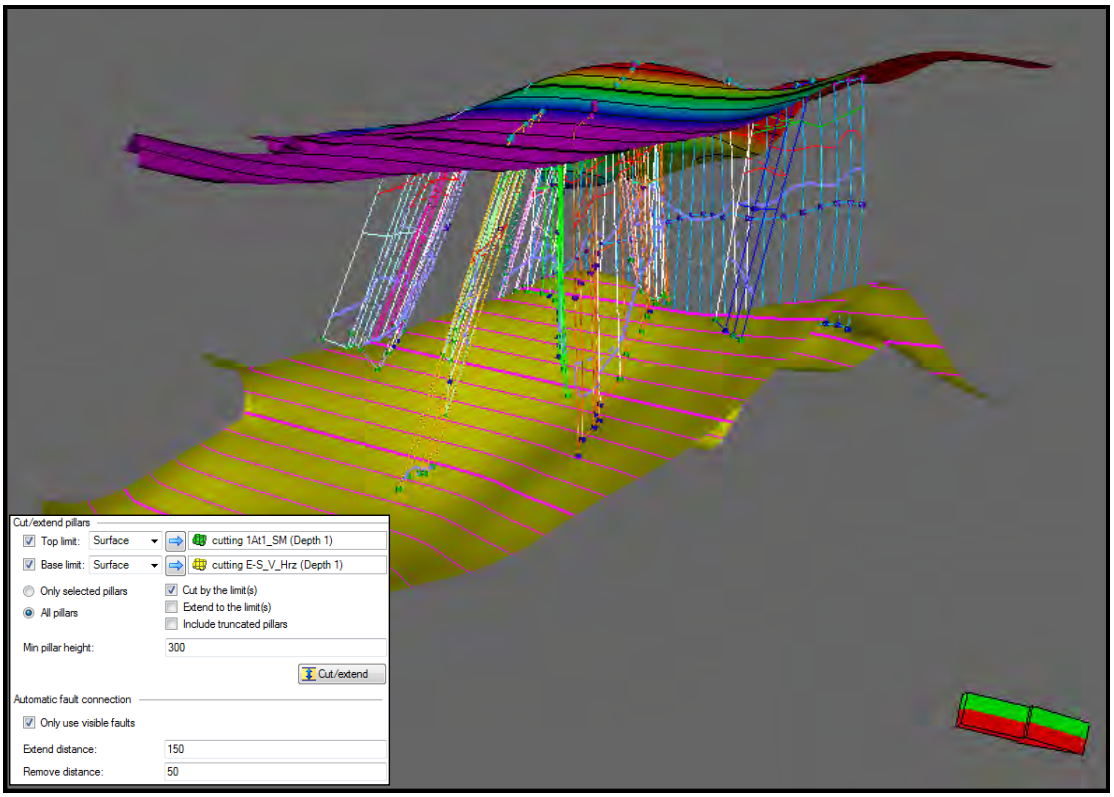

Figure 5.7 An illustration showing the fault truncation process.

5.3 Stratigraphic Modelling

Seismic surfaces interpreted by the geophysicists are usually fewer in number than the actual geological zones present in the geologists model (Zakrevsky, 2011). This can be attributed to the differences in scale dealt with by these disciplines. This therefore informs the sequence of stratigraphic modelling i.e. begin with the modelling of the seismic surfaces and then further refine the stratigraphic model by defining the geological zones which are beyond the resolution of the seismic. These zones can be based on constant thickness between two surfaces or isochore calculations (in the form of maps) derived from well to well cross-sections in the software package or manually using thickness proportion maps (Zakrevsky, 2011). The modelling of the zones together with the layering that follows it, is often based on the conceptual sedimentary model taking into account the source of sediment, sediment transport direction and mode of sediment transport all within the interpreted sedimentary environment.

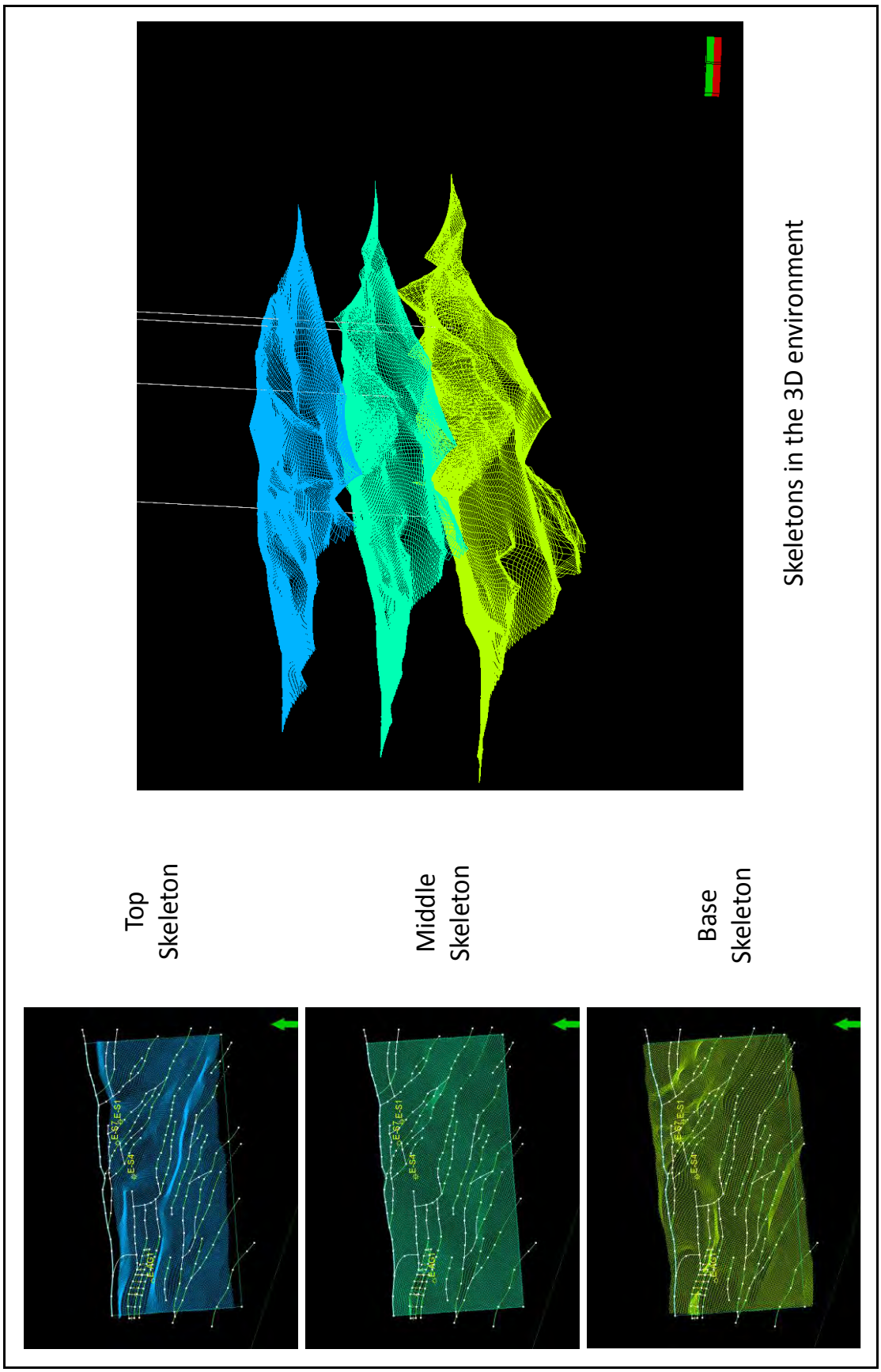

Figure 5.8 The 3 surface skeleton grid – Result from pillar gridding process.

Dubrule (1998; p10) appropriately describes the layering as being able to "reflect the distribution pattern of geological heterogeneities in space", while honouring the stochastic and statistical principles meted out by the model.

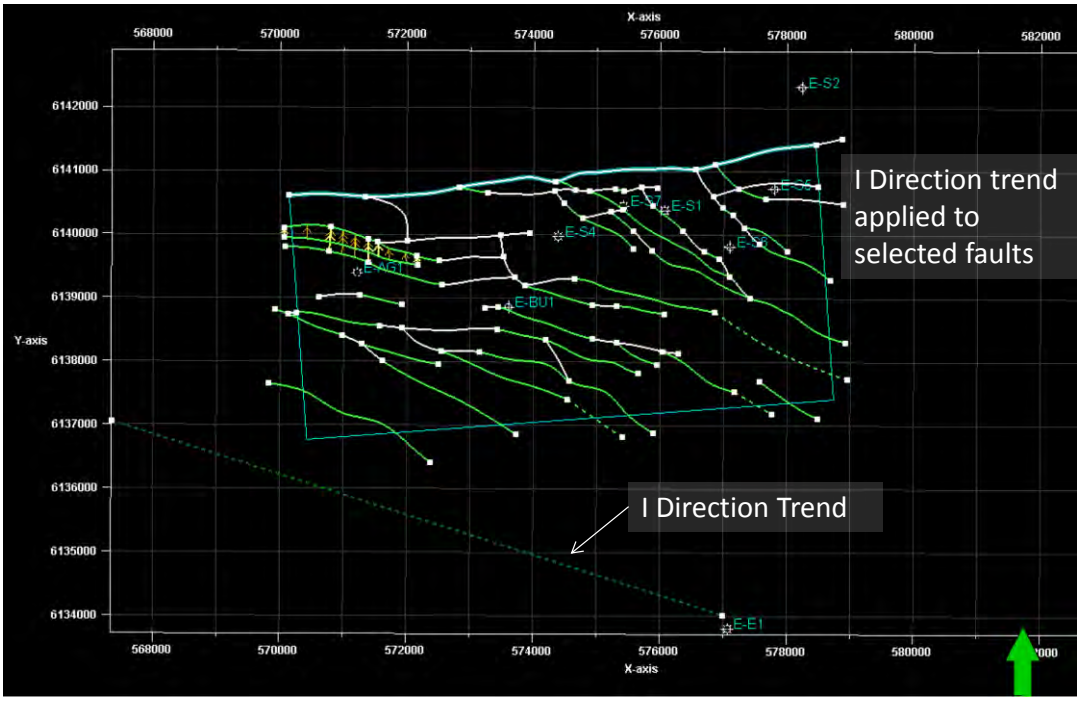

Figure 5.9 2D pillar gridding process. Faults coloured green indicate an applied trend. Cells will remain orthogonal to these faults.

5.3.1 Horizon Modelling

The seismic surfaces were gridded and used as input for stratigraphic modelling from which modelled horizons were created (Figure 5.11). The horizons were tied to the well markers in order to honour the well data. The horizons were then individually adjusted using fault-horizon intersection lines according to the fault displacement and structural pattern. This involved the adjustment of each individual fault and every horizon level through a time consuming iterative process (Figure 5.12).

5.3.2 Zones and Layering

After the modelling of the horizons, zones were defined between the horizons (1At1, BUSM and V). These zones were further subdivided into subzones in

order to better represent the stratigraphy where the markers are below seismic resolution or the layers are laterally discontinuous. Four subzones were created between the 1At1 and Bottom Upper Shallow Marine horizons and were based on sedimentological zones interpreted in the E-M field according to the stratigraphy (discussed in detail under the section on sedimentology).

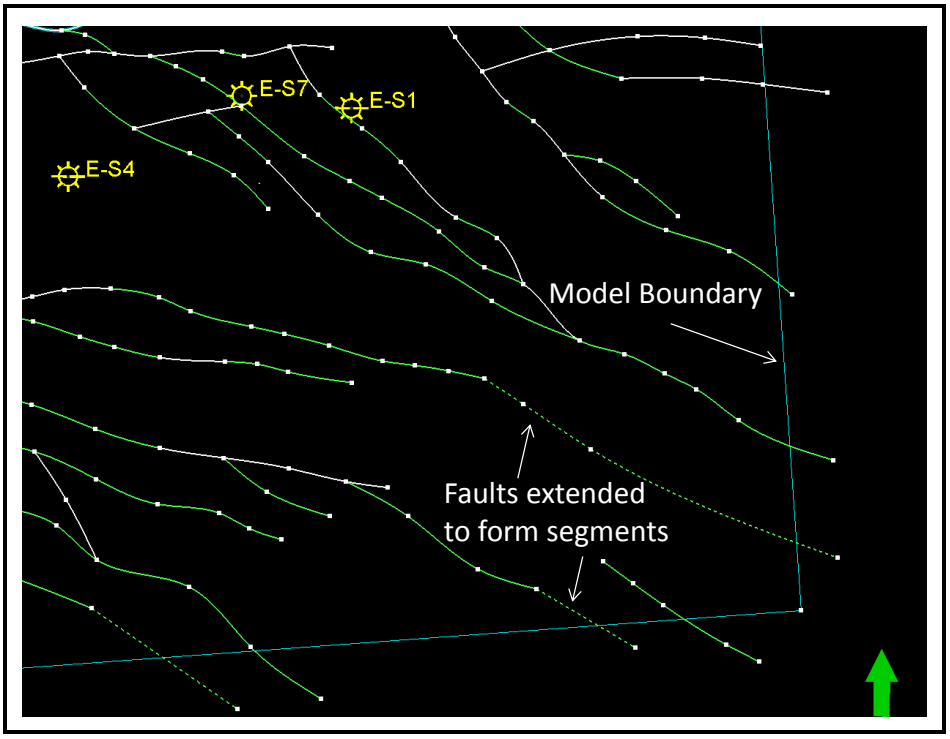

Figure 5.10 Fault segments extended to the model boundary for segment delineation.

The Top of the Upper Shallow Marine (TUSM) is difficult to resolve in the seismic data over the E-S area and therefore marker data from logs was used to control this top. The 1At1 to Top Upper Shallow Marine isopach was modelled as a zone using the "rest" thickness input method. The "rest" method calculates the residual thickness without any specified thickness. The modelling software builds all other zones in the model towards this zone and whatever part of the model is left will form part of the "rest" zone. The 1At1 to Top Upper Shallow Marine zone or Pre-1At1 Estuary Unit (El Saadi Zone 1) is suited to this type of input method as it lies directly beneath the 1At1

erosional unconformity and by its nature is a layer with inconsistent thickness.

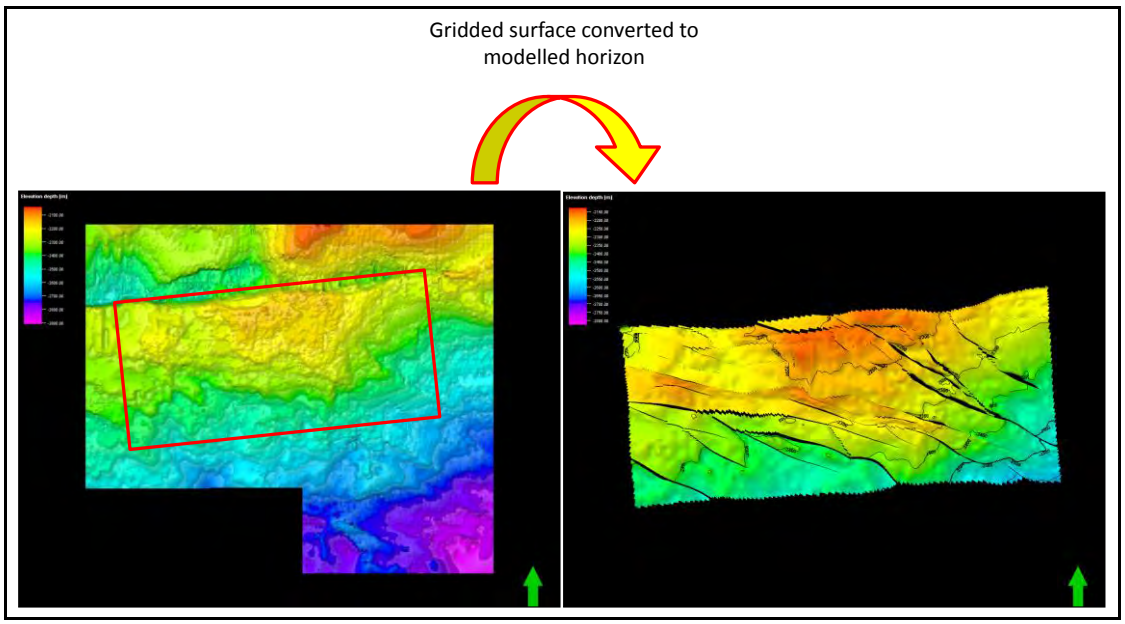

Figure 5.11 Process converting gridded surfaces to modelled horizons.

Similarly, a lower sand package (USM-Lower / El Saadi Zone 4), a middle fluvio-deltaic (Fluvio Deltaic / El Saadi Zone 3) interval and an upper sand separated into two units (USM-2A and USM-2B / El Saadi Zone 2A and 2B) were modelled as separate zones (Figure 5.13a). An “isochore” thickness input method was used for all these zones. The “isochore” input type uses isochores as an input to guide the modelling of the zones. This division separates zones of common heterogeneity. This is important for the statistical interrogation applied to the data because a variogram can only be meaningfully interpreted if it is applied to a region/zone with similar geological patterns (Caers, 2005).

Thereafter the model was divided into layers with each zone having its own layering parameters (Figure 5.13b). The Pre-1At1 Estuary Unit zone was modelled with a 2m cell thickness using a “follow the base” zone division. The USM-2B, USM-2A and the Fluvio-Deltaic zones were layered using a 1m cell thickness and like the Pre-1At1 Estuary Unit, a “follow the base” zone division was applied. The USM-Lower and Fluvial (Wickens Zone IV) zones were “proportionally” layered having 59 and 200 layers respectively. The “follow

the base “method builds the layers from the horizon at the bottom of zone, remaining conformable to the base till the zone’s top bounding horizon (Figure 5.14). In the “proportional” method, layering is kept at proportional thicknesses throughout the zone, adjusting as the thickness of the entire zone changes.

During the modelling phase of the study, the aforementioned zone designations were divided into two modelling zones due to the specific and mutually exclusive modelling methods and parameters used for these two modelling zones. Modelling Zone 1 consists of the Pre-1At1 Estuary Unit, USM-2A, USM-2B, Fluvio-deltaic and USM-Lower zones while Modelling Zone 2 consists of the Fluvial zone.

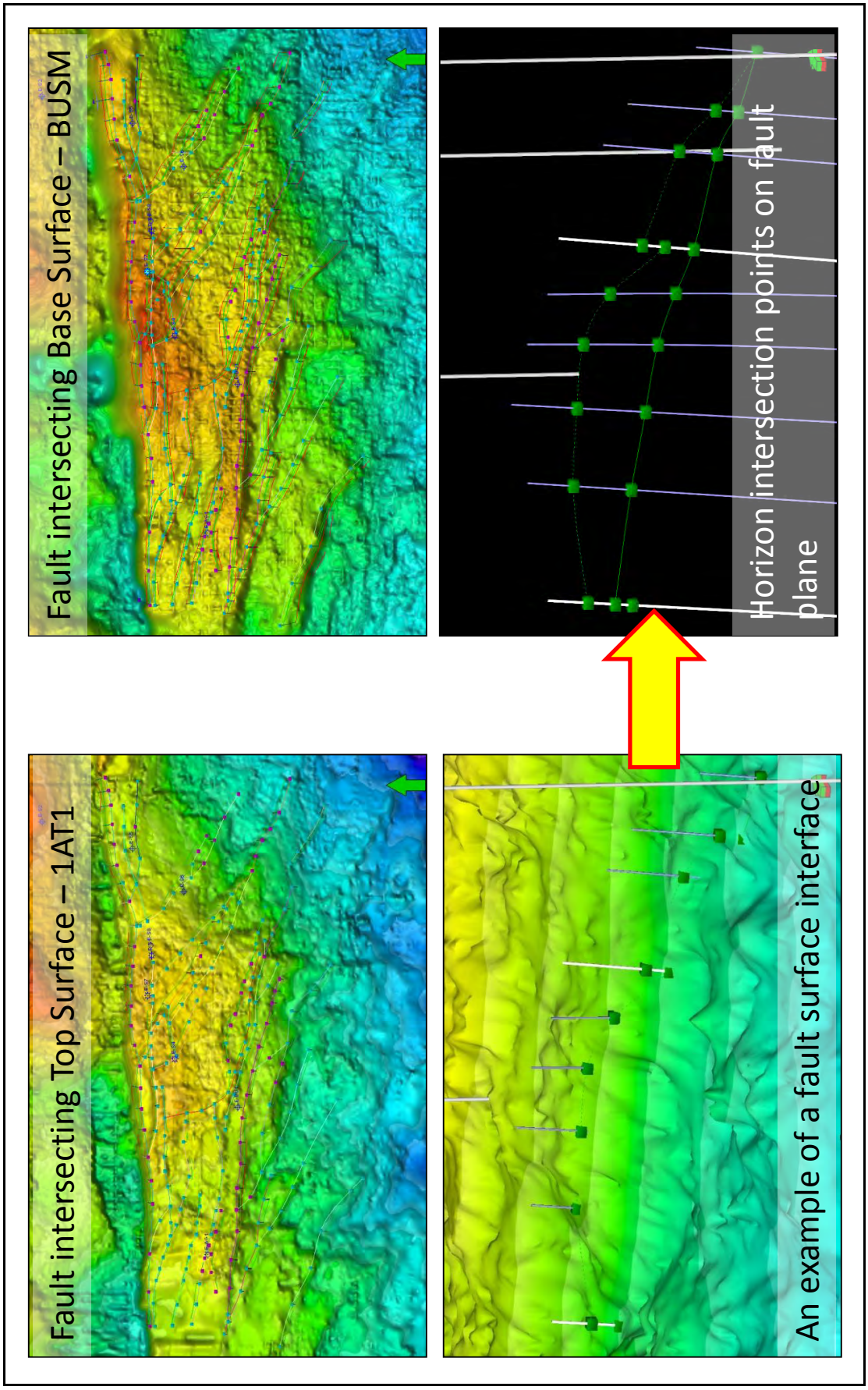

Figure 5.12 Horizon-Fault editing process.

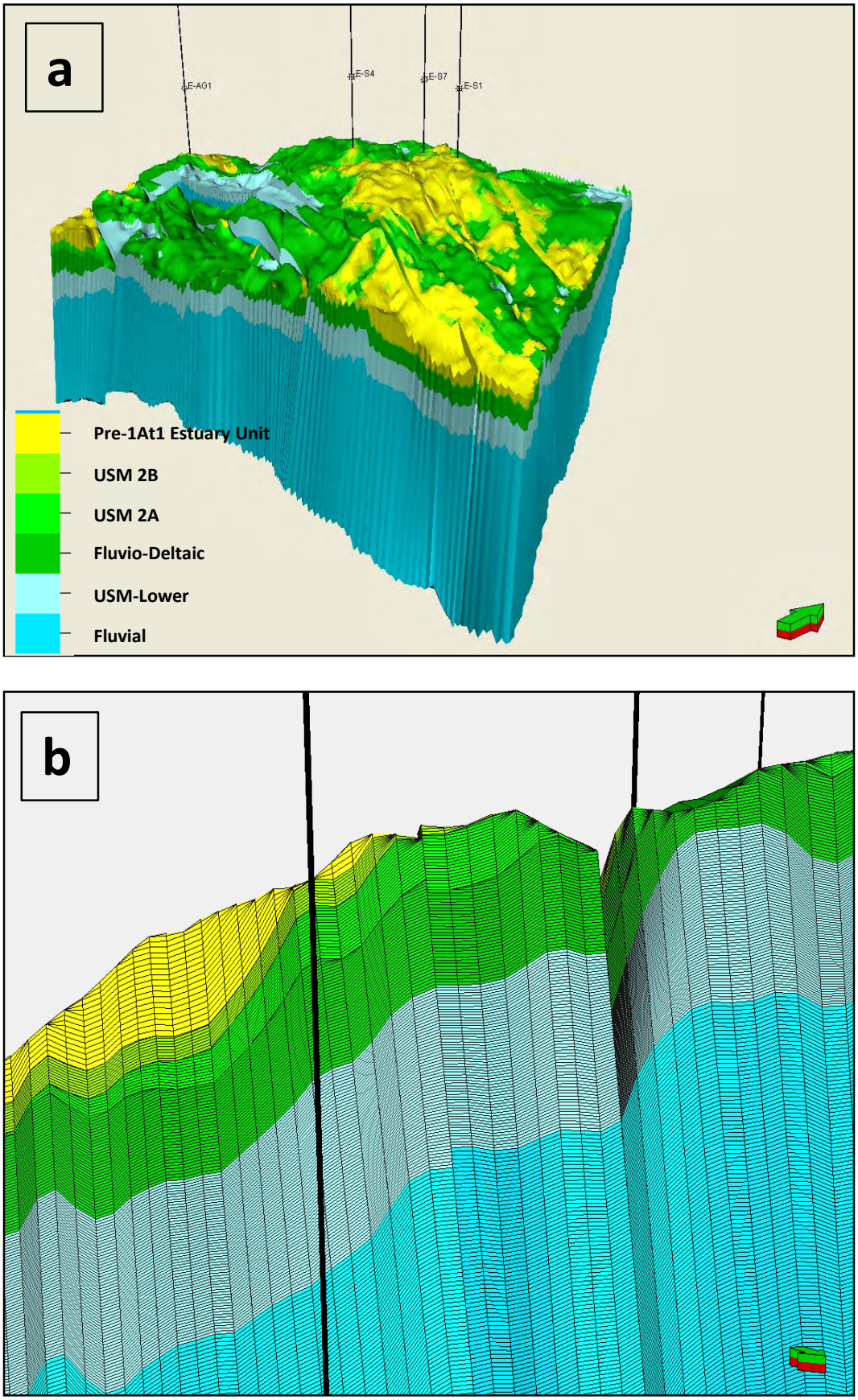

Figure 5.13 (a) The 3D model subdivided into zones. (b) Layering in the model.

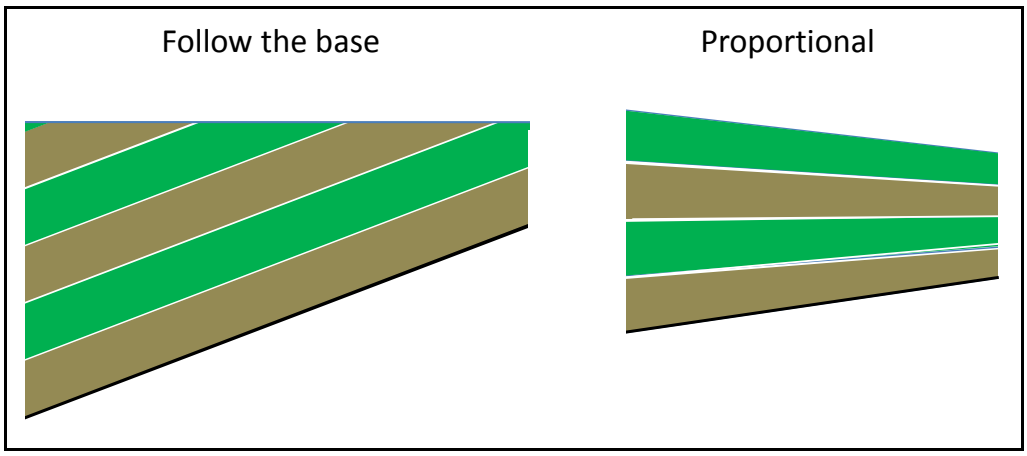

Figure 5.14 Layering types.

5.4 3D Parameter and Property Modelling

The Segment Property

This property was referred to in the section on pillar gridding. Preparation was made by extending the faults to the model boundary in order to separate the model into various segments. Each segment is given a name which is the segment property value. This property is created through a geometrical modelling process and assists in situations where information is needed or needs to be calculated in specific blocks. It also serves as an effective filtering application. Figure 5.15 shows the Segment property in 3D and 2D.

The result of the previous steps (structural model and stratigraphic model) is a multi-zone 3D model as seen in Figure 5.13a and b. Logs were first created for each property using petrophysical equations, and where core data was available it was used as input and as a QC.

Upscaling

The processed logs are inherently fine scaled and before they were introduced into the model for population, the logs were upscaled. The upscaling process decreases the resolution of the logs by averaging out samples over specific distance increments. In other words, it is used to populate the raw data into the present model, averaging the log values in

each cell. The distribution law or averaging method for parameters is specific for different properties. Porosity and water saturation should be averaged arithmetically and permeability should be harmonically or geometrically averaged (Zakrevsky, 2011). The result is a “coarser” log which enables quicker computing time in the preparation of the model. It is important to note that even though the logs are upscaled, they must still be representative of the original fine scale data in order to produce an acceptable and usable result. During the subsequent steps a set of discrete (facies/Flow Zone Indicator) and continuous properties (porosity, water saturation, permeability) are modelled using the processed, upscaled logs.

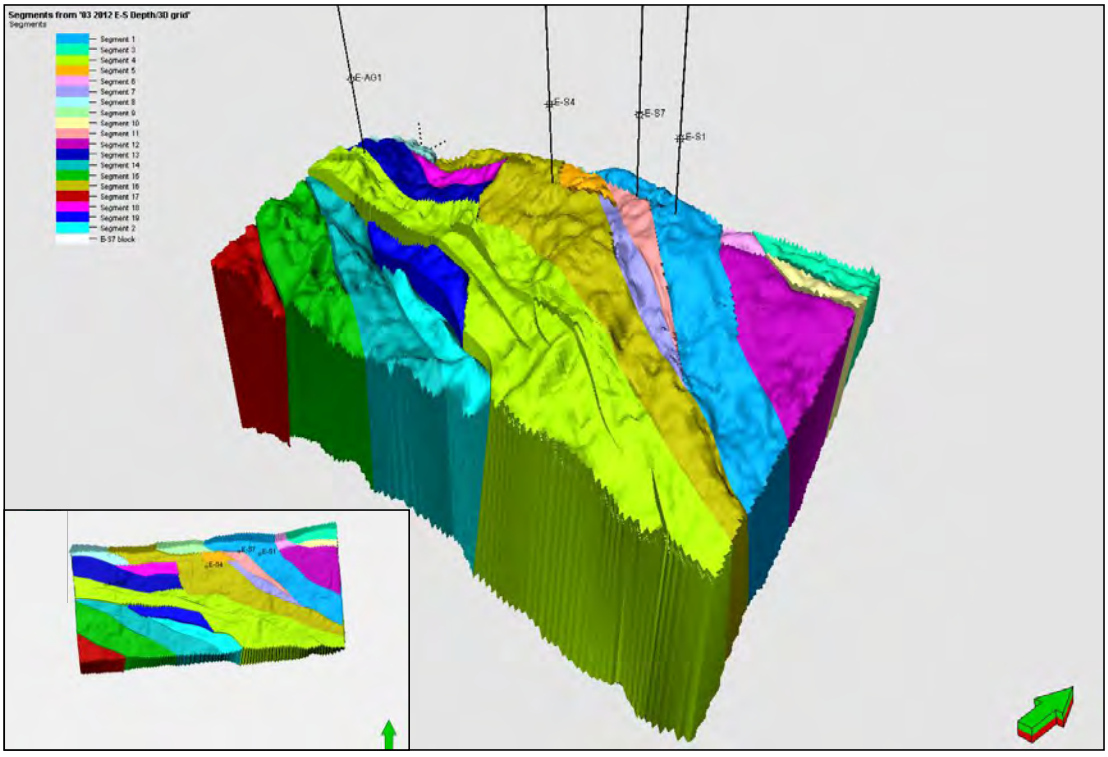

Figure 5.15 3D model showing the Segments property.

Data Analysis

The data analysis process is used to prepare the upscaled data (e.g. truncate outlier data) of each property based on the log data before statistically distributing the property throughout the model volume. The data analysis focuses on applying a statistical distribution to the properties, which is normal or lognormal. After analysing the data distribution using a series of

transforms, representative variograms are constructed for the vertical and horizontal directions. These variograms may or may not be edited based on the discretion of the interpreter. Vertical variograms are used with a higher degree of confidence because they are obtained directly from the wells and are thus generated based on a fine sampling rate. Horizontal variograms have a stronger statistical component and other trends must be applied based on knowledge of the sedimentary environment and lithology and other reservoir parameters.

Figure 5.16 broadly illustrates the upscaling and data analysis process and results.

Variogram Choice

In this study, the exponential variogram model was used for all property modelling. As mentioned earlier, the exponential and spherical models produce very similar results but this model was chosen over the spherical model in order to introduce a little more variability in the outcome due to the small data set available. The variogram azimuth and ranges in the major and minor directions are based on the understanding of the sedimentology and depositional environment. The vertical ranges were set small enough to be able to capture the vertical heterogeneity while maintaining a range commensurate with the cell thickness. The vertical range for Modelling Zone 2 was smaller than that of Modelling Zone 1 in order to better represent the highly heterogeneous fluvial succession. In general, a small nugget value was chosen to incorporate a degree of variance in the modelling but was adjusted when needed.

Figure 9

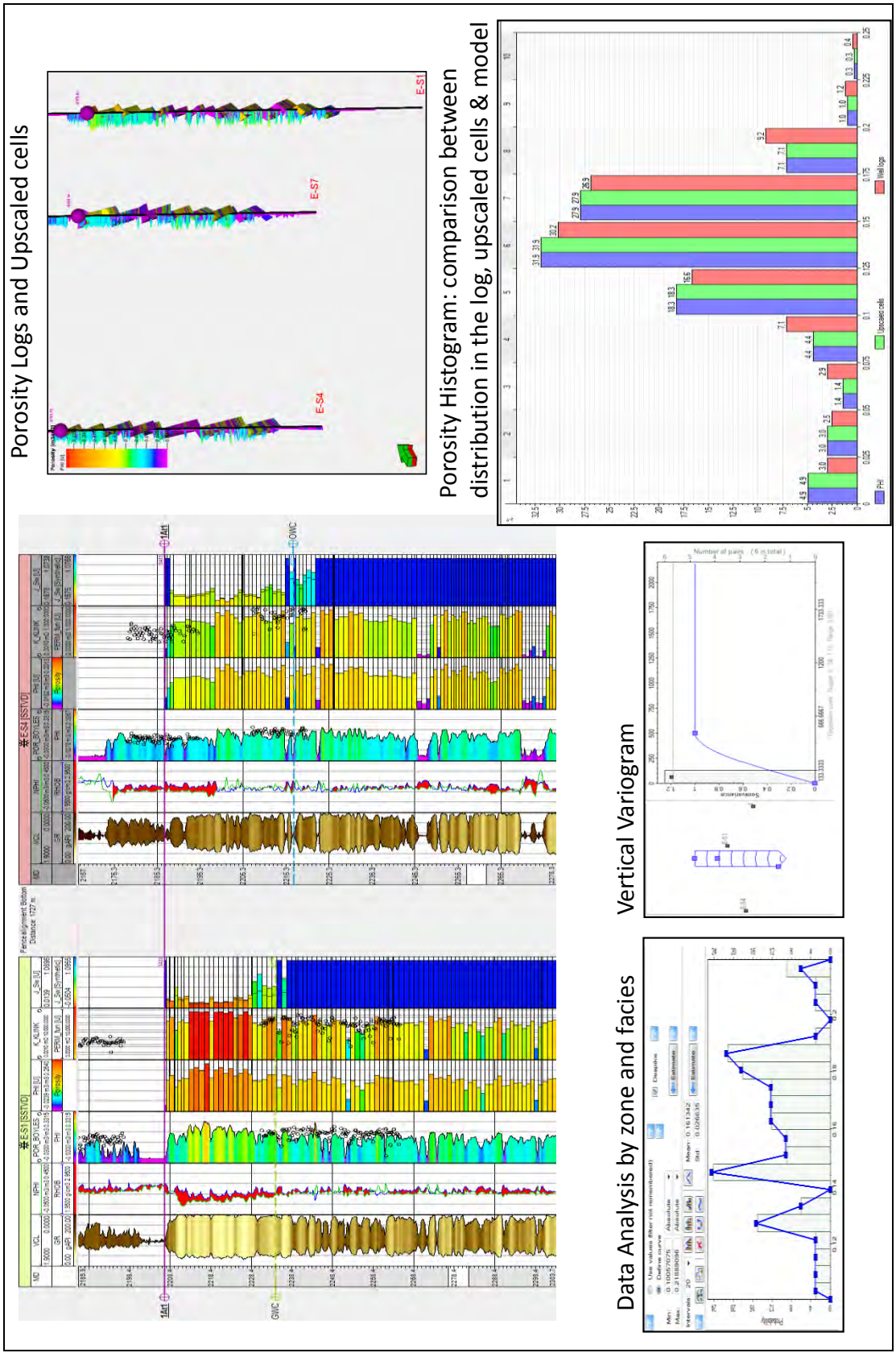

Figure 5.16 A broad overview of the Upscaling and Data Analysis processes.

5.4.1 Facies Modelling

Dubrule (1998) highlights the value of identifying and using genetic facies associations and relationships within each geological interval from the well data and then correlating these units between wells resulting in a significant reduction of uncertainty in areas away from existing wells. On the other hand, Zakrevsky (2011) discusses a modelling workflow which excludes the building of a facies volume. He explains that by interpolating the porosity property using Kriging over the entire area (porosity data must be dense and across all intervals in the model) and then calculating and building the permeability volume through the use of a poro-perm relationship, the reservoir engineer or dynamic modelling specialist can use a specified cut-off value which will disable some cells before running the flow simulation. He thereafter goes on to cite two disadvantages of such an approach, the first of which is that this method only works in an extensively drilled reservoir having very simple geology with fairly homogeneous properties. The second disadvantage is that rock property distribution is not representative without the use of a facies volume to guide it. The facies model is responsible for preserving the geological sense of the conceptual model built by the geologist and maintains consistent distributions (both statistically and geologically) even in cases where properties are highly variable.

Facies can be modelled either deterministically or stochastically via numerous methods (Zakrevsky, 2011). Seismic geobody extraction can be used as an input for a deterministic type of facies distribution while an object (object based) or Sequential Gaussian/Indicator simulation (pixel or cell based) is a stochastic type. The Multi-point statistic method, using a training image to populate facies, or Truncated Gaussian simulation are other types of pixel based stochastic modelling methods but these will not be discussed further in this dissertation. The transition from pixel-based modelling (sometimes referred to as two-point statistics) to object modelling represents a change from a technique which is flexible to a more restrictive but geologically plausible one (Figure 5.17). Although object modelling methods are known to better handle trends, the ultimate choice of whether to use pixel

or object based methods depends on the conceptual model and the geologist's prerogative, but both methods can be combined, using different methods for different zones within a single model.

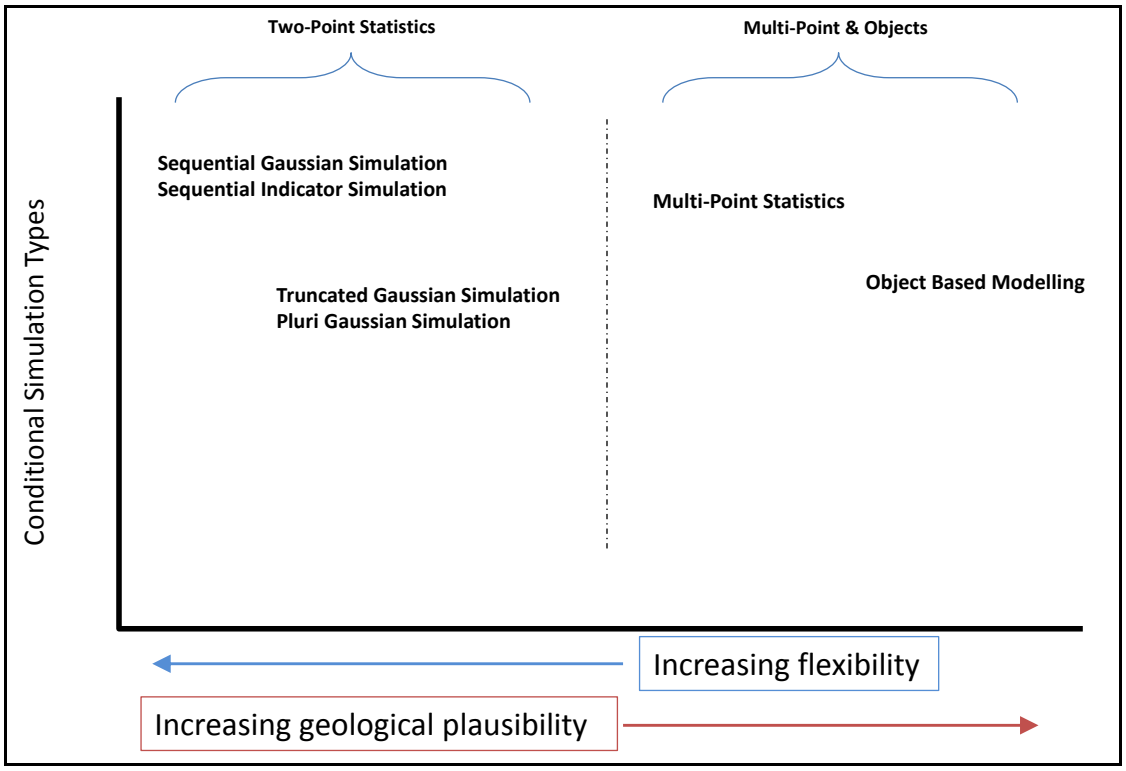

Figure 5.17 Types of Conditional Simulation.

The main difference between object based modelling and Sequential Indicator simulation lies in the way heterogeneities are quantified (Dubrule, 1998). With object modelling, each geological body is modelled as an object using a specific geometry and statistical information about its size (Dubrule, 1998). Both Dubrule (1998) and Goodwin and Brown (1998) have highlighted the use of width-thickness relationships to control the distribution of geological bodies in the object modelling method. Another factor controlling the distribution in the object modelling method is that the total proportion of each body type with respect to the total model volume is kept constant. In other words the percentage of channel sandstone within a specific zone will remain constant while producing different equally possible scenarios for every single model run (Dubrule, 1998).

The most obvious advantage of object modelling is that the modeller is able to capture the geological context through the use of geologically inspired

shapes. It is for this reason that this type of method is highly suitable for modelling fluvial or submarine fan environments and is also flexible with regard to incorporating trends and different facies proportions in the reservoir volume (Zakrevsky, 2001; Caers, 2005). In general terms, object modelling works well when data is a little sparse, or where genetic body dimensions are small compared to well spacing, as the algorithm has more freedom to model the different bodies within the limits of the input parameters. In a situation where there are numerous wells, the parameters of the bodies chosen by the modeller may not be able to match the well data leading to conflict in the mathematical systems of the modelling software and possible termination (Zakrevsky, 2011; Caers, 2005). Object models can therefore be described as being more rigid than pixel based models due to the task of fixing objects (sometimes large objects like long sinuous channels) to match a set of well data and this challenge of matching object parameterisation to actual subsurface data is seen as the most perplexing impediment in the object modelling process (Caers, 2005).

The Sequential Indicator simulation (SIS) method uses the same basic algorithm as that of Sequential Gaussian simulation (SGS) but is used to model discrete variables such as facies rather than continuous variables like porosity and permeability (PetroWiki, 2013). Both Sequential Indicator and Sequential Gaussian simulation, as the name suggests, populate the cells within a grid sequentially. Each cell is populated with a facies (SIS) or petrophysical property (SGS) one cell at a time along a random path until every cell is populated (Caers, 2005). The property value assigned to a specific cell is dependent on the values assigned to all previous cells along the path, thus arranging the reservoir model with a particular configuration of geological continuity (Caers, 2005).

Sequential Indicator simulation involves the use of an Indicator Variogram to build a discrete cumulative density for each discrete property, in this case for each facies type (Bohling, 2005; Dubrule, 1998). In other words, a variogram can be created for each facies with specific anisotropy and correlation lengths representing the spatial continuity for each facies in the relevant

geological environment (Caers, 2005). To understand this better, the Indicator Variogram can be thought of as a facies log, having an assigned cumulative probability to each of the facies in the log. Using the Indicator Variogram the experimental indicator variogram is calculated along the well data and can be described to measure the difference between measurements as a function of distance between them (Dubrule, 1998). Essentially, the variogram does not control the distribution of parameters by means of defined shapes and sizes and therefore can produce results that do not look geologically plausible. However, it will always maintain conformance to the statistical limits assigned by the modeller and thus provides a better handle on the uncertainty associated with property distribution in the inter-well space of the model (Dubrule, 1998).

Facies was modelled first as it was used as a bias in the modelling of subsequent continuous properties.

Petrophysical Log Processing

The Volume of Clay (VCL) log was processed from the gamma ray log through a normalisation process assigning the minimum VCL value to a clean sand value (sand line) and the maximum VCL value to a shale value (shale line) on the gamma ray logs. Thus the equation used to create the VCL logs is:

$$VCL = (GR - GRmin) / (GRmax - GRmin) \quad \ldots\ldots (2)$$

Where:
VCL = Volume of Clay
GR = The gamma ray log
GRmin = The sand line value
GRmax = The shale line value.

The VCL log was then corrected using the following logical equation:

If VCL < 0, 0
Or if VCL > 1, 1 ……..…… (3)
Where:
VCL = Volume of Clay.

The use of this equation (3) is for QC purposes as it helps to remove all spurious value from the processed log. In addition, it may be applied to any other logs where a similar result is needed.

Facies Definition

A facies log template was added to the list of global well logs as a discrete well log. Thereafter four facies were defined using VCL and porosity cut-offs: Sandstone, Tight Sandstone, Shaly Sandstone and Shale. Figure 5.18 shows a cross-plot of porosity vs VCL displayed with data from wells in the E-S field and facies classes superimposed on the data. The table below summarises each facies class with its respective cut-offs.

Facies	VCL cut-off	PHI cut-off
Sandstone	<0.37	>0.07
Shaly Sandstone	>0.37 & <0.60	
Tight Sandstone	<0.37	<0.07
Shale	>0.60	

Table 2: Volume of Clay and porosity cut-offs defining different facies classes.

These cut-offs were expressed by means of a logical equation to produce a facies log.

Upscaling and Data Analysis

The facies log was then upscaled using the “most of” averaging method and the “neighbour cell” cell penetration method. The neighbour cell method

averages log values from all cells adjacent to the upscaled cell which belongs to the same layer as the upscaled cell. The “most of” averaging method is suitable for discrete logs like Facies. It selects the most represented discrete value in the log for each cell.

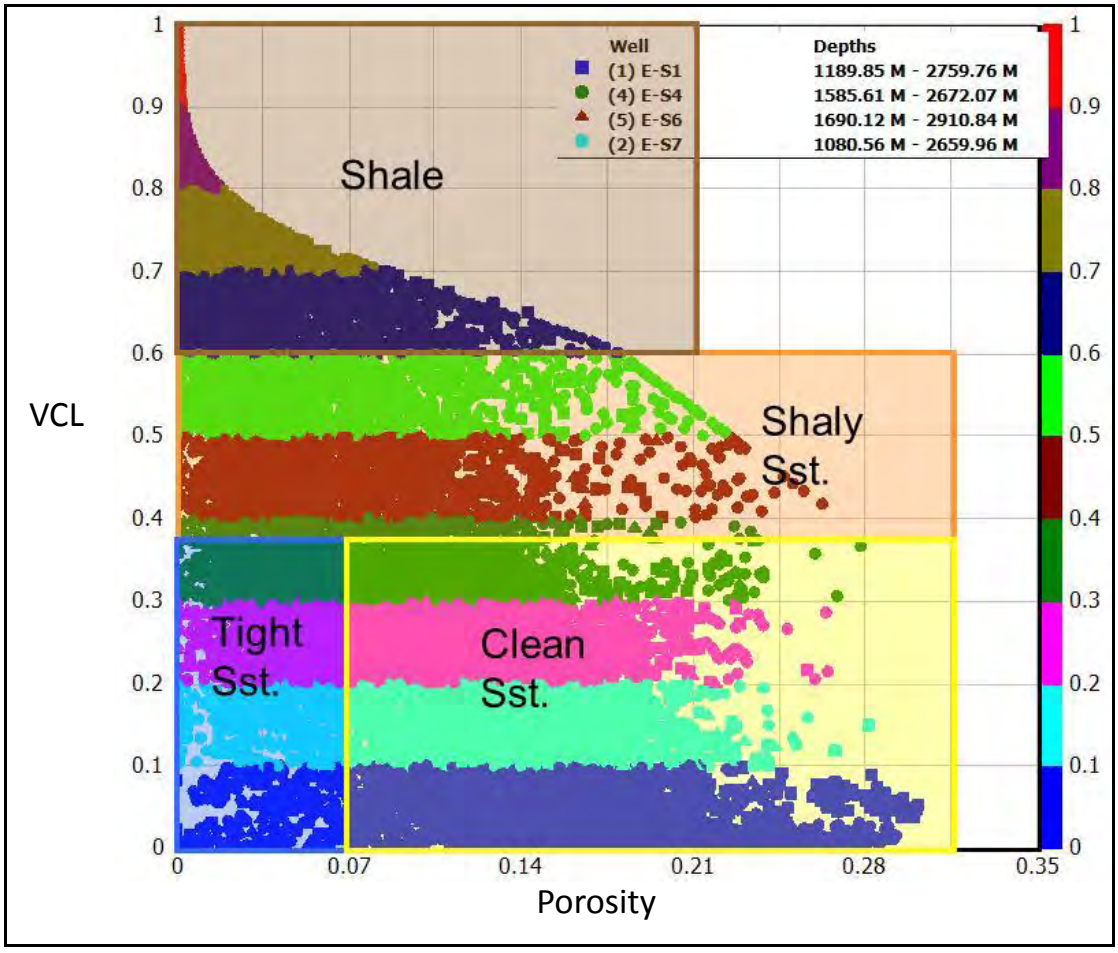

Figure 5.18 Cross-plot of porosity and Volume of Clay with facies classes superimposed on data from wells in the E-S field.

Data analysis of the upscaled facies data was done per zone with the data being represented in the form of probability curves based on the original facies proportion percentage (Figure 5.19).

Modelling Zone 1

Facies modelling was done per zone using the Sequential Indicator simulation statistical method. Another potentially viable method would have been to use the Truncated Gaussian simulation method; however the Sequential Indicator simulation method is suited to properties like facies

because it is a discrete property and lends itself to the low number and uneven distribution of wells drilled in and around the area of the 3D model. Furthermore, facies variability is high, having only two broad rock types i.e. sand and shale.

An exponential variogram was chosen for modelling the spatial distribution of the Pre-1At1 Estuary Unit, USM-2A, USM-2B, Fluvio-deltaic and USM-Lower zones.

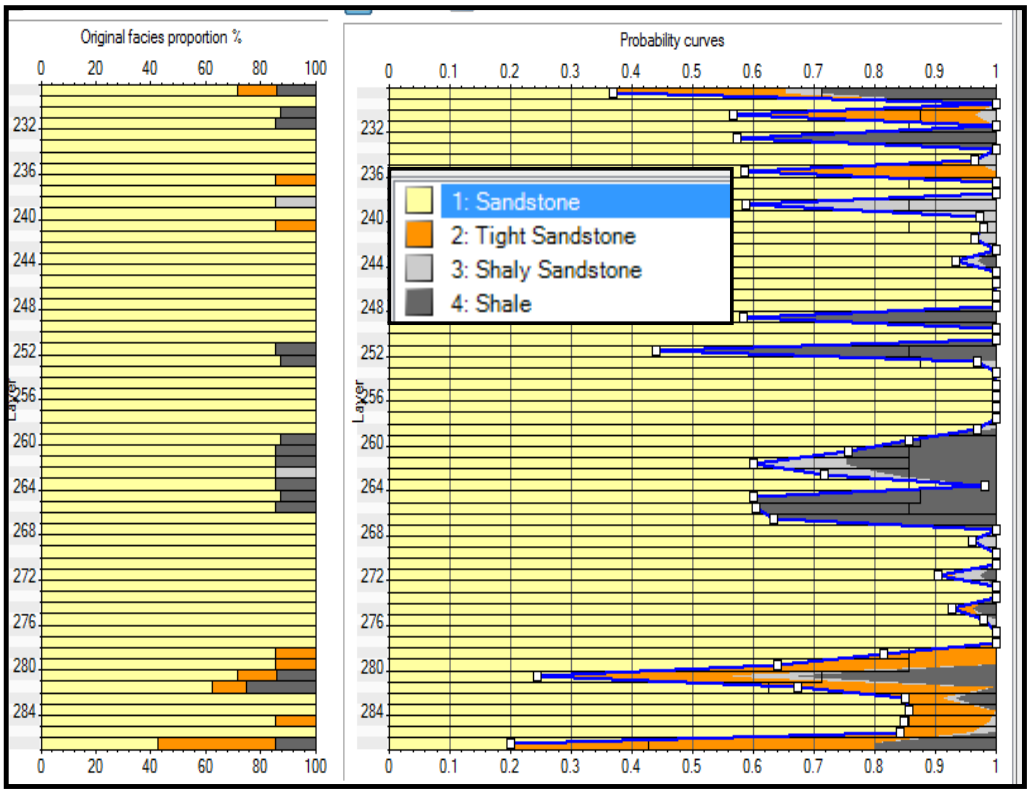

Figure 5.19 Example of probability/proportion curves from the Data Analysis of facies.

For the Pre-1At1 Estuary Unit zone a circular horizontal range was used equating to 1000m with a vertical range of 2m and a nugget of 0.01 (figure 5.20). Moreover the tight sandstone facies was excluded from this zone due to it being absent from log data. Overall, this zone has a lack of data due to the rarity of it being intersected by wells in the field and therefore it was not modelled with the probability curves from the data analysis.

The facies for USM-2A, USM-2B, Fluvio-deltaic and USM-Lower zones were all modelled using the same statistical parameters. The variogram used had a range of 2400m in the major direction (-84°, roughly E-W) and 1200m in the

minor direction. The vertical range was set at 1m and the nugget at 0.01 (figure 5.20).

Modelling Zone 2

The geological parameters of the fluvial bodies in Zone 2 are based on a combination of previous work done by Goodwin & Brown (1998) and some unpublished work done in the nearby F-A field. Elton Charlies & Gervasio Robles (Pers. Comm.) did some work in the F-A field (located east of the E-S field) in order to discern the palaeo-direction of the fluvial channels. The parameters used regarding the width of the channels was adapted from what was published by Goodwin & Brown (1998) and in some places the ranges were modified. For the amplitude and wavelength parameters, it was more difficult to obtain an empirical value, and therefore reasonable values based on the sedimentology and depositional environments were assumed. The ranges used were also managed in order to maintain realistic outcomes.

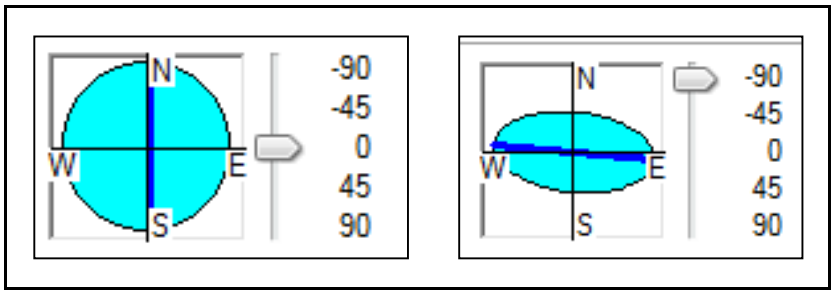

Figure 5.20 Variogram range & orientation for Pre-1At1 Estuary Unit zone (left) and remainder of Modelling Zone 1 (right).

Facies in the Fluvial zone were modelled using the stochastic object modelling algorithm. Two facies bodies, adaptive channels and ellipse, were identified. The channel bodies are divided into two elements, channel sand and levee, with specific parameters. The channel sand was ascribed to the sandstone facies (38.14%) and the levee to the tight sandstone facies (9.47%) with both making up 42% of the total facies to be modelled for this zone. The percentages do not add up exactly because by default stratigraphically lower objects are replaced by higher objects. In this case, the channels will replace some percentage of the levees while keeping the total fraction of the channel bodies (channel bodies = channels + levees) constant.

For each facies body, a set of parameters must be stochastically defined in order to capture the spatial and architectural distribution of the bodies. Below is a summary of the parameters followed by tables populated with the data ranges used for modelling the fluvials (Figure 5.21).

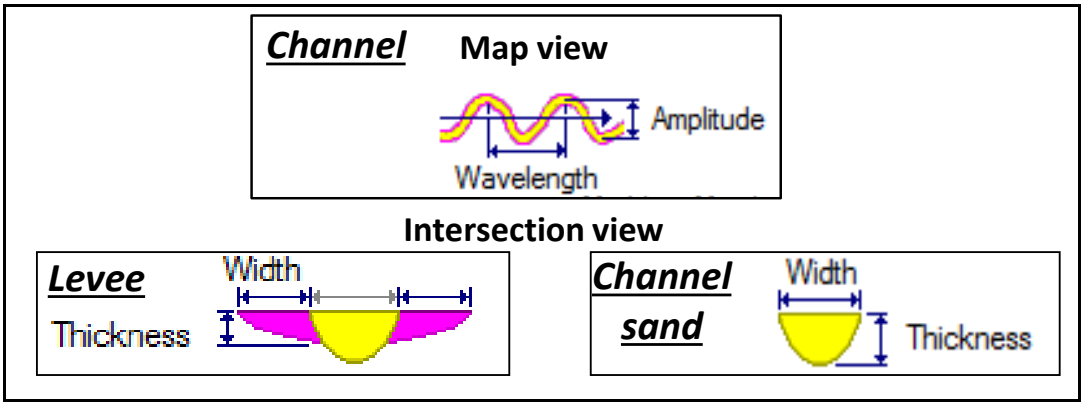

Figure 5.21 Facies modelling parameters used for Modelling Zone 2 – Adaptive Channels.

Parameters for the entire adaptive channel (i.e. channel sand and levee) are (Table 3):

Orientation: is the average azimuth of the channels.

Amplitude: the average transverse distance covered during one wavelength.

Wavelength: the average distance between two consecutive channel turns on the same side.

Relative Sinuosity: is the additional channel length compared to the minimum channel length required to honour the amplitude. Increasing values translate to increasing sinuosity. The most optimum range is between 0.1 and 0.4 with values above 1 having very little effect on sinuosity.

Parameter	Distribution	Minimum	Mode	Maximum
Orientation	Triangular	0°	8°	16°
Amplitude	Triangular	100m	600m	600m
Wavelength	Triangular	1000m	2000m	4000m
Rel. Sinuosity (Ratio)	Triangular	0.1	0.25	0.4

Table 3: Summary of parameters for modelling fluvial bodies.

Parameters for the channel sand are (Table 4):

Width: it is the average channel width.

Thickness: it is the average channel thickness or depth.

Parameter	Distribution	Minimum	Mode	Maximum
Width	Triangular	150m	300m	450m
Thickness	Triangular	5m	12m	18m

Table 4: Summary of parameters for channel sand characteristics.

Parameters for the levee are (Table 5):

Width: Average levee width on each side of the channel as either a fraction of the channel width or horizontal distance units. The fraction of channel width option was used in this study.

Thickness: Average levee thickness as a fraction of channel thickness.

Roughness, one of the parameter settings, is measured between 0 and 1, where 0 produces a smooth levee that closely follows the shape of the channel and 1 produces a very irregular levee.

Parameter	Roughness	Distribution	Minimum	Mode	Maximum
Width	0.2	Triangular	0.3	0.5	0.7
Thickness	0.2	Triangular	0.5	0.7	0.9

Table 5: Summary of parameters for levee characteristics.

No other trends were applied to the adaptive channels.

The shaly sandstone facies was represented by the ellipse type facies body and was assigned to be 12% (initially) of the facies model. As explained, by default in the modelling software, an object replaces stratigraphically lower objects in the model; therefore the initial specified percentage fraction may subsequently change. The shaly sandstone was allowed to replace only the shale (background facies) and therefore did not affect the percentage of adaptive channels.

The “body shape” of the shaly sandstone was chosen to be an ellipse and its “radial profile” rounded.

Parameters for the ellipse facies body are (Table 6):

Orientation: the azimuth of the body's main axis.

Minor Width: is the horizontal dimension across the direction given by the orientation.

Major/Minor Ratio: is the ratio of horizontal dimension along the orientation direction and minor width direction.

Thickness: is the vertical thickness of the body.

Parameter	Distribution	Minimum	Mode	Maximum
Orientation	Triangular	0°	10°	20°
Minor Width	Triangular	300m	800m	1200m
Maj/Min Ratio	Triangular	0.8	1	1.2
Thickness	Triangular	2m	5m	10m

Table 6: Summary of parameters for ellipse body characteristics.

No other trends were applied to the ellipse facies body.

The shale facies was assigned as the background facies of the model and accounts for approximately 35% of the total facies in the model.

The triangular distribution method is suitable for modelling these objects because it allows for the minimum, maximum and mode parameter values to be fixed, thus giving the user more control.

Figures 5.22 and 5.23 show the facies model along a cross-section through the main wells and at different stratigraphic levels.

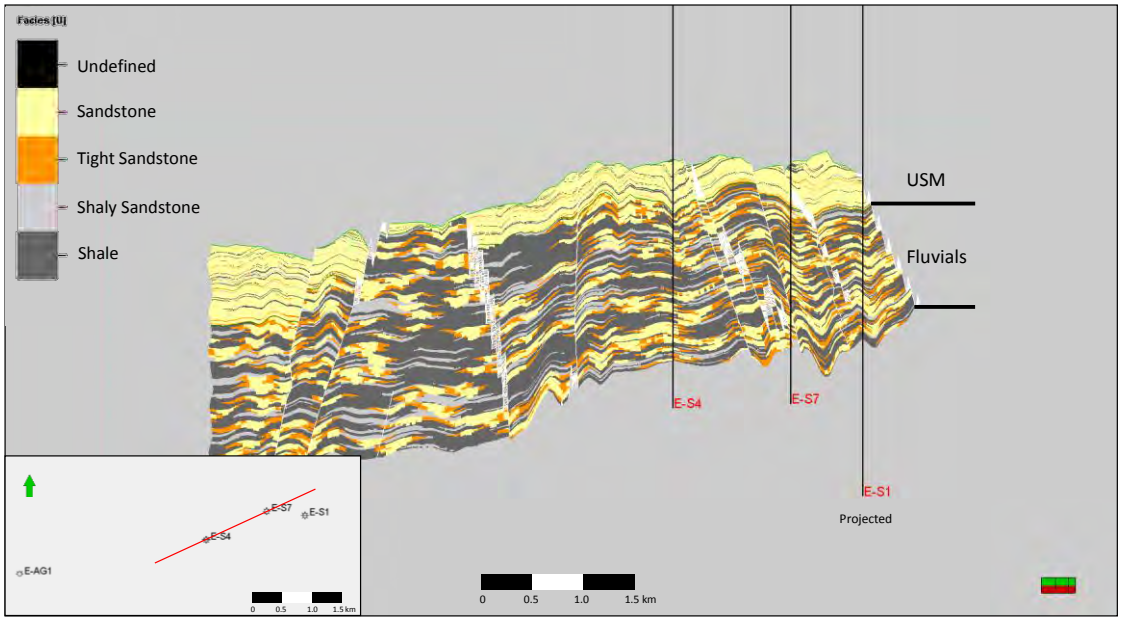

Figure 5.22 Facies model: Cross-section through the main wells.

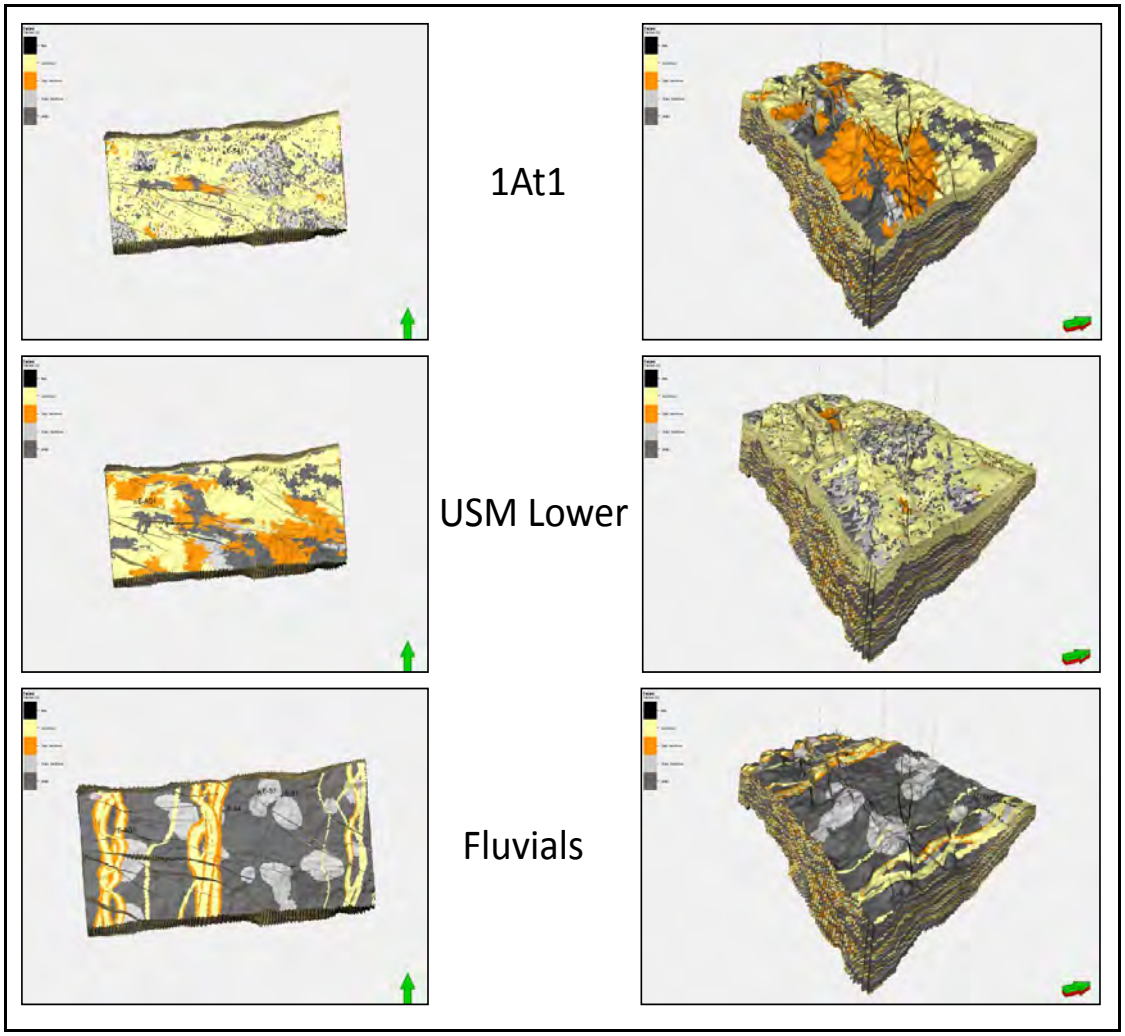

Figure 5.23 Facies model shown at different stratigraphic levels.

5.4.2 Porosity (Φ)

Porosity was the first petrophysical (continuous) property to be modelled as it is used as a control for all the other properties in the model. Both porosity and permeability can be modelled using a constant value per facies type or by using spatially variable geostatistical methods depending on the variability of the petrophysical properties (Caers, 2005). The geostatistical approach involves modelling the porosity first, and thereafter using an acceptable porosity/permeability relationship to model permeability (Caers, 2005).

Petrophysical Log Processing

The total porosity was obtained from a corrected density log using the following equation:

Φ_t = (Matrix Density – RHOBlog) / (Matrix Density – Density of Fluid) ……. (4)

Where:

Matrix density (g/cm^3) = density of the lithology matrix calculated by the petrophysicist over a particular interval in a well.

RHOBlog (g/cm^3) = density at each sample point of the Density log curve.

The Total Porosity was thereafter used to calculate the Effective Porosity using the equation below:

$\Phi_e = \Phi_t \times (1 - VCL)$ …….. (5)

Porosity measured from cores was also loaded into the software program. The measured core data was corrected, i.e. it was shifted vertically to match the log data (Figure 5.24). This correction compensates for any discrepancies due to stretch in the drill pipe which results in different “driller” and “logger” depths.

Upscaling and Data Analysis

The effective porosity was upscaled using the facies distribution as a bias so as to correspond high porosity with sandy facies and low porosity with shale

facies. Furthermore, the porosity was averaged arithmetically using the "neighbour cell" cell penetration method.

Data analysis was carried out per zone and per facies with the data being represented in the form of probability curves using a series of transform parameters in order to produce a close to normal distribution where possible.

Modelling Zone 1

Porosity was modelled using the Gaussian Random Function simulation distribution method for all zones in Modelling Zone 1 using an exponential variogram which was defined as per facies. The Gaussian Random Function simulation differs from Sequential Gaussian simulation in that it is not a sequential algorithm, which allows the algorithm to be parallelised, making it faster than the SGS algorithm. Another difference is that the Gaussian Random Function simulation method has a built-in collocated co-simulation option which removes the bias associated with the variance of the simulated property having the tendency to be higher than expected (Petrel, 2014).

By using facies as a bias, heterogeneity in reservoir continuity is captured already. A variogram incorporating spatial correlation characteristics for porosity in each facies group was created.

The variogram range for most of the facies groups was set at 1200m in the major (E-W) and 600m in the minor (N-S) horizontal directions. The vertical range used was 1m and a nugget of 0.01 was assigned. The variogram for the tight sandstone facies was designed differently, depending on the sand content of the zone. For the shalier zones (Fluvio Deltaic and USM_Lower zones), the variogram was set using the same parameters described above, while for the sandier zones, where this facies is less likely to occur (this is deduced from the data distribution in the data analysis), a circular variogram with a horizontal range of 5000m was set. The vertical range was set at 10m and a nugget of 0.0001 was used. This low nugget value was chosen to force the algorithm to tend towards the actual log data because this facies can be highly localised.

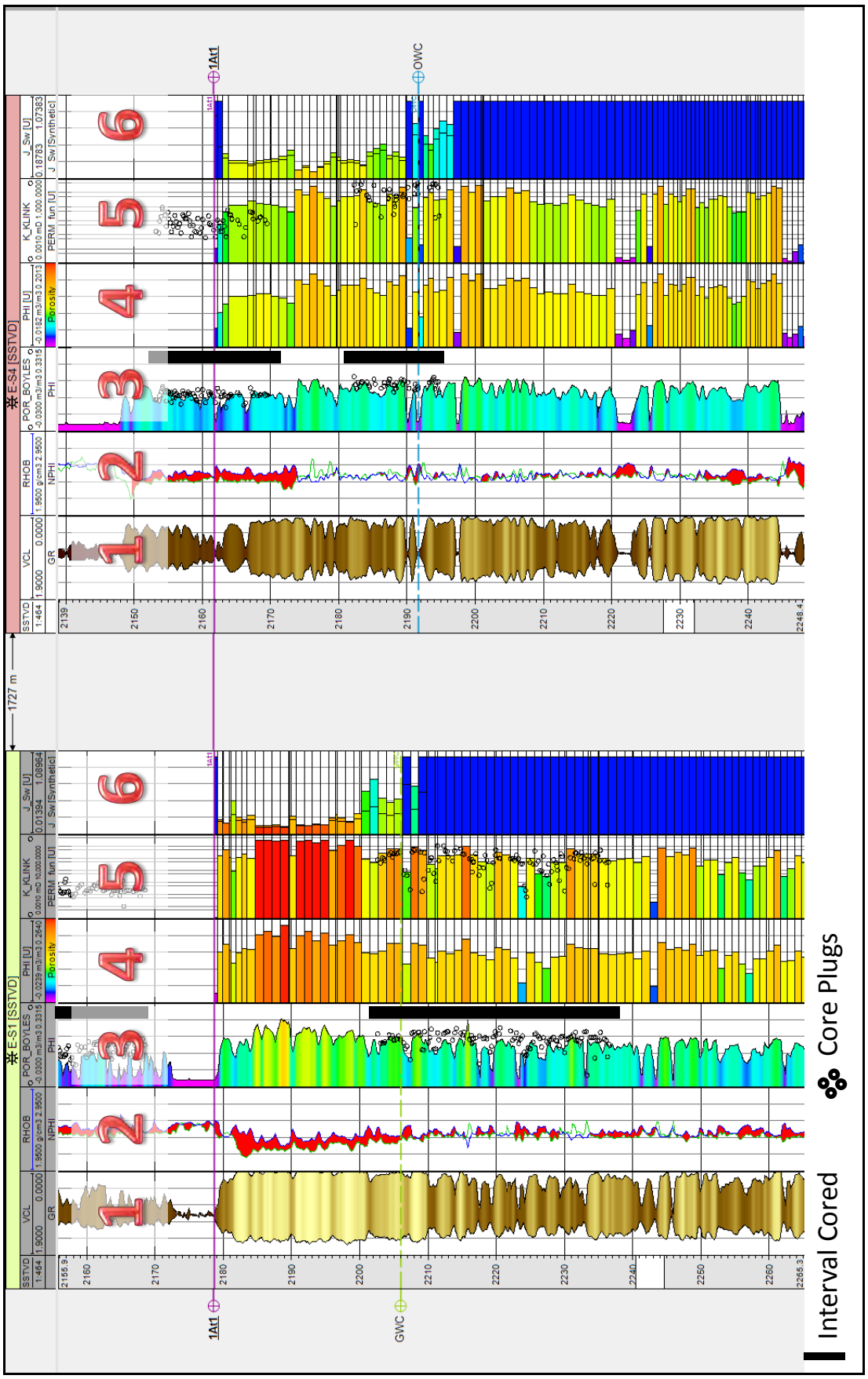

Figure 5.24 Well section showing core porosity matched to log porosity data (Track 3). Flattened on the 1At1 marker.

Modelling Zone 2

Porosity in Modelling Zone 2 was also modelled using the Gaussian Random Function simulation distribution method using an exponential variogram and the variogram parameters were the same for all facies groups. The major trend direction has an azimuth of 10° (roughly N-S) and a horizontal range of 1200m. The perpendicular minor direction has a range of 600m and the vertical range is 1m. A nugget of 0.1 was set for the fluvial zone to account for the high facies variability expected in this zone (Figure 5.25). Furthermore, the porosity was modelled incorporating transforms resulting from the data analysis.

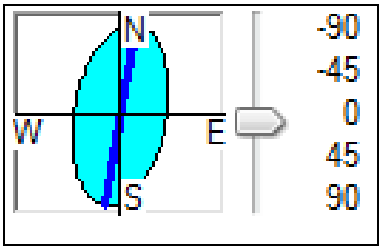

Figure 5.25 Variogram range & orientation for porosity in Modelling Zone 2.

Figures 5.26 and 5.27 show the porosity model along a cross-section through the main wells and at different stratigraphic levels.

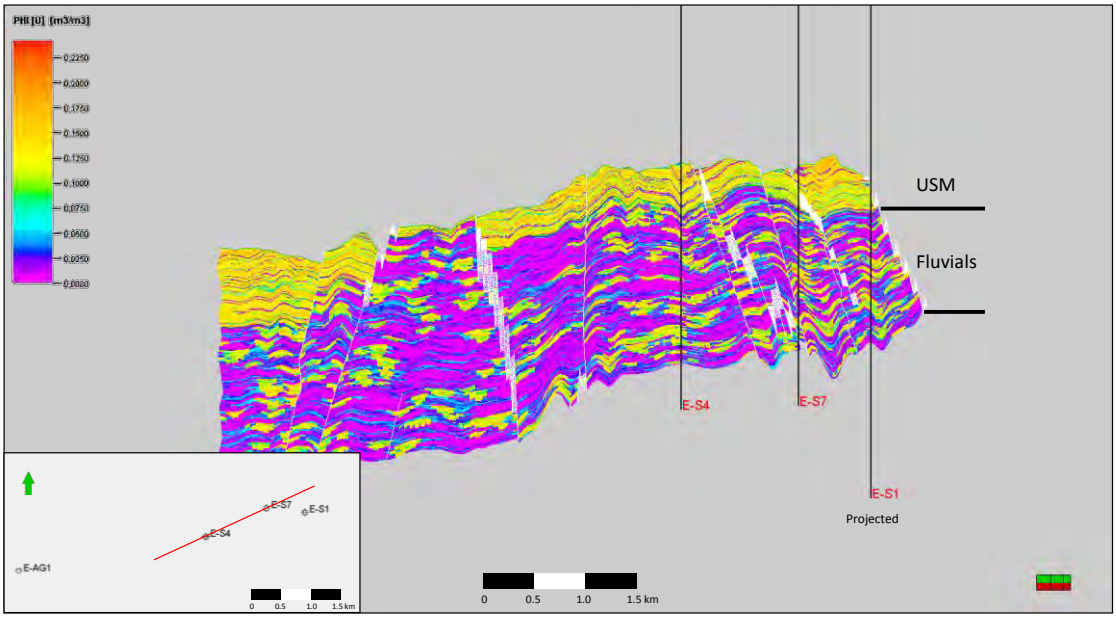

Figure 5.26 Porosity model: Cross-section through the main wells.

5.4.3 Volume of Clay (VCL)

The VCL property is required to follow the same trend as porosity and is used later during the fault-seal analysis process where VCL across the faults is calculated.

Petrophysical Log Processing

The log processing for VCL was done as a precursor for the facies modelling (See Section **5.4.1** Facies Modelling).

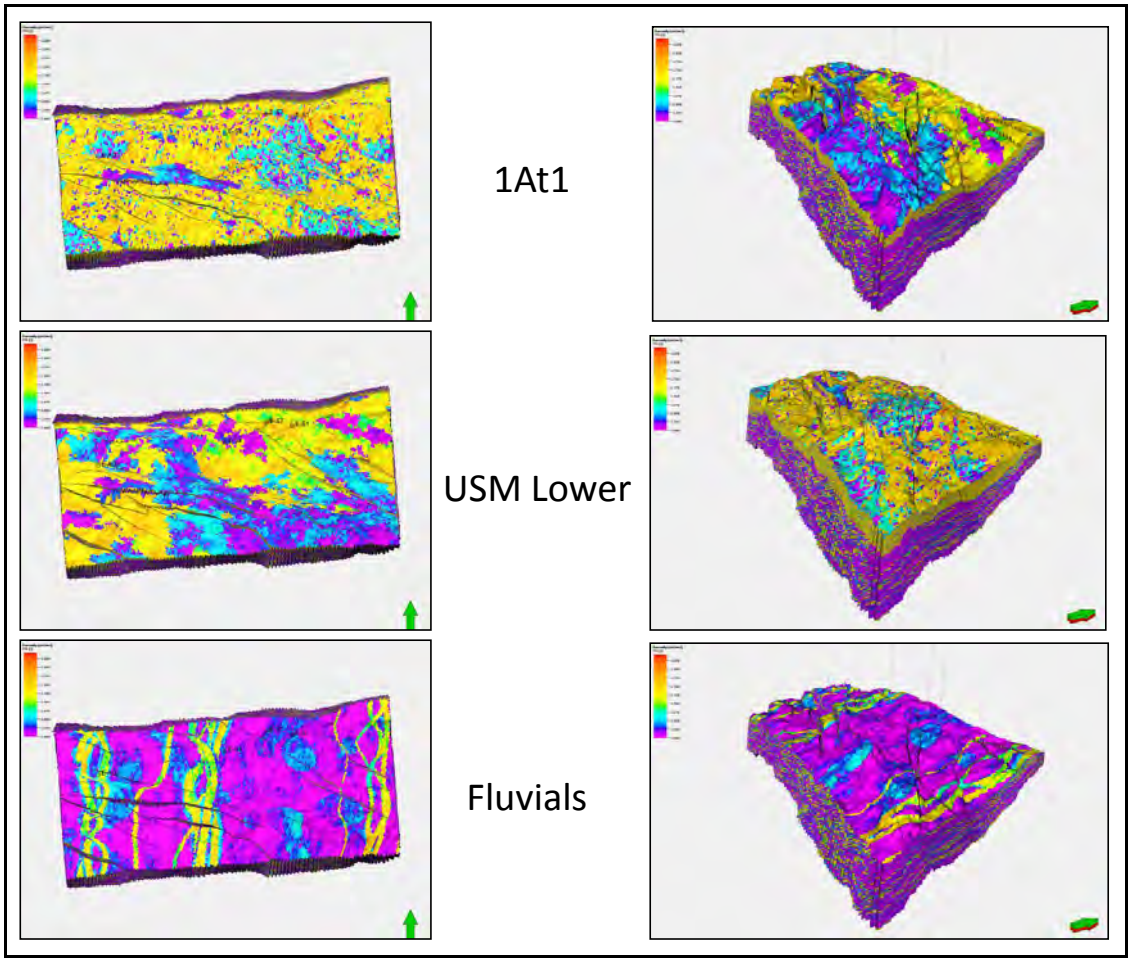

Figure 5.27 Porosity model shown at different stratigraphic levels.

Upscaling and Data Analysis

Like porosity, the VCL log was upscaled arithmetically using the “neighbour cell” method and data analysis was done per zone and per facies.

Modelling Zone 1

Volume of Clay was also modelled using similar parameters to that of porosity. A Gaussian Random Function simulation distribution was applied using an exponential variogram having an orientation of -84° and an anisotropy range of 1200m in the major direction and 600m in the minor direction, with a vertical range of 1m and a nugget of 0.01. In the Pre-1At1 Estuary Unit, USM-2A and USM-2B zones (the sandier zones), the variogram for the tight sandstone facies was set up with a circular range of 5000m, a 10m vertical range and a nugget of 0.0001.

In addition, a Co-kriging function was applied to all the facies in Modelling Zone 1 using the porosity volume (i.e. the porosity model) as a secondary variable and applying a Collocated Co-kriging method. When compared to the "local varying mean" method, the Collocated Co-kriging method incorporates a correlation coefficient allowing the user to better control the influence of the secondary variable. The secondary variable provides information about small-scale variation in modelling space and therefore allows the primary variable to be affected by sudden changes in the secondary variable.

Modelling Zone 2

All facies in the fluvial zone were modelled using the Gaussian Random Function simulation distribution method using an exponential variogram. The parameters used were the same as those set for porosity in this particular zone.

Figures 5.28 and 5.29 show the Volume of Clay model along a cross-section through the main wells and at different stratigraphic levels.

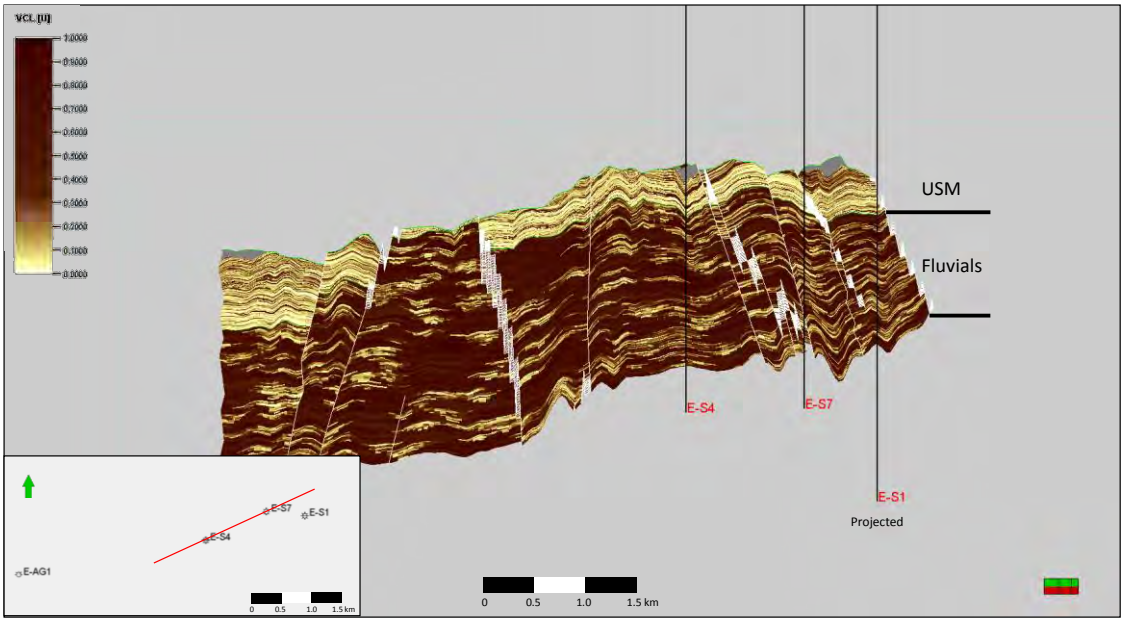

Figure 5.28 Volume of Clay model: Cross-section through the main wells.

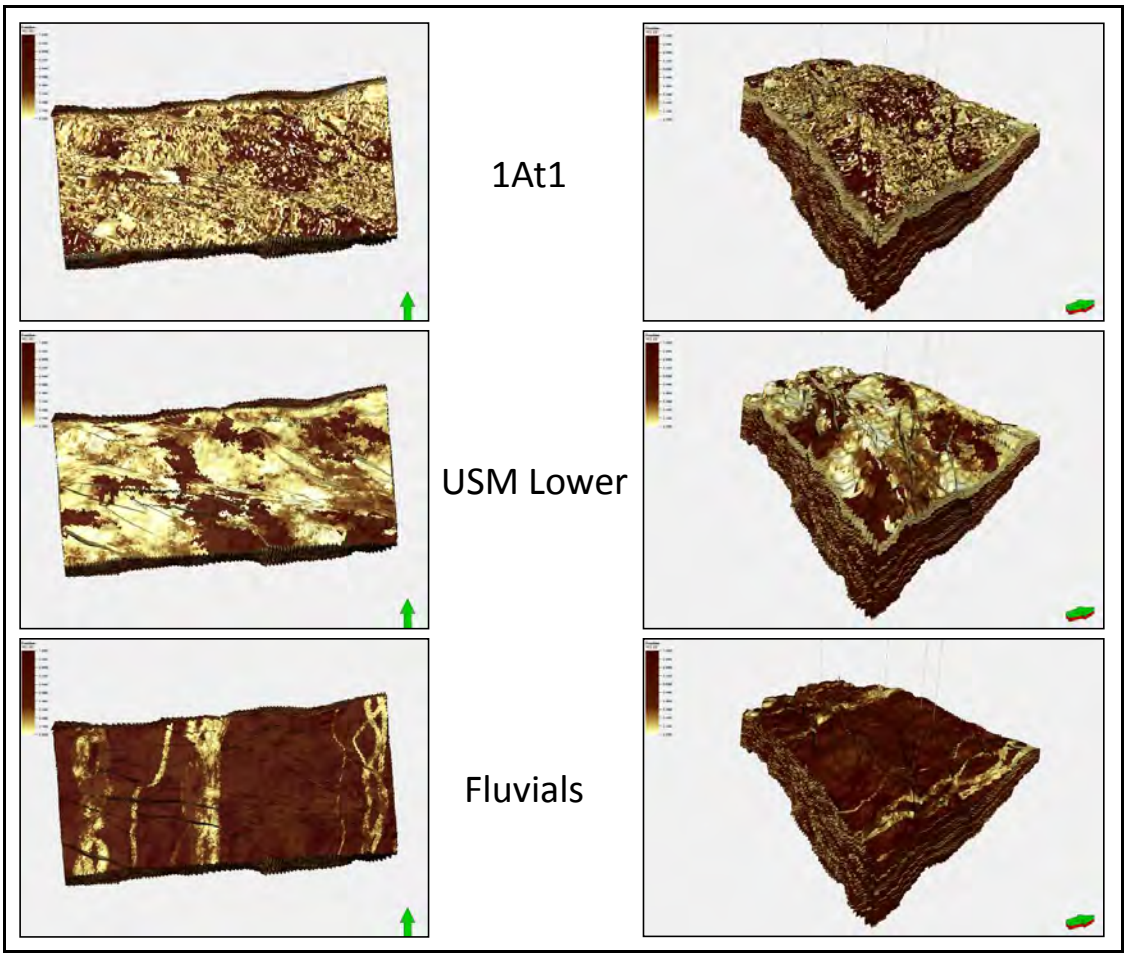

Figure 5.29 Volume of Clay model shown at different stratigraphic levels.

5.4.4 Permeability (K)

A permeability model can be achieved by using a combination of core data and the transform obtained from the cross-plot of core porosity vs core permeability (Klinkenberg). A linear regression between log permeability and porosity is created for each facies thereby producing a permeability model directly from the modelled porosity (Caers, 2005). The drawbacks of this method are that it does not cater for any unique permeability trends (spatially) which differ from the trends seen in the porosity model, and it could underestimate the presence of legitimate extreme values (Caers, 2005). A permeability model can also be created using Collated Co-Kriging. In this method permeability has its own variogram which differs from the porosity variogram with unique spatial characteristics and isotropy, and porosity serves as a *co-variable* with its statistical relationship quantified with a correlation coefficient using a linear correlation cross-plot of porosity and permeability from core data (Caers, 2005).

The method adopted in this workflow uses porosity as a co-variable (i.e. the second method described above) but the variogram parameters for both porosity and permeability were set to be the same.

Petrophysical Log Processing

Porosity and permeability core data were plotted against each other to evaluate the trend. Usually a trend line is used to best fit the data and the equation of the line provides a mean to apply this trend to the entire model. In this case two trends were identified from the cross plot between core porosity and core permeability using a porosity cut-off of 0.07 (Figure 5.30). Above this cut-off the trend correctly matches porosities with permeabilities. However, below the cut-off, low porosities incorrectly correspond to relatively higher than expected permeabilities due to limitations of the core analysis methodology. Therefore the trend below the cut-off is made steeper so as to relate the low porosity values to lower, more realistic permeabilities.

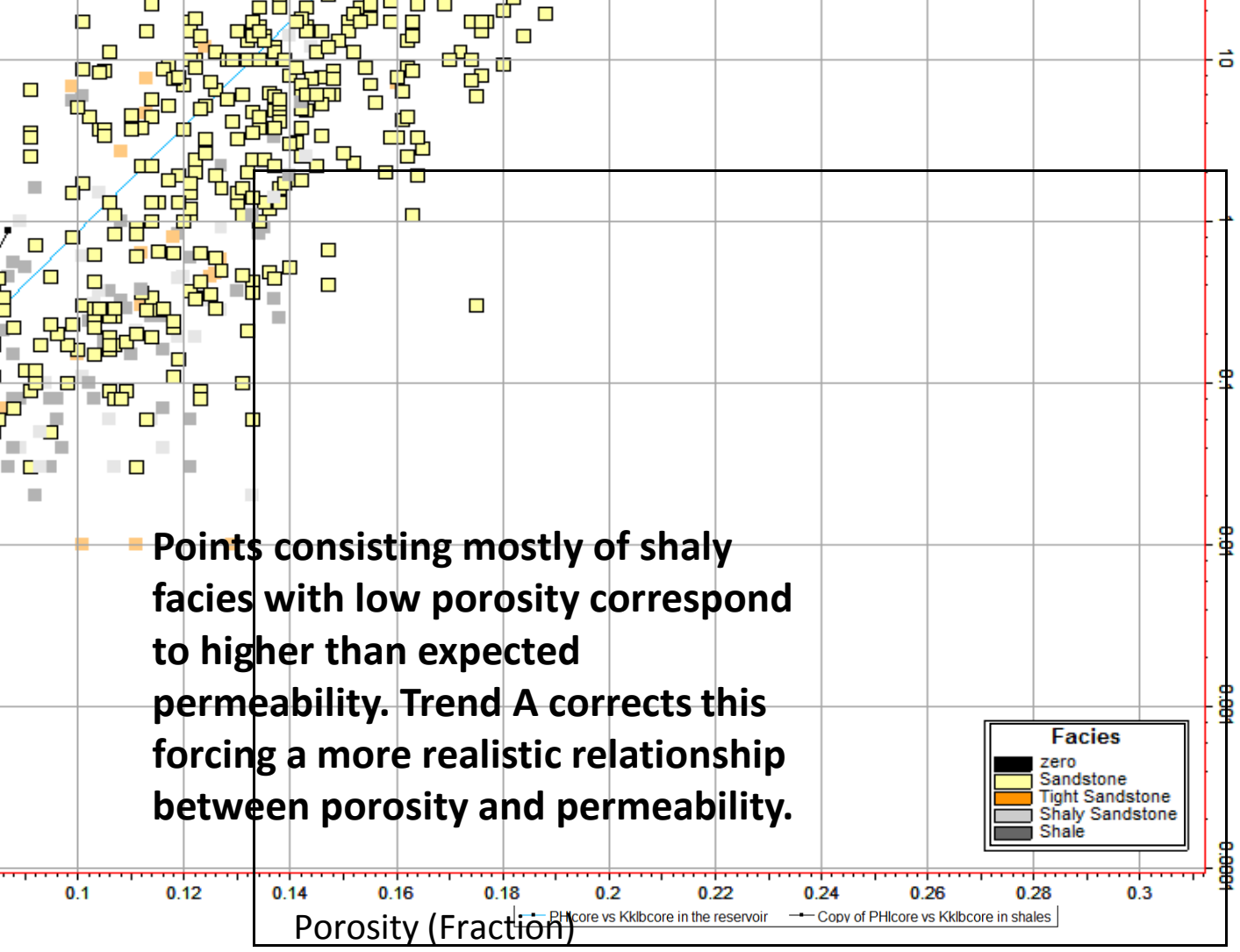

Figure 5.30 Poro-perm cross-plot using core data. Two separate trends were identified using a cut-off of 7% porosity. Data points are painted with corresponding facies.

Upscaling and Data Analysis

Using the equations of both trends, a permeability log was generated and then like porosity, upscaled using the facies distribution as a bias. The equations used to create the permeability log were implemented using the following statement:

PERM = If (PHI >= 0.07, Trend A, Trend B) …… (6)

Where:

PERM = Permeability

PHI = Porosity

Trend A = the trend above the porosity cut-off

Trend B = the trend below the porosity cut-off.

It is important to note that the direct use of the produced equation in the property model population makes the poro-perm (Φ/K) relationship fit exactly onto a straight line; whereas the use of upscaled logs results in a data cloud with a representative trend, making it the better method as it captures the uncertainty involved in the statistical distribution.

Permeability was averaged using the “median” method using the “neighbour cell” cell penetration method. The “median” method sorts all the values within a cell and will choose the centre value in terms of magnitude.

Data Analysis was done per zone and since permeability is a lognormally distributed parameter, a logarithmic function was added to the transform workflow. In addition, a 3D trend function was also added to the transform workflow. Porosity was used as the comparative property i.e. a co-variable, for trending in order to directly relate the permeability to the porosity trend. The use of the 3D trend obviated the need for analysing the data as per facies because the porosity trend used had already been subjected to this and thus has the facies conditioning embedded in it already.

Modelling Zone 1

Permeability in this field is deemed to be closely related to porosity and was modelled using the same variogram settings. A Gaussian random function simulation distribution method was used for all zones in Modelling Zone 1 using an exponential variogram and was modelled per zone but wasn’t conditioned to facies. In the data analysis phase, a porosity trend function was already incorporated having a facies bias embedded in it. The variogram range for all the facies groups was set at 1200m in the major (E-W) and 600m in the minor (N-S) horizontal directions. The vertical range used was 1m with a nugget of 0.01.

Modelling Zone 2

Permeability in Modelling Zone 2 was also modelled using the Gaussian Random Function simulation distribution method using an exponential variogram with variogram parameters being the same for all facies groups.

The horizontal range in the major and minor trend directions were defined as 1200m and 600m respectively with the major axis having a roughly N-S azimuth (10°). The vertical range used was 1m with a nugget of 0.1.

Figures 5.31 and 5.32 show the permeability model along a cross-section through the main wells and at different stratigraphic levels.

5.4.5 Water Saturation (Sw and J_Sw)

Petrophysical Log Processing

The modelling of water saturation (Sw) was more complex than that of the other properties in the model. It involved combining the water saturation provided by the petrophysicist and water saturation using the Leverett J Function approach. The water saturation log generated by the petrophysicist was obtained from the Waxman-Smits and Archie equations. In this study, the water saturation value used was obtained from the Dual-Water method (Waxman-Smits equation developed for muddy sandstones) because it is generally more accurate. However, the reservoir sandstones have a low shale content, therefore both (Archie and Dual Water) methods produce similar results.

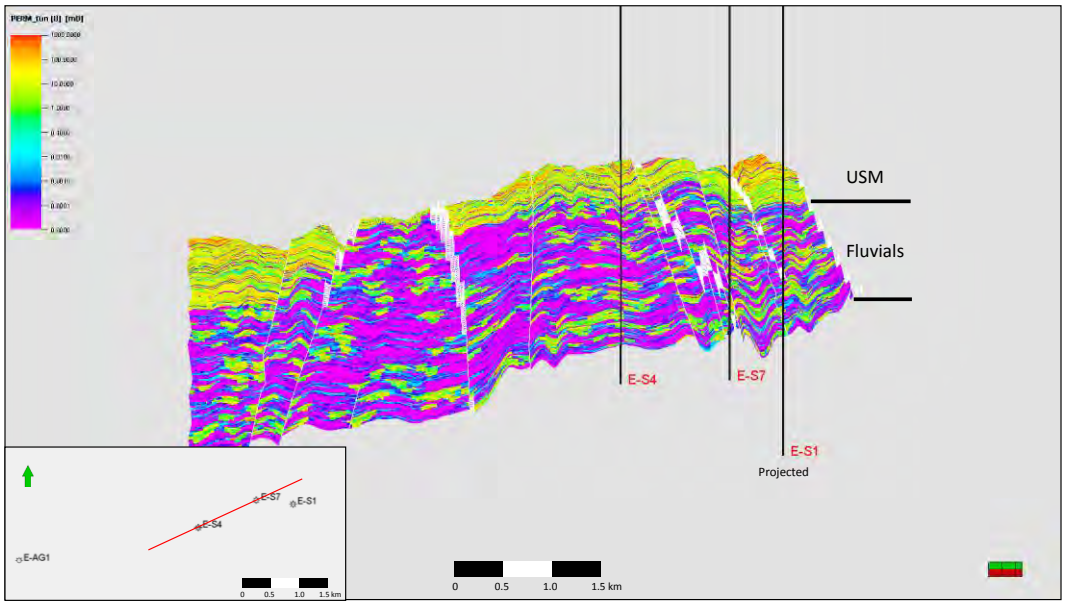

Figure 5.31 Permeability model: Cross-section through the main wells.

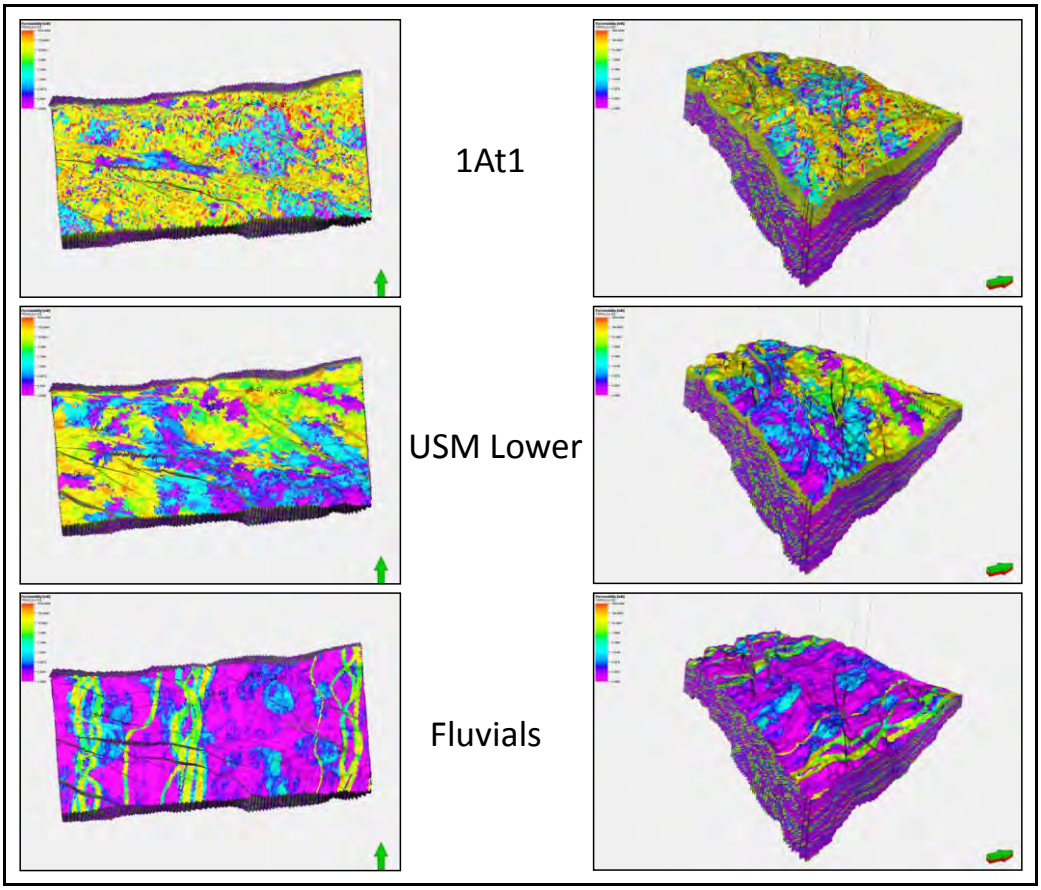

Figure 5.32 Permeability model shown at different stratigraphic levels.

Petrophysical Log Processing: Flow Zone Indicator (FZI)

The Flow Zone Indicator approach (Amaefule et al., 1993) was applied using the facies to differentiate between zones of varying hydrocarbon flow potential. The benefit of a Flow Zone Indicator, which is obtained from the Flow Zone Indicator equation (equation 7), is that it solves the divergence problems at the population level which can occur with co-dependant variables. The mentioned procedure allowed individual J functions to work in the appropriate flow zones.

The Flow Zone Indicator (FZI), proposed by Amaefule et al. (1993), is a derivative of the Rock Quality Index (RQI) and Normalized Porosity Index (NPI) where:

$$RQI = 0.0314 * \sqrt{\frac{K}{\varphi_E}} \qquad NPI = \frac{\varphi_E}{(1-\varphi_E)} \qquad FZI = \frac{RQI}{NPI}$$

The equation can thus be re-adjusted as:

$$FZI = \frac{0.0314 * \sqrt{\frac{K}{\varphi_E}}}{\frac{\varphi_E}{(1-\varphi_E)}} \quad \text{..... (7)}$$

Where:

K = Permeability

Φ_E = Effective Porosity

Flow Zone Indicator values typically range from zero to 6. Higher values correspond to better flow capacity rock types. It may be required to truncate or clip the data in order to remove any illogical data points.

In this model, two flow zones were identified, A zone of poor flow and a zone of good flow. Due to the homogenous, tabular and clean nature of the reservoir it wasn't deemed necessary to create multiple zones. A Flow Zone Indicator of >0.5 corresponds to good flow while a Flow Zone Indicator <0.5 corresponds to poor flow. Furthermore, the Flow Zone Indicator value of 0.5 corresponds to porosity and permeability values of 7% and 0.1mD respectively (Table 7). Flow Zone Indicator values greater than 0.3 where porosity values were less than 2.5% were interpreted as being unrealistic and were adjusted to 0.3 using the following logical equation:

FZI = if (FZI >=0.3 AND PHI<=0.025, 0.3, FZI) ……..…. (8)

Where:

FZI = Flow Zone Indicator

PHI = Porosity

This over-estimation is due to the initial shale trend gradient being too shallow and implementing this equation normalises the Flow Zone Indicator property. In addition, any porosity values greater than 24% and permeability values greater than 2500mD were seen as anomalous and were clipped.

Flow Zone Indicator was plotted on top of a poro-perm cross-plot to illustrate two distinct flow zones (Figure 5.33).

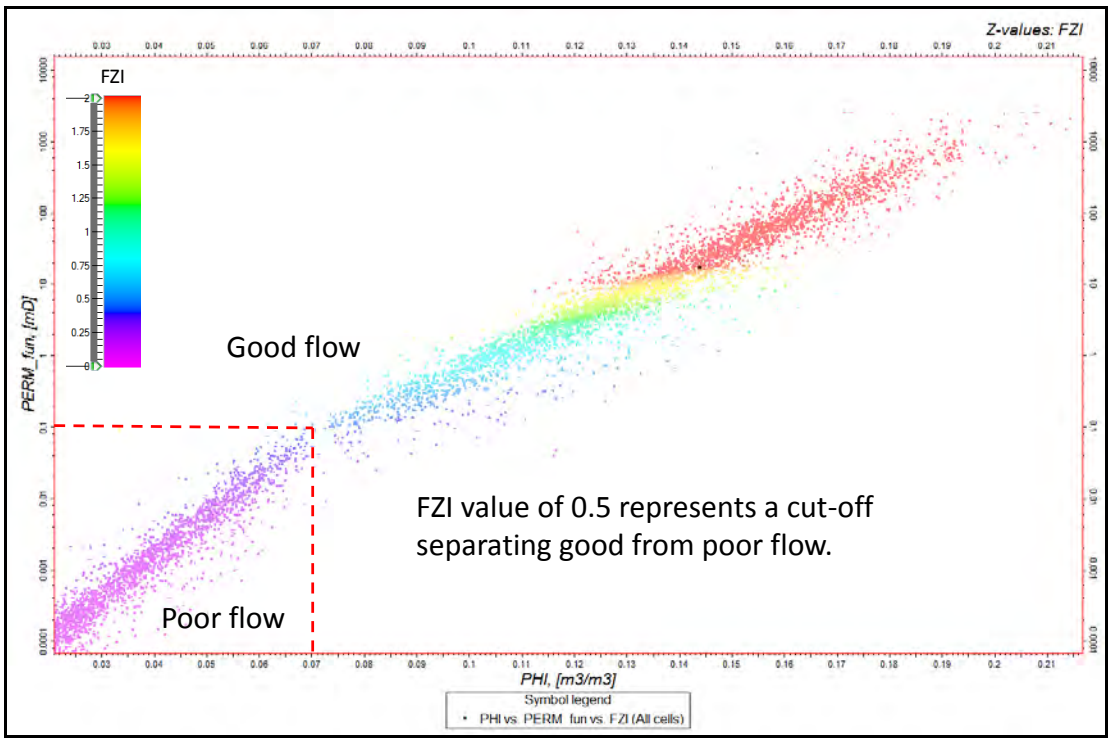

Figure 5.33 Poro-perm cross plot using data from the model with the Flow Zone Indicator property painted on each data point.

FZI Facies	Range of FZI	Φ cut-off	K cut-off
Poor Flow	FZI < 0.5	<0.07	<0.1
Good Flow	FZI > 0.5	>0.07	>0.1

Table 7: Flow Zone Indicator facies with relevant cut-off values.

Modelling Zone 1: Overview

Neither Flow Zone Indicator nor J Function water saturation were derived from statistical distribution methods. These properties were generated directly from defined equations (Equations 7 and 9) using a calculator in the modelling software. The equation for water saturation using J function is given below:

$$Sw = \left(\frac{0.005845 * Ht * \sqrt{\frac{Kh}{\varphi}}}{a} \right)^{\frac{1}{b}}$$

..... (9)

Where:

φ = modelled porosity,

Kh = modelled horizontal permeability

Ht = cell height from the gas-water contact

Parameters a and b depend on Flow Zone Indicator /Lithologies.

(Note: the J function equation had been re-formulated to eliminate the need for direct capillary pressure data which is not always available).

The J-function water saturation was modelled empirically using the water saturation (Sw) log data provided by the petrophysicist and cross-plotting it with the Height Above Contact property. Using the J function equation, water saturation was populated into the model and the data points displayed on a water saturation vs Height Above Contact cross-plot. The variables a and b were adjusted for each Flow Zone Indicator, matching the J function model data to the data from the wells until the best match was found. This was done in an iterative process, whereby each flow zone is characterised by specific a and b values (Table 8).

FZI Ranges	a	b
FZI < 0.5	0.15	-1.8
FZI > 0.5	0.16	-3

Table 8: Flow Zone Indicator ranges and defined values of a and b variables (J function).

Modelling Zone 1: Individual Contact Regions

Wells in the E-S region have discovered both oil and gas in the Upper Shallow Marine reservoir. The E-S4 and E-AG1 wells have encountered oil while E-S1 and E-S7 have intersected gas. In addition, each well intersected individual hydrocarbon contacts. In order to create a single water saturation property which captures the different J function distributions/populations with individual hydrocarbon contacts, a property called “Contact Regions” was created.

Hydrocarbon contacts were defined for each region using the Contact filter, thus allowing for each contact to only be active within stipulated segments of the model. The contacts were then modelled individually (each field contact modelled separately) using a geometric modelling method i.e. Above Contact method, resulting in individual properties of Height Above Contact (Ht) extrapolated over the whole model, unconstrained by any field boundaries (Figures 5.34 and 5.35). A “mock” hydrocarbon volume map was then created for each contact in order to distinguish different geographic regions of variable Height Above Contact (Figure 5.36).

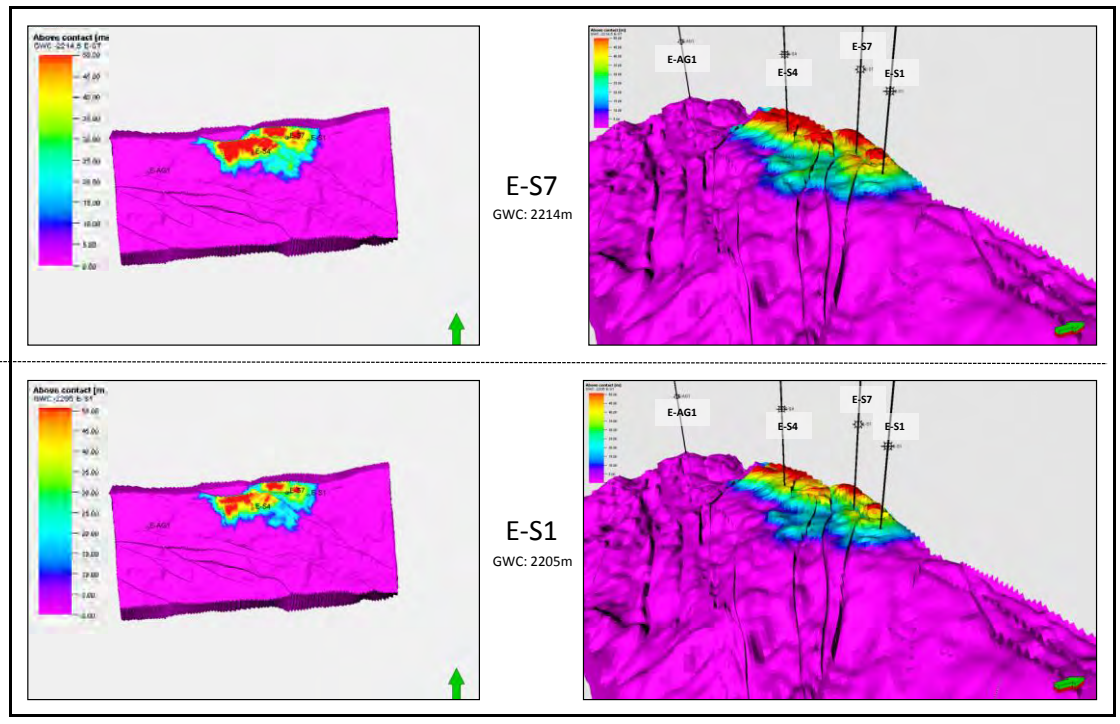

Figure 5.34 Hydrocarbon contacts for each well modelled individually without any areal constraints. E-S7 and E-S1. Scales identical for all four panels.

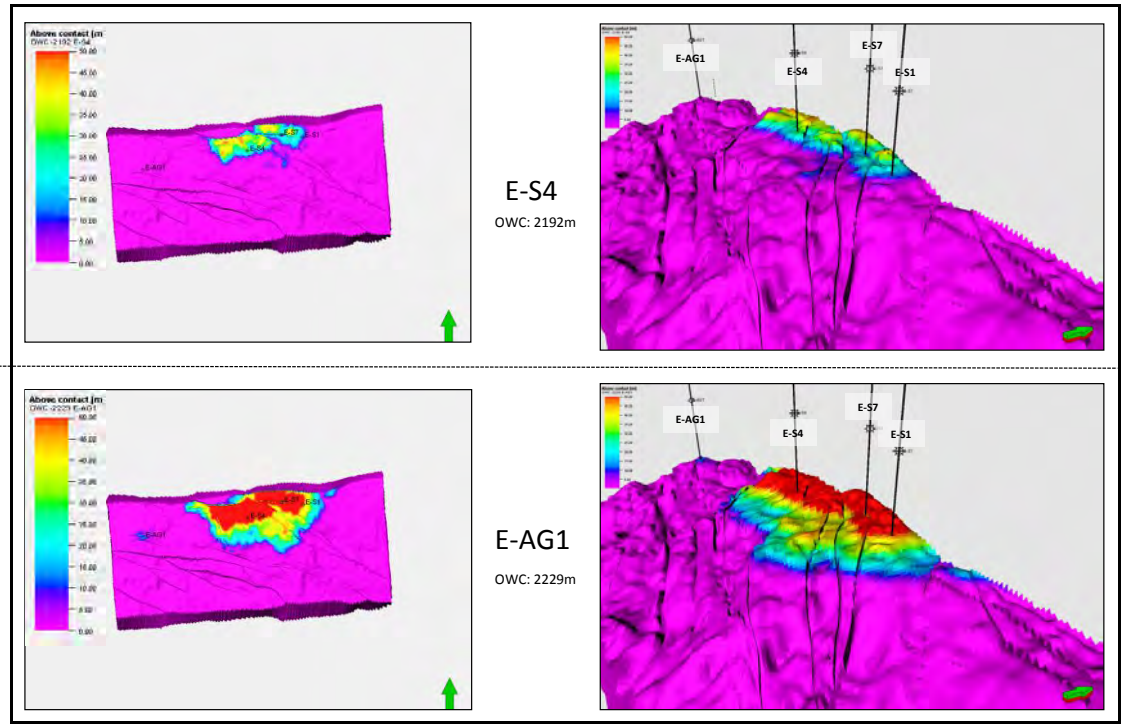

Figure 5.35 Hydrocarbon contacts for each well modelled individually without any areal constraints. E-S4 and E-AG1. Scales identical for all four panels.

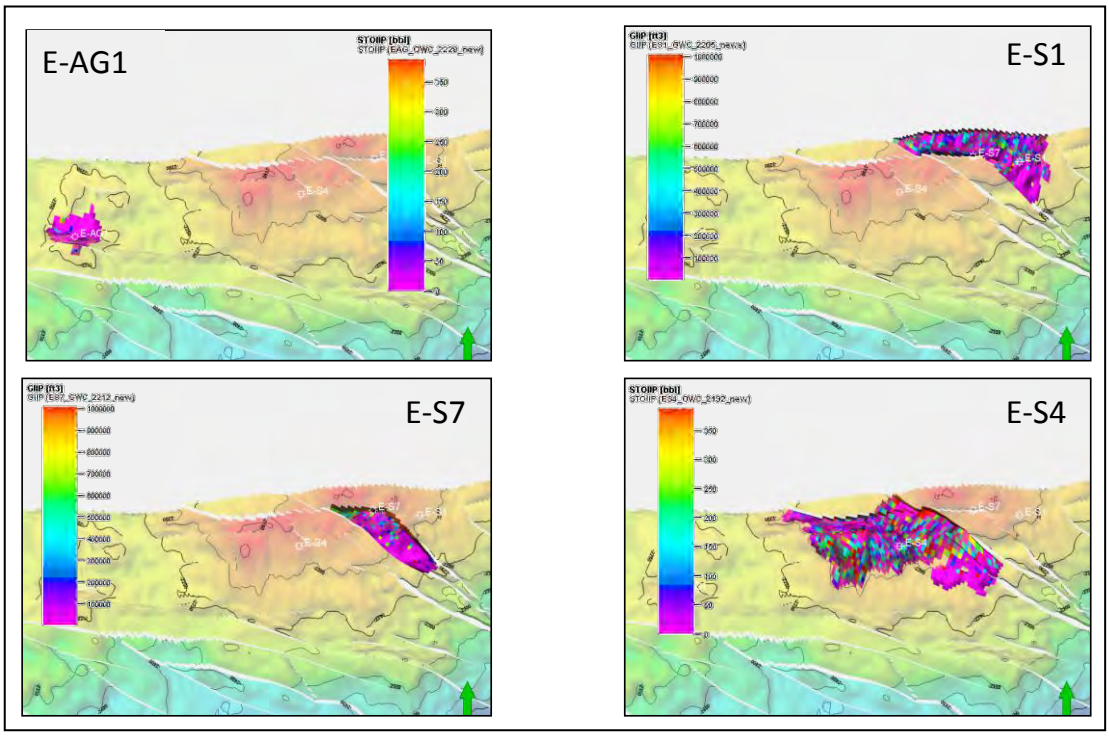

Figure 5.36 Mock hydrocarbon volume maps overlain on the 1At1 structure map - created in order to distinguish different geographic regions.

These volume maps were used to create the Contact Regions property using the following logical equation:

ContactRegions= If(ES1_Region<>U,2,If(ES4_ Region <>U,3 If(ES7_ Region <>U,4, If(EAG1_ Region <>U,1,0)))) ..…….....…. (10)

Where:
U = Undefined,
ES1_ Region,
ES4_ Region,
ES7_ Region &
EAG1_ Region
are the mock volume maps for each specified region;
And, numbers 0 to 4 are contact region codes (Table 9).

Figure 5.37 shows the Contact Regions property corresponding with regions and colours in the table below.

Contact Region Code	Contact Region Name	Colour
0	Water_Region	
1	E-AG1_Region (Oil)	
2	E-S1_Region (Gas)	
3	E-S4_Region (Oil)	
4	E-S7_Region (Gas)	

Table 9: Contact Regions codes, names and corresponding colour table.

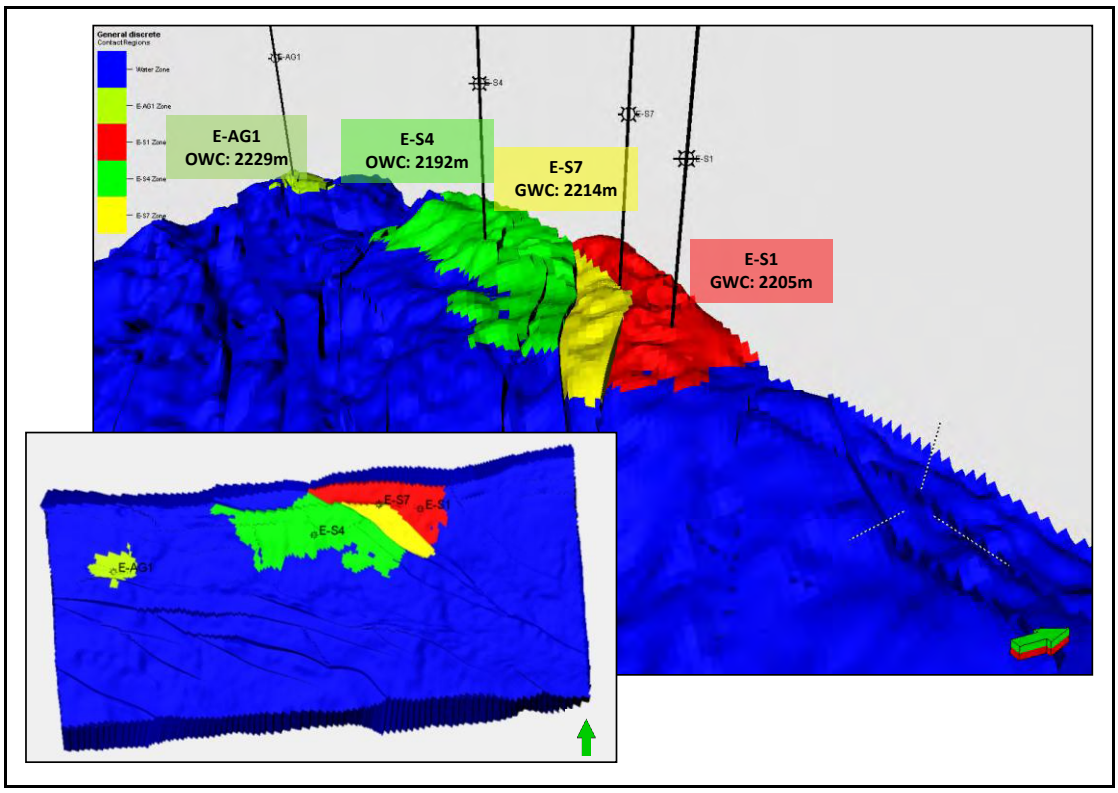

Figure 5.37 Contact Regions property.

Modelling Zone 1: Merging Contact Regions using the Ht Property

With the Contact Regions property defining the geographical extent of each contact's area of influence, the Height Above Contact (Ht) property was used to integrate all the contacts into one map while respecting the influence of each contact on its specific area (Figure 5.38). Height Above Contact is expressed in metres and increases towards the top of the structure from the base of the contact and is defined using the following logical equation:

Ht= If (ContactRegions=1, E-AG1_Ht,
If (ContactRegions=2, E-S1_Ht,
If ContactRegions=3, E-S4_Ht,
If (ContactRegions=4, E-S7_Ht, 0)))) ……..…… (11)

Where:
E-AG1_Ht,
E-S4_Ht,

E-S1_Ht &

E-S7_Ht

are the individual Height Above Contact property maps (Figures 5.34 and 5.35) modelled geometrically using the “Above Contact” method.

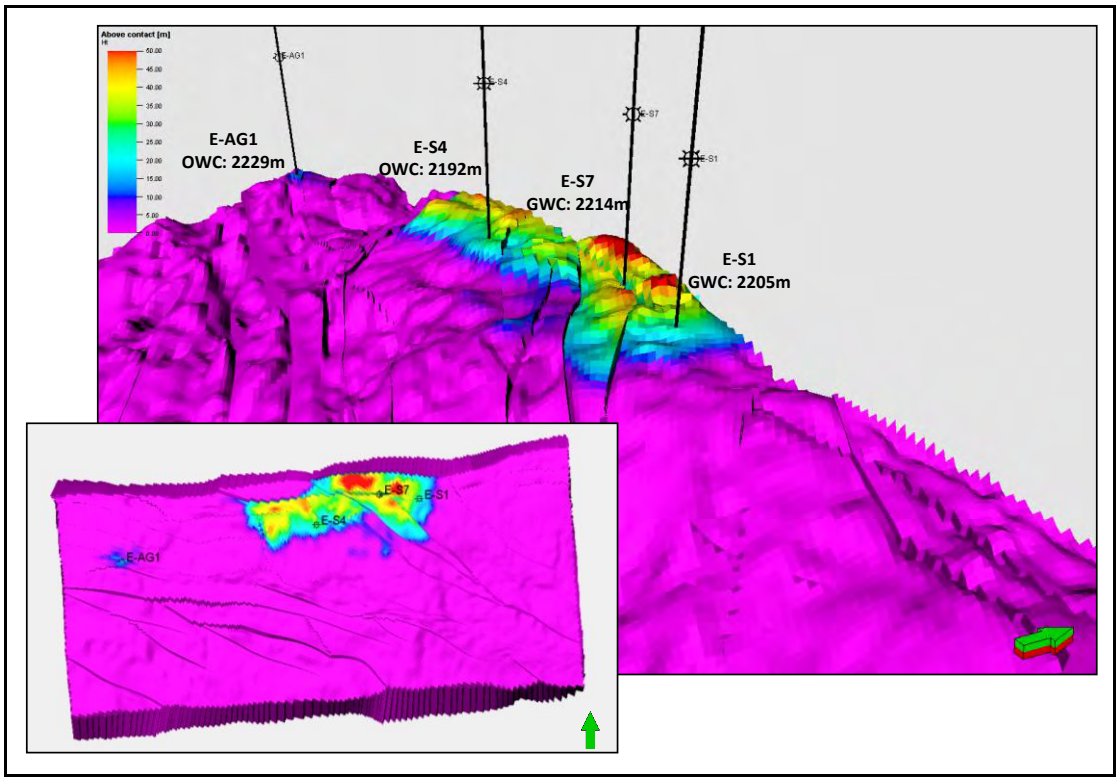

Figure 5.38 Height Above Contact (Ht) property.

Modelling Zone 1: Implementing the J Function

A cross-plot of water saturation (log data) vs Height Above Contact was generated in order to empirically derive the J function equation for each hydrocarbon region (Figure 5.39). The Height Above Contact data from the model was converted to a log in order to plot it correctly with water saturation (Figure 5.40). The cross-plot can be interpreted to have two broad trends corresponding to wells with gas (E-S1 and E-S7) and wells with oil (E-S4 and E-AG1). For each of these broad J Function trends, two J Function equations were applied corresponding to the defined flow zones. Using this thought process, equation 9 was used to calculate the J Function water saturation. The modelled J Function water saturation plotted against height with Flow

Zone Indicator transposed on the data points can be seen in Figure 5.41. The logical equation is given below:

J_Sw= If (ContactRegions = Water Region, (Sw=1), If (ContactRegions = EAG1_ Region Or ContactRegions= ES4_ Region,
If (FZI>=.5, J Function for oil wells, J Function for poor flow),
If (FZI>=.5, J Function for gas wells, J Function for poor flow)))…… (12)
Where:
J_Sw = Water Saturation derived from the J Function &
FZI = Flow Zone Indicator.

The J Function water saturation (J_Sw) was not applied to Modelling Zone 2 (the fluvial section) and therefore at this stage the fluvial section was modelled with a water saturation of 1 using the equation below (Figure 5.42):

J_Sw=If (J_Sw>=1, 1, J_Sw) …… (13)
Where:
J_Sw = Water Saturation derived from the J Function.

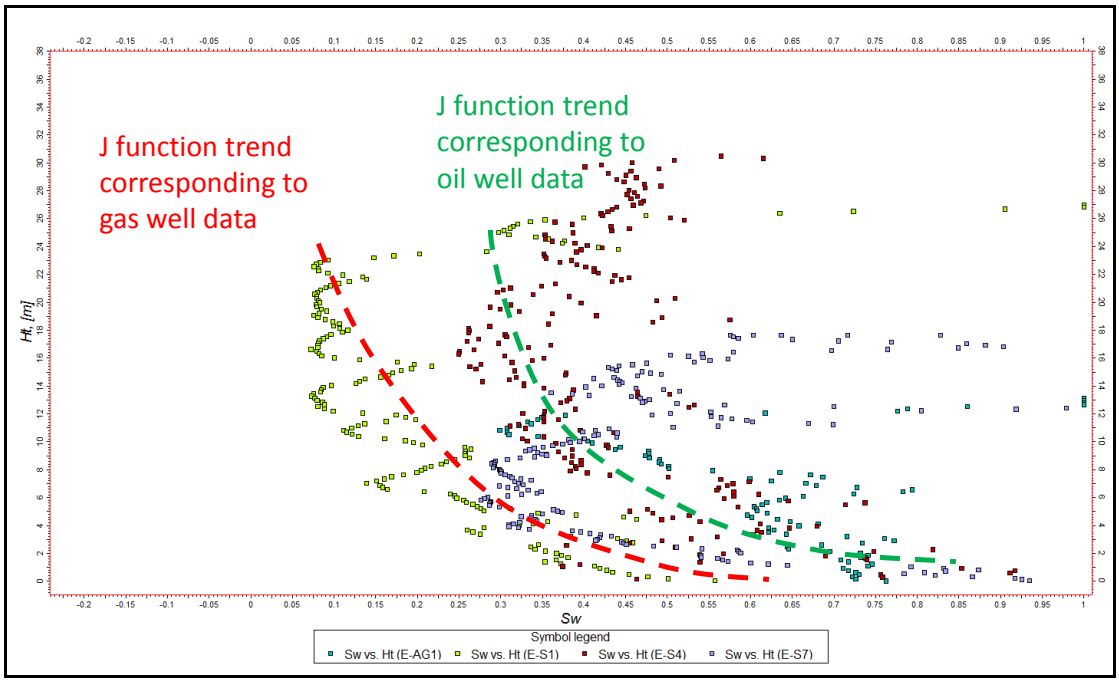

Figure 5.39 Sw (core) vs Height Above Contact cross plot. Two trends can be identified resulting in different J-function equations. This is expected as one is representative of the gas wells (red) while the other is representative of the oil wells (green).

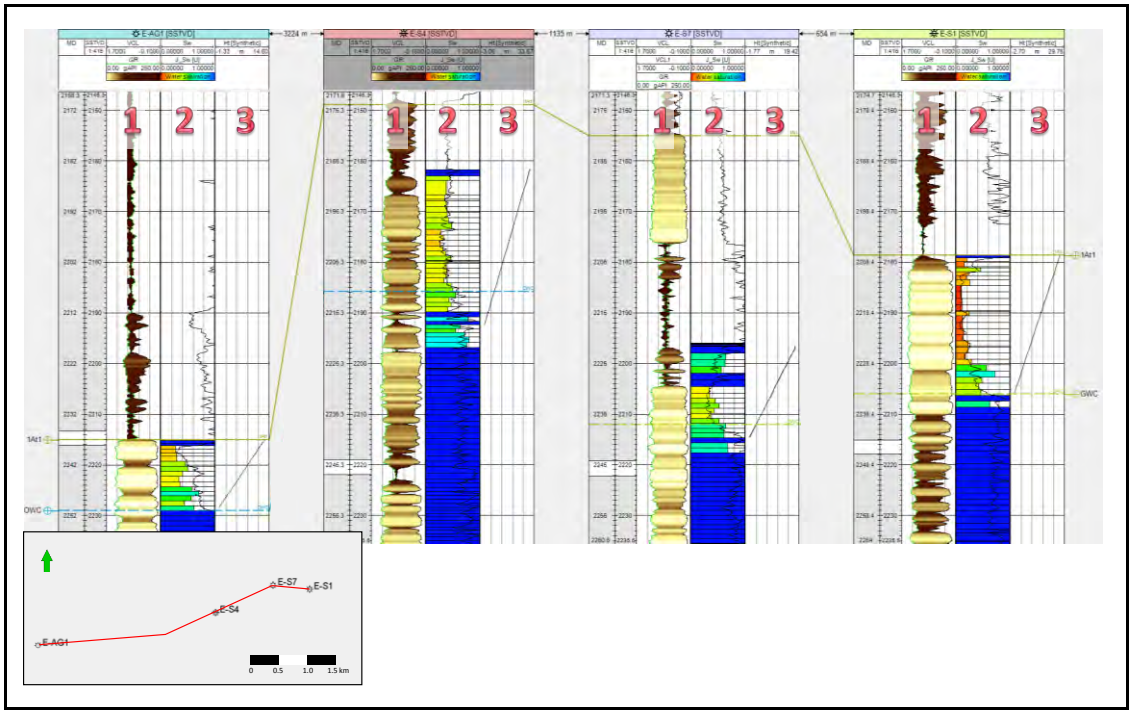

Figure 5.40 Height Above Contact property converted to a log (Track 3). Used as a QC against Sw in order to check that height continues to increase above the contact. The J function Sw is also plotted with log Sw to make sure it is representative of reality.

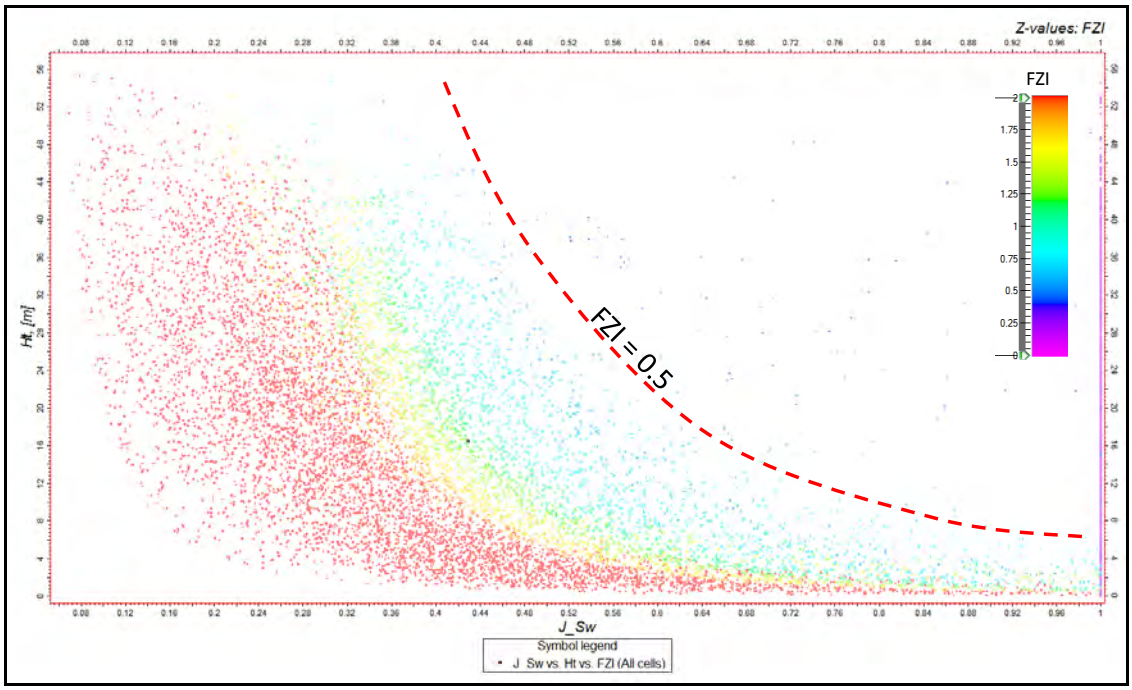

Figure 5.41 J function water saturation vs Height Above Contact with Flow Zone Indicator transposed.

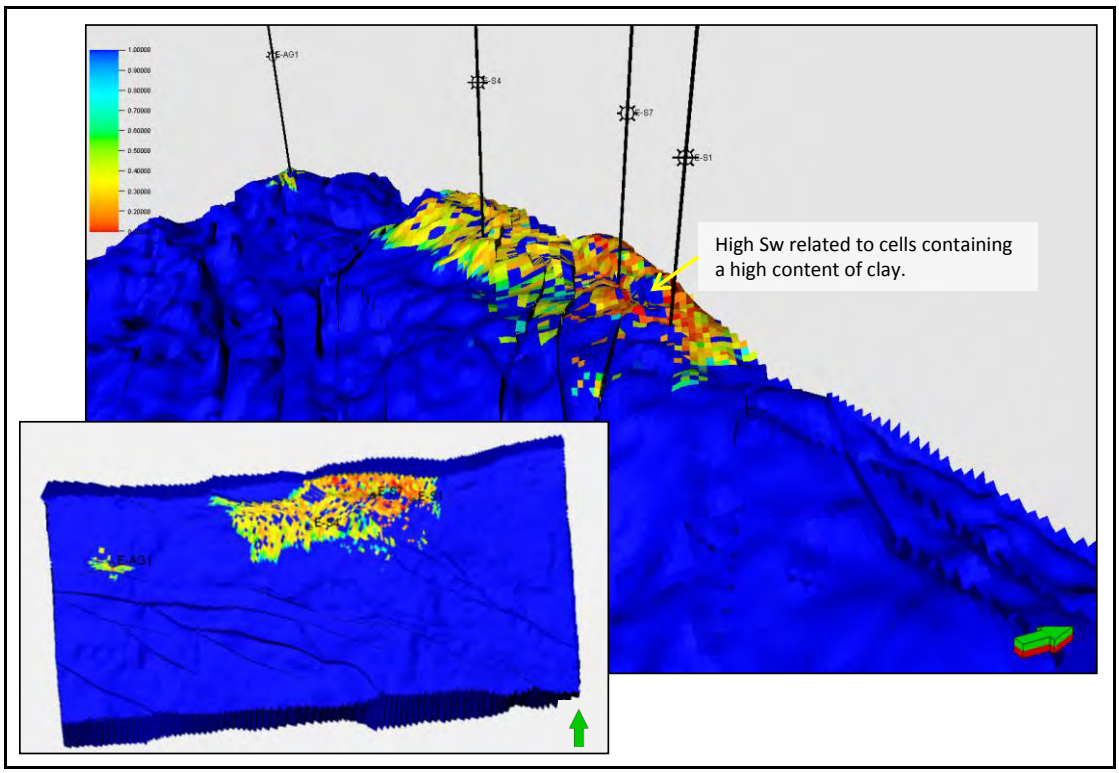

Figure 5.42 J-function water saturation model for Modelling Zone 1 only. Fluvial zone Sw is made to equal one.

Zone 2: Upscaling and Data Analysis

The water saturation log was upscaled using the facies distribution as a bias in order to match low water saturations with reservoir facies and high water saturations with shale facies. Water saturation was averaged arithmetically using the “neighbour cell” cell penetration method.

Data analysis was carried out per facies using a series of transform parameters in order to produce a distribution close to normal where possible. A 3D trend was also added to the transformation process with porosity being used as the trend property. The 3D trend function allows one to rescale the trend property using a user defined trend function.

Modelling Zone 2

Water saturation in Modelling Zone 2 was modelled using the Gaussian Random Function simulation distribution method using an exponential variogram where variogram parameters were the same for all facies groups. The horizontal range in the major and minor trend directions were defined as

1800m and 700m respectively with the major axis having a roughly N-S azimuth (10°). The vertical range used was 1m with a nugget of 0.001.

Merging of Sw and J_Sw

Modelling of the fluvial zone resulted in a water saturation that was stochastically populated. In order to preserve the J Function water saturation defined for Modelling Zone 1 while maintaining the water saturation stochastically modelled for Modelling Zone 2, an equation was formulated to merge both the water saturation properties into a single property (Figure 5.43):

Sw=If (ContactRegions= Water_Region, Sw, J_Sw) ..…….. (14)

Where:
Sw = water saturation for the fluvial zone (Modelling Zone 2)
J_Sw = J function water saturation (Modelling Zone 1).

5.4.6 Net/Gross Ratio (NG)

Petrophysical Log Processing

The net/gross ratio log was calculated based on porosity and permeability cut-offs (Table 2) using the logical equation below:

NG=If (VCL<.37 And PHI>=.07, 1, 0)…….…… (15)

Where:
NG = Net/gross ratio
VCL = Volume of Clay
PHI = Porosity.

Using Equation 5 together with Equation 15 is justified in this case because Equation 5 removes the VCL associated with the total porosity, which is the

negligible amount of clay present within an otherwise clean reservoir. Formula 15 separates between reservoir and non-reservoir (result is 0 or 1) using VCL and porosity cut-offs. This is used to populate the effective porosity in reservoir and not non-reservoir. Using total porosity instead of effective porosity here would over-estimate the result.

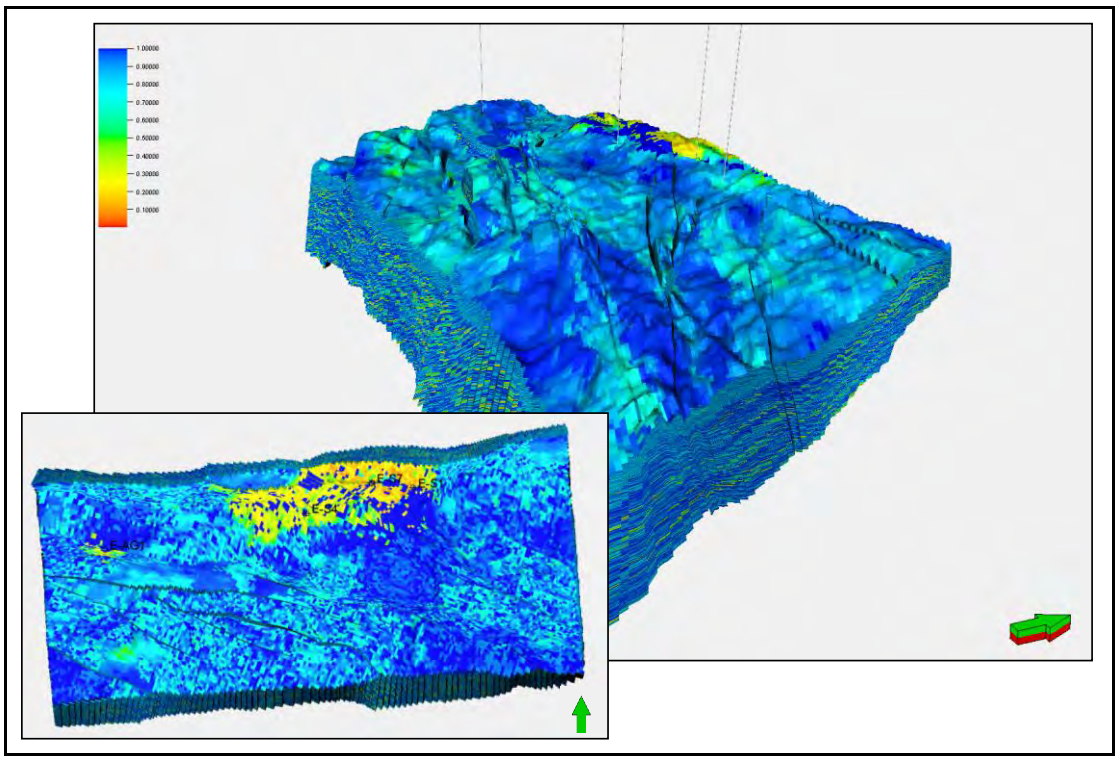

Figure 5.43 J-function water saturation modelled with stochastically populated fluvial zone water saturation.

Upscaling and Data Analysis

Net/gross ratio was averaged arithmetically using the “neighbour cell” cell penetration method without using the facies as a bias. Using facies as a bias for net/gross after it has been used as a bias for porosity will result in an incorrectly reduced hydrocarbon volume when used for volumetric calculations. The effect of using a facies bias during the population of other properties causes the property in question to use the most common facies type within each cell and average the data associated only with the most common facies type while all other facies types are ignored. The net/gross log is a binary log representing reservoir and non-reservoir rocks, and using a bias will result in averages which are either 1 or 0 i.e. 100% reservoir or

100% non-reservoir. Without the facies bias, the ratio between 1 & 0 will be calculated within each cell irrespective of the facies resulting in a representative net/gross property throughout the model.
Data analysis was carried out per zone and per facies and was once again represented by probability curves.

Modelling Zone 1

After the log upscaling, the net/gross property was populated into the model using the porosity as a secondary variable driver for sandstone facies within each zone. A high correlation co-efficient of 99% was chosen in order for the porosity to have a strong impact on the net/gross, resulting in a strong correlation between high porosity values and high net/gross reservoir rocks. Furthermore, it helps to avoid any miss-match between porosity and net/gross and ensures that good porosity will be associated with reservoir rock thus providing a more accurate volumetric calculation.
A Gaussian Random Function simulation distribution method was used for all zones in Modelling Zone 1 using an exponential variogram and was modelled per zone, and except for the Pre-1At1 Estuary Unit zone, all the zones were conditioned to facies. The variogram range for all facies was set at 1200m in the major (E-W) and 600m in the minor (N-S) horizontal directions. The vertical range used was 2m with a nugget of 0.01.

Modelling Zone 2

Permeability in Modelling Zone 2 was also modelled using the Gaussian Random Function simulation distribution method using an exponential variogram with variogram parameters being the same for all facies groups. The horizontal range in the major and minor trend directions were defined as 1200m and 600m respectively with the major axis having a 10° azimuth. The vertical range used was 1m with a nugget of 0.1.

Figures 5.44 and 5.45 show the net/gross model along a cross-section through the main wells and at different stratigraphic levels.

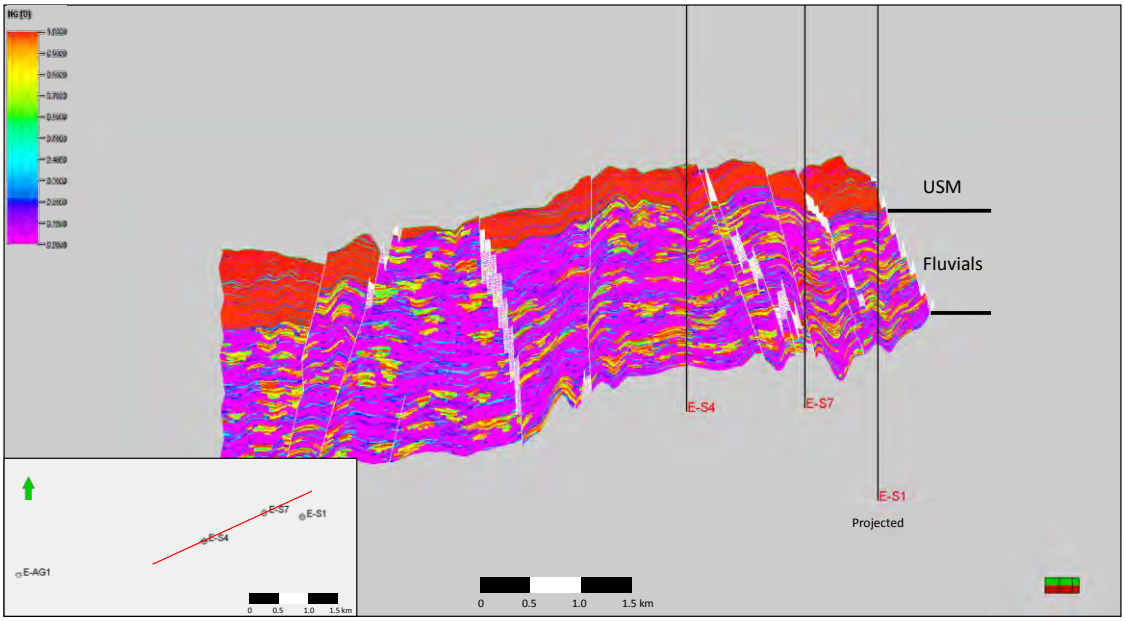

Figure 5.44 Net/gross model: Cross-section through the main wells.

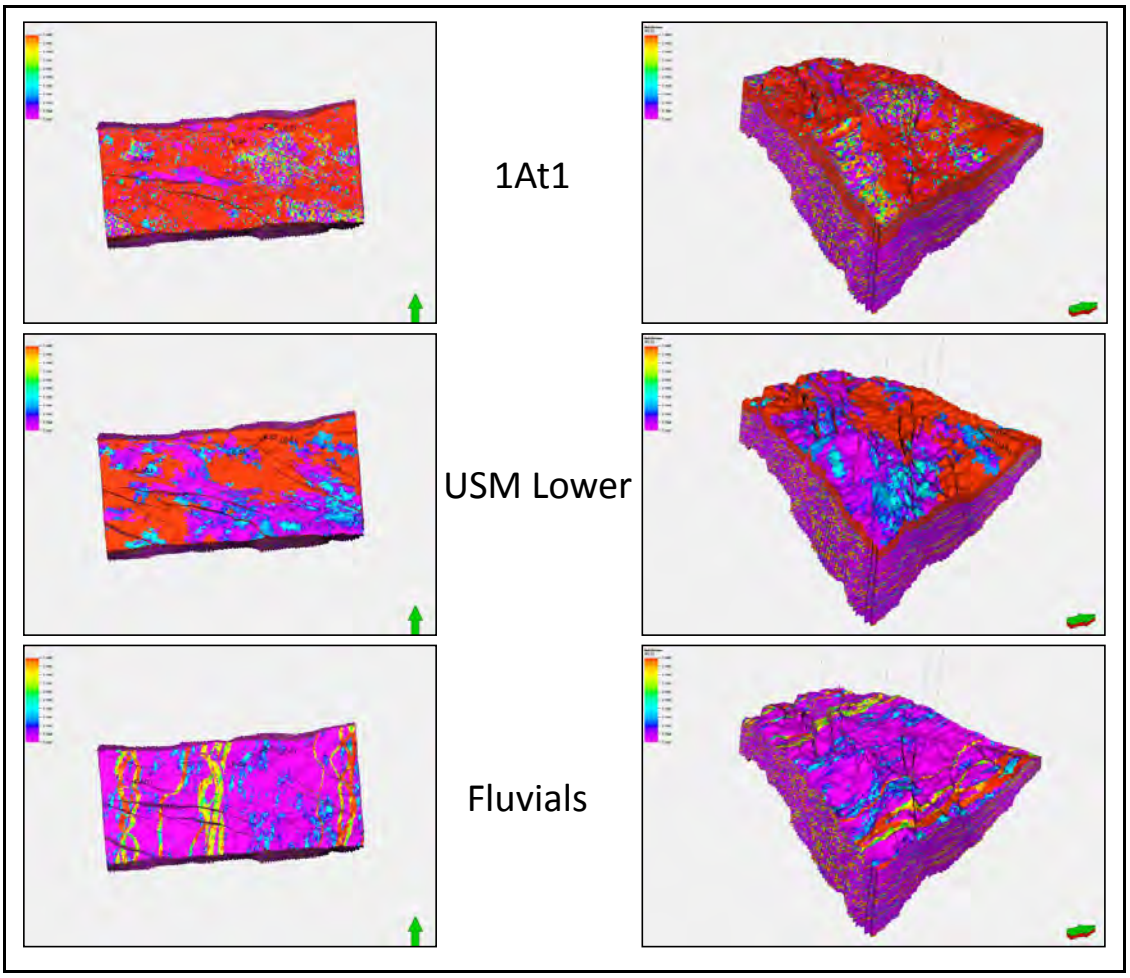

Figure 5.45 Net/gross model shown at different stratigraphic levels.

5.5 Previous Studies Incorporating Modelling of the E-S Field
(These studies were undertaken before the E-S7 well was drilled)

5.5.1 Goodwin and Brown, 1998

Goodwin and Brown (1998) were the first to stochastically model the fluvial interval in the E-S area (they used Roxar Reservoir Management Software (RMS)). Due to the heterogeneous nature of the fluvials, difficulties arose when attempting to calculate the net reservoir, correlating individual sand bodies throughout the field, as well as determining the volume of sandstone connected to a single well. The use of an amplitude map assisted in defining the extent of the fluvials.

They described the fluvial interval as consisting of an upper and lower depositional unit. The upper depositional unit was interpreted as a meandering river system, and the lower unit, having thinner beds and being more interbedded, was described as a braided stream system. Core descriptions were done in order to identify different facies within their related depositional environments. Fielding (1986) showed, using field data, that channel sandstone thicknesses can be empirically related to palaeo-channel depth. Thereafter, Fielding and Crane (1987) used channel width estimates to predict particular depositional environments. A probability distribution of the thickness/width relationship was defined from the average minimum, median and maximum sand thickness and then used to model facies. Analogues proposed by Crane (1982) indicate a higher likelihood to form potential reservoirs corresponding to higher channel deposit proportion (CDP). CDP values between 0.5 and 0.75 relate to thick sandstone bodies, however, the E-S/E-AG area is characterised by a lower average CDP of 0.43 with a wide range (0.22 – 0.70) indicating a large degree of lateral variability. Goodwin and Brown (1998) used triangular distributions to populate the trends and relationships described above into the facies model using three genetic facies: fluvial channel, crevasse splay and flood plain. The petrophysical model was created using a Kriging algorithm conditioned to the

facies, so as to relate better porosity and water saturation to channel sandstones and poorer petrophysical properties to siltstone and claystone facies.

The total GIIP reservoired in the fluvials was calculated to be 335 Bcf.

5.5.2 Fouché et al., 1997

Fouché et al. (1997) carried out an interpretation of the E-S and surrounding fields using the then newly acquired 3D survey. The report details the geophysical work done from the actual seismic interpretation through to structural interpretation, depth conversion and map creation. They have suggested that the fault between E-S1 (gas) and E-S4 (oil) is perfectly sealing based on a theory of gas flushing. They postulated that gas migrating from the east has displaced the oil that may have been present in the E-S1 trap and has continued to move westwards, partly flushing the E-S4 trap (attic gas has been interpreted to exist due to the oil in E-S4 being close to bubble point), bypassing the E-AG1 closure and eventually flushing the E-M structure leaving only an oil rim. Gas present in the fluvials, together with the absence of oil, has been explained by the effect of a younger erosional unconformity cutting through the Upper Shallow Marine into the fluvial section or by migration from the south rather than the east.

A set of probabilistic volumetrics for each of the 3 fields (E-S1, E-S4 and E-AG1) was produced using a Monte Carlo Analysis using a triangular distribution for each of the volumetric parameters i.e. Net/Gross, porosity, water saturation and expansion/shrinkage factors. Water saturation was made semi-dependent on porosity using a 0.75 dependency coefficient.

The P50 hydrocarbon in place has been published as 1.3 and 9 MMbbl for the E-AG1 and E-S4 areas respectively and 28 Bcf for the E-S1 area.

5.5.3 PGS, 2000

This report deals with the evaluation of the E-S field based on the interpretation of the E-S 3-D seismic survey carried out by PGS in 1999/2000.

It focusses on both the Upper Shallow Marine and fluvial intervals and explains the use of log and core data to create a complex zonation scheme from which hydrocarbon volumetrics were calculated.

Using existing RFT (Repeat Formation Test) data, PGS interpreted different hydrocarbon contacts within the E-S field which helps explain the inferred sealing nature of the faults separating the E-S1 block from the E-S4 block.

The deterministic hydrocarbon volumes for the E-S1, E-S4 and E-AG1 areas in the Upper Shallow Marine interval were 26.1 Bcf (GIIP), 6.8 MMbbl (STOOIIP) and 1 MMbbl (STOOIIP) respectively (A probabilistic approach was also taken but will not be quoted here; the P50 volumes derived from the probabilistic approach closely resemble the deterministic volumes).

The fluvial interval (referred to as Zone 5 by PGS in their report) was divided into 14 individual zones based mainly on gamma ray log character together with density and neutron logs. The assumption made is that this zonation model can be applied to the whole field making each zone continuous across a segment without any erosional effect (this assumption carries a high element of risk). The fluvial section is postulated to be more structurally complex than the Upper Shallow Marine interval with a larger number of faults having greater throws.

Within the fluvial interval, the concept of a series of stacked hydrocarbon columns was introduced, contrary to the previous single connected column interpretation. The Repeat Formation Test (RFT) data shows that aquifer points for all the wells do not fall on the same trend, leading to the conclusion that each fluvial sand has its own pressure regime and hydrocarbon contact, and they are therefore isolated between the existing wells. Deterministic GIIP for the fluvial interval in the E-S1, E-S4 and E-AG1 segments is 49, 105 and 69.3 Bcf respectively.

5.5.4 Frewin et al., 2001

Frewin et al. (2001) aimed to compare/review and validate the results produced by the Goodwin and Brown (1998) and PGS (2000) studies and

assess the justification of a commercial development plan. In doing so, a revised static model based on the model created by Goodwin and Brown (1998) was created to address the uncertainties in the fluvial volumetrics.

The hydrocarbon contacts (based on RFT data) as well as the volumetrics for the Upper Shallow Marine interval are similar in both the Goodwin and Brown (1998) and PGS (2000) studies and therefore a re-calculation of the Upper Shallow Marine volumetrics was not warranted. Frewin et al. (2001) did however question the validity of up-dip attic gas in the E-S4 region, indicating that the actual bubble point of the oil could not be determined with confidence.

The fluvial volumetrics were conversely markedly different. The approaches taken in the studies were different, with PGS (2000) using a regional zonation model with gas-water contact or Gas Down To values derived from Repeat Formation Test (RFT), while Goodwin and Brown (1998) used a static model approach using a regional gas-water contact. Through a geophysical investigation it was found that Goodwin and Brown (1998) mapped Horizon V as being the Base Lower Shallow Marine (BLSM) while PGS (2000) interpreted it as being the Top Lower Shallow Marine (TLSM), resulting in a 90m difference in the fluvial interval's average gross thickness. The way in which the field extent was defined was also different, and in fact, it is seen as the main contributing factor to the large volume difference between the two studies. While PGS (2000) used separate contacts for each of the wells, Goodwin and Brown (1998) used a regional contact coupled with the lateral extent of the amplitude map which resulted in a much bigger area. Frewin et al. (2001) have also highlighted the risk of assuming that the fluvial channels are connected or continuous between wells. With the data available Frewin et al. (2001) have also suggested that PGS's (2000) regional correlation of sand and the multi-zonation is unrealistic thus raising doubts over their volumetric calculations.

In reviewing the Goodwin and Brown (1998) static model, Frewin et al. (2001) found some parts of the workflow which they did not agree with. These

included the extensive field area definition, inconsistent petrophysical modelling and using an amplitude map to trend sandstones which did not agree with the structural model. Using this 1998 model as a base, they revised the model to produce various stochastic geological models reflecting minimum, most-likely and maximum scenarios of the reservoir parameters. In doing so, fifty realisations of each property were run.

The model was built incorporating five major faults previously used by Goodwin and Brown (1998). The cells in the model were set at 100 * 100m with a height of 2.5m. The layering in the model was built from the top down and was confined to only one zone due to consistency of facies and sedimentary characteristics within the entire fluvial interval. Borehole data (petrophysical logs) were upscaled with a facies bias using the arithmetic averaging method.

Facies parameters and relationships were based directly on those modelled by Goodwin and Brown (1998), keeping facies volume percentages fixed for all realisations i.e. 35% reservoir facies (channel sandstones) and 20% splay (floodplain facies filled the rest). A rule called “erode before reject” (in the Roxar Reservoir Management Software) was applied which allows reservoir facies to erode (or replace) or be eroded by splay facies during the modelling process. The parameters used in the facies modelling are tabled below.

Porosity and water saturation were modelled using a variogram and univariate statistics. The variograms together with the data histograms were defined in the Data Analysis phase and applied to the fifty facies realisations. Tables 10 and 11 summarise the parameters defined for the fluvial bodies.

Although fifty realisations were processed for the facies model, Frewin et al. (2001) highlighted the need to attribute a stochastic component to other elements of the volumetric calculation e.g. the bulk rock volume, as well as to quantitatively evaluate other uncertainties affecting the model (different sized polygons used in the different studies and different gas-water contacts) and therefore describe this model as being deterministic rather than probabilistic.

The volume of gas in the fluvial interval was cited for the entire polygon area and was calculated as minimum: 108 Bcf, most likely: 116 Bcf and maximum: 129 Bcf. Fluvials in the E-AG1 area were not considered in the economical evaluation of this study due to the disseminated and anomalous nature of the amplitude anomaly when compared to the defined trend on the map. The economic evaluation yielded a negative NPV using a gas price of $1.50/Mscf. It was recommended that an appraisal well be drilled in order to better characterize the fluvial reservoir.

Channel Sandstone				
Parameter	**Distribution**	**Minimum**	**Mid**	**Maximum**
Orientation	Triangular	280	320	370
Thickness	Triangular	2.5	6	20
Amplitude	Expression	3 × Width		
Wavelength	Expression	5 × Width		
Width	Expression	12.1 × Thickness		

Table 10: Summary of parameters for channel sandstone characteristics (Frewin et al., 2001).

Splay				
Parameter	**Distribution**	**Minimum**	**Mid**	**Maximum**
Width	Triangular	50	500	5000
Thickness	Triangular	.25	3	13
Length	Expression	1.5 × Width		

Table 11: Summary of parameters for splay characteristics (Frewin et al., 2001).

5.5.5 Frewin, 2005

The E-S accumulation was identified as an integral element of the South Coast Gas Development Project. The project required that representative reservoir models be built for proper reservoir characterization and thereafter upscaled for reservoir simulation and economic sensitivity studies. Frewin

(2005) built three geological scale models; representing the downside, most likely and upside case; using a 25m × 25m grid size and 259 layers, and three simulation scale models using a 100m × 100m grid size and 48 layers. The number of layers was optimally chosen in order to capture the heterogeneity and modelled petrophysical parameters

This study was done in the Petrel modelling software and horizon and fault data were imported from the previous Roxar Reservoir Management Software model. Although not many changes were made with regard to the Upper Shallow Marine interval, this new study aimed to combine the Upper Shallow Marine and Fluvial into a single static model.

In order to explain the gas present in E-S1 with the absence of gas in E-S5, a stratigraphic break is assumed to occur between the two wells. The positioning of this break is also tested at different positions corresponding to multiple field extents representing the minimum (downside) to maximum (upside) model scenarios, although the exact location is uncertain.

The facies logs created for each well were upscaled using the “most-of” method and the facies property was then populated in the model using object modelling. For the Upper Shallow Marine, shale objects were modelled into a background of sand assuming a shale percentage for the most likely case to be slightly higher than what was seen in the logs (the log shale percentage was used in the upside case). This takes into account the high possibility, which is most likely the reality, to encounter shale bodies in-between the existing wells. For modelling the fluvial zone, sand channels and crevasse splays were modelled into a background of shale.

The porosity property was modelled using Sequential Gaussian simulation (SGS) and was biased to the facies model. Shale porosity was made to equal zero and absolute values from the input logs were used to define the most-likely porosity model case. Porosity distribution for the upside and downside cases were controlled by an output distribution. The permeability and water saturation models were defined using transforms using the height above the contact as well as field extent polygons to constrain the modelling.

The gas in-place estimates based on the geological grid for the Upper Shallow Marine downside, most likely and upside cases are 28, 32 and 41 Bcf respectively; while that of the fluvial interval are 20, 47 and 76 Bcf respectively. The volumes calculated using the simulation grid were very similar to those mentioned above.

5.6 Volumetric Results from this Study and Discussion

The hydrocarbon volumetrics were calculated for each contact region using their specific hydrocarbon contacts (Table 12).

Contact Region Name	Contact Type	Contact Depth
E-AG1 Zone	Oil-water contact	-2228m
E-S1 Zone	Gas-water contact	-2205m
E-S4 Zone	Oil-water contact	-2192m
E-S7 Zone	Gas-water contact	-2212m

Table 12: Summary of hydrocarbon contacts in the E-S field and surrounding.

The cumulative in-place gas volume for the E-S1 and E-S7 contact regions was calculated to be 16.8 Bscf using porosity and hydrocarbon saturation from the model. The average porosity and water saturation being 13% and 70% respectively is consistent with data from logs. Using a gas recovery factor of 75% together with a gas expansion factor (Bg) of 170 the recoverable gas was calculated to be 12.6 Bscf (both the gas expansion factor and recovery factor values are based on data from existing fields in the Bredasdorp Basin).

The E-AG1 contact region has a very low oil volume (27 Mbbl) and therefore will not be considered as a future development target.

The in-place oil volume in the E-S4 region was calculated to be 11.6 MMbbl. A recovery factor of 11%, based on historical data (Willis et al., 1987), was used together with an oil shrinkage factor (Bo) of 1.3 to produce a recoverable oil volume of 1.3 MMbbl. The recovery factor does seem to be quite low, and should therefore be re-assessed. If the recovery factor is found to be correct, secondary stimulation methods would need to be investigated in order to make the E-S4 region a viable prospect. The average porosity in the E-S4 reservoir is 13.3% and the average hydrocarbon saturation is 59.6%.

Table 13 below summarises the volumetric results calculated for the individual contact regions.

		Contact Regions			
GAS	**OIL**	**E-S1**	**E-S7**	**E-S4**	**E-AG1**
Bulk Rock Volume (MMm^3)		26	12	36	1
Net Rock Volume (MMm^3)		22	8	30	1
Porosity (%)		13.6	12.5	13.3	
Permeability (mD)					
Hydrocarbon Saturation (%)		69.8	70.8	59.6	
Bg/Bo (%)		170	170	1.3	1.3
GIIP (Bscf)		12.508	4.307		
Gas recoverable (Bscf)		9.381	3.231		
STOIIP (MMbbl)				11.62	0.25
Oil recoverable (MMbbl)				1.3	0.027
Recovery Factor (%)		75	75	11	11

Table 13: Summary of hydrocarbon volumetrics in the E-S field and surrounding.

Volumetrics were not calculated for the fluvial succession (Modelling Zone 2). Previous studies have published large volumes for the fluvials in the field based on many different assumptions. The fact remains that the uncertainty is high, and considering the confined extent of the prospective channel reservoirs together with the vertical stacking pattern which shows there to be mainly discrete channels at different levels, it would be difficult to predict with confidence the position of the channels. Consequently, the challenge would be to design a cost effective and viable development plan to drain the hydrocarbon volume associated with these discrete bodies.

The Upper Shallow Marine gas volume calculated in this study can be described as being slightly more pessimistic when compared to previous studies. This could be attributed to differences in the structural as well as marker interpretation which is something unique to every interpreter. It is

possible that the structural interpretation favoured a bigger structure over the E-S4 area resulting in a slightly higher in-place oil volume. In addition, the use of a J function water saturation instead of the direct population of log water saturation could also have affected the gas volumes calculated in this study.

The higher oil-in-place volume could lead to a shift in focus from historically wanting to develop the gas in the E-S field to now primarily making the field an oil development. This would also provide higher revenues due to the more favourable economics of oil over gas.

The table below summarises and compares in place volumes from previous studies with the current study.

	USM		FLUVIAL	
	OIL (MMbbl)	GAS (Bscf)	OIL (MMbbl)	GAS (Bscf)
This Study	11.87	16.8		
Goodwin and Brown (1998)				335
Fouche et al. (1997) p50	10.3	28		
PGS (2001)	7.8	26.1		223.3
Frewin et al. (2001) most likely				116
Frewin (2005) most likely		32		47

Table 14: Summary and comparison of in-place hydrocarbon volumetrics in the E-S field and surrounding, from different studies.

6 FAULT-SEAL ANALYSIS

6.1 Introduction to Fault-Seal and Literature Review

Reservoir compartmentalisation can be described as “the segregation of a petroleum accumulation into a number of individual fluid/pressure compartments” and “(compartmentalisation) occurs when flow is prevented across ‘sealed’ boundaries in the reservoir” (Jolley et al., 2010; p1).
Faults play an integral part in forming hydrocarbon traps. The sealing nature of these discontinuities is the main attribute that leads to the trapping of hydrocarbons in a fault-trapped petroleum system. Understanding fault-seal and its effect on fluids is important when evaluating the viability of any hydrocarbon prospect. The major issue related to evaluating fault seals is that the actual sealing nature of the fault is not apparent by looking at any readily available data (at least in oil field terms) related to the physical architecture or properties of the fault itself. The most common indicator is usually fluid behaviour either side of the fault in question. Recognising a fault seal could come from noticing varying fluid contacts or differing pore pressure measurements in adjacent compartments or blocks (Yielding et al., 2010). Fault rock is a term used to describe the rock which forms within the actual fault zone and consists of rock fragments and grains of varying sizes which are representative of the stratigraphy crossed by the fault.

From a broad perspective, seals can either be described as being *static* or *dynamic*. Static seals are regarded as completely sealing being able to seal entirely over geological time, while dynamic seals are very low permeability baffles which allow fluids to flow and pressures to equilibrate across them, albeit very slowly, over geological time, but act as significant seals over production time (Jolley et al., 2010). Dynamic seals are primarily controlled by the permeability and thickness of the fault rock whilst static seals are governed by capillary properties (Yielding et al., 2010). The importance of understanding the impact of fault seal and compartmentalisation has really

come to the fore in recent times. The mechanical evolution of a field over production time versus the state of the field before drilling it, and understanding and evaluating this change, is something that is often overlooked (Fox and Bowman, 2010).

Fault seals can also be more specifically defined as being either juxtaposition seals or reservoir-reservoir seals. Juxtaposition seals occur when reservoir rock is positioned against low permeability rock e.g. sand against shale. Reservoir-reservoir seals can be divided into membrane seals and hydraulic seals (Yielding et al., 1997). Membrane seals are controlled by the capillary entry pressure of the seal rock. This is the minimum pressure required to push hydrocarbons into, and water out of a rock (or for hydrocarbons to pass through the easiest pathway in the rock). In other words, sealing will occur as long as the buoyancy pressure of the hydrocarbon phase does not exceed the capillary entry pressure associated with the fault rock (Ingram et al., 1997). The capillary entry pressure is dependent on pore-throat size, and in general, the smaller the pore throat size, the higher the capillary entry pressure needed for seal failure to occur, corresponding to larger hydrocarbon columns that can potentially be supported (Bretan, et al., 2003). A membrane seal will hold a hydrocarbon column measured from the free-water level (FWL) up to a point where the capillary pressure is equal to the capillary threshold pressure (Cerveny et al., 2004; Figure 6.1).
A Hydraulic seal can be said to be breached when the capillary entry pressure is greater than the rock strength causing the seal to rupture.
Where reservoir-reservoir relationships exist across a fault zone, the sealing nature of these faults largely depends upon the fault rock properties which in turn are dependent upon the rocks present across the different stratigraphic intervals. Cerveny et al. (2004) have documented numerous factors which affect fault rock properties and a fault's ability to seal. These include the local facies distribution, reservoir fluid types and saturations, pressure differentials across faults and juxtapositions across faults.

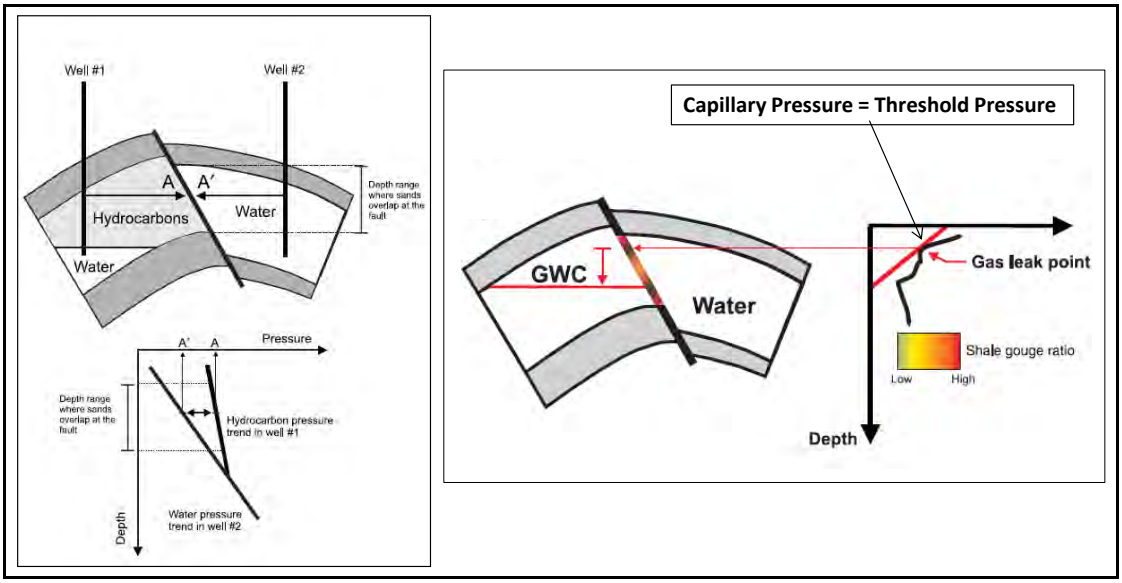

Figure 6.1 The pressure differential across a fault or capillary pressure will determine the hydrocarbon column height. A fault will leak at the point where capillary pressure is equal to the threshold pressure of the fault rock (after Bretan et al., 2003).

Different fault rocks form under different deformation conditions, and their propensity to seal is related to these conditions and also lithological factors, the main one being clay content. It has been identified that a strong relationship exists between fault rock clay content and the sealing capacity of a fault; and most algorithms used to calculate fault seal use this information as input variables (Jolley et al., 2010). Fault rocks can be classified based on their clay content and range from those formed by the interaction of quartz-rich lithologies to phyllosilicate-framework fault rocks and to clay smear series with increasing clay content (RDR, 2013 & Cerveny el al. 2004). A fault cutting through different stratigraphic units may incorporate different lithologies into the fault zone (RDR, 2013). When the stratigraphy is dominated by ductile clay layers, the movement along the fault zone is likely to form clay/shale smears. These smears form a low permeability barrier along a fault zone connecting the source layer either side of the fault.

In more brittle formations (well consolidated or cemented), the fault rock consists of fractured crushed material which forms a heterogeneous gouge. The sealing capability is driven by the content of shale or clay in this gouge.

Equations such as the Clay Smear Factor (CSF; used in environments dominated by ductile clay layers) and the Shale Gouge Ratio (SGR; used in environments where brittle formations dominate) have been developed to measure fault-seal quantitatively.

The Clay Smear Factor determines the amount of throw relative to the shale bed thickness for which a shale smear is continuous (RDR, 2013). The Clay Smear Factor equation is defined by the fault throw divided by the bed thickness, and as long as the Clay Smear Factor is smaller than one, the clay smear will be continuous.

The Shale Gouge Ratio calculates the average clay moving past a single point on a fault. The method assumes uniform mixing of clays within a fault from all lithologies cut by that particular fault.

6.2 Fault-Seal Workflow

The fault-seal analysis was done in the Petrel software using the Rock Deformation Research (RDR) structural and fault analysis module. The process was carried out using all the faults in the model but the investigation was limited to the faults separating the E-S1 and E-S4 blocks. The first step was to apply the relevant modelled properties to the fault planes in the model. Then the clay content was calculated using one of the clay mixing models and their specific equations (Shale Gouge Ratio, Clay Smear Factor, etc.). Thereafter, hydrocarbon column heights and hydrocarbon contact depths were calculated as separate properties in order to evaluate the potential of sealing or leaking at each grid cell along the fault plane.

The workflow carried out was based on that taught by Rock Deformation Research and is detailed below under the relevant processes.

6.2.1 Fault Property Analysis

6.2.1.1 Volume of Clay (VCL)

The fault seal analysis process uses data from the geocellular model already created. The Volume of Clay property from the cells in contact with the fault

planes (either side of the faults) was extracted and assigned to the adjacent position on the fault plane. Three separate properties were created simultaneously during this process. The actual VCL property either side of the fault accounted for two of these properties while another calculation called a “maximum cross-fault calculation” accounted for the third (Figure 6.2). This third calculation provides the maximum value within the grid cells considering values both sides of a particular fault. In other words, it takes the higher of the two Volume of Clay values either side of the fault. This process provides an understanding of the lithological compositions which are in contact with the fault together with the nature of the juxtapositions and is the first step towards clay content prediction in the fault zone (or fault rock).

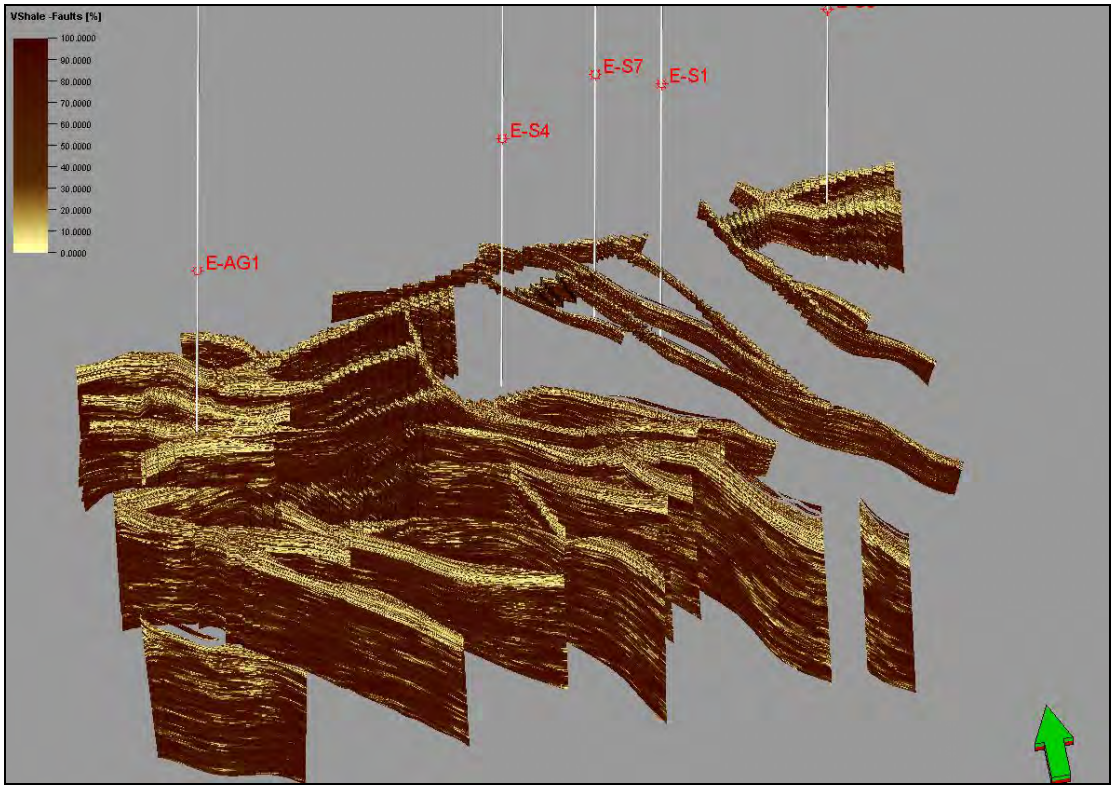

Figure 6.2 Volume of Clay property distributed along all fault planes. Display shows the “maximum cross-fault calculation”.

6.2.1.2 Fault Clay Content Prediction

This process involves measuring the clay content of the faults using a choice of different methods and equations. The method used is “Clay from grid property model”. This method uses a Volume of Clay (VCL) property from the 3D grid together with the variation in displacement along the faults, via clay-

mixing (Shale Gouge Ratio) or clay-smearing models (Clay Smear Factor); in order to predict fault clay content.

The Shale Gouge Ratio clay mixing model was chosen to govern this calculation and together with the VCL property, a Shale Gouge Ratio property across the fault planes was produced (Figure 6.3). The choice of the Shale Gouge Ratio over that of the Clay Smear Factor mixing model was based on the knowledge that the reservoir rocks and the interbedded shales are hard and brittle.

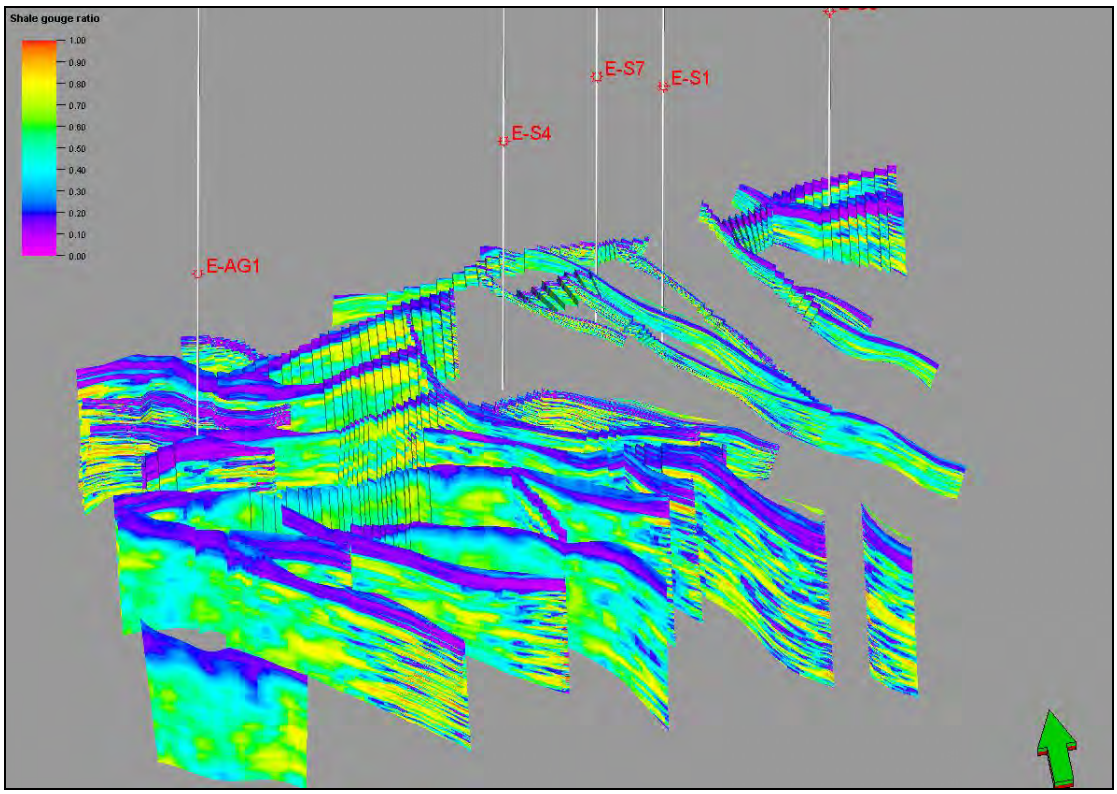

Figure 6.3 Shale Gouge Ratio property distributed along all fault planes.

6.2.1.3 Column Height Prediction and Contact Depth

The column height prediction process is essentially a seal capacity calculation. Using the clay content prediction from the previous step, in this case Shale Gouge Ratio, together with threshold pressure modelled simultaneously during this process (Figure 6.4), a column height property is generated giving a value for the maximum possible column height of hydrocarbon, supported at every cell in the fault plane.

The process used the Shale Gouge Ratio property as an input to represent the fault clay content and distribution. With regard to the threshold pressure, two options are available. Estimating threshold pressure from data gathered from actual core samples would be ideal as the relationship between fluids, clay content and pressures are analysed on field calibrated data in the area of study. This data was not available for this study and an alternative approach was taken. Maximum column height was calculated using a global multi-sample trend of clay content and threshold pressure. In this study, the Bretan et al. (2003) global equation/trend was used due to it requiring less data than the Sperrevik et al. (2002) equation/trend (these are the two options provided by the software). Bretan et al. (2003) have explained the use of seal failure envelopes which relate threshold pressure or across-fault pressure difference to Shale Gouge Ratio based on varying burial depths. The resultant column height property can be seen in Figure 6.5.

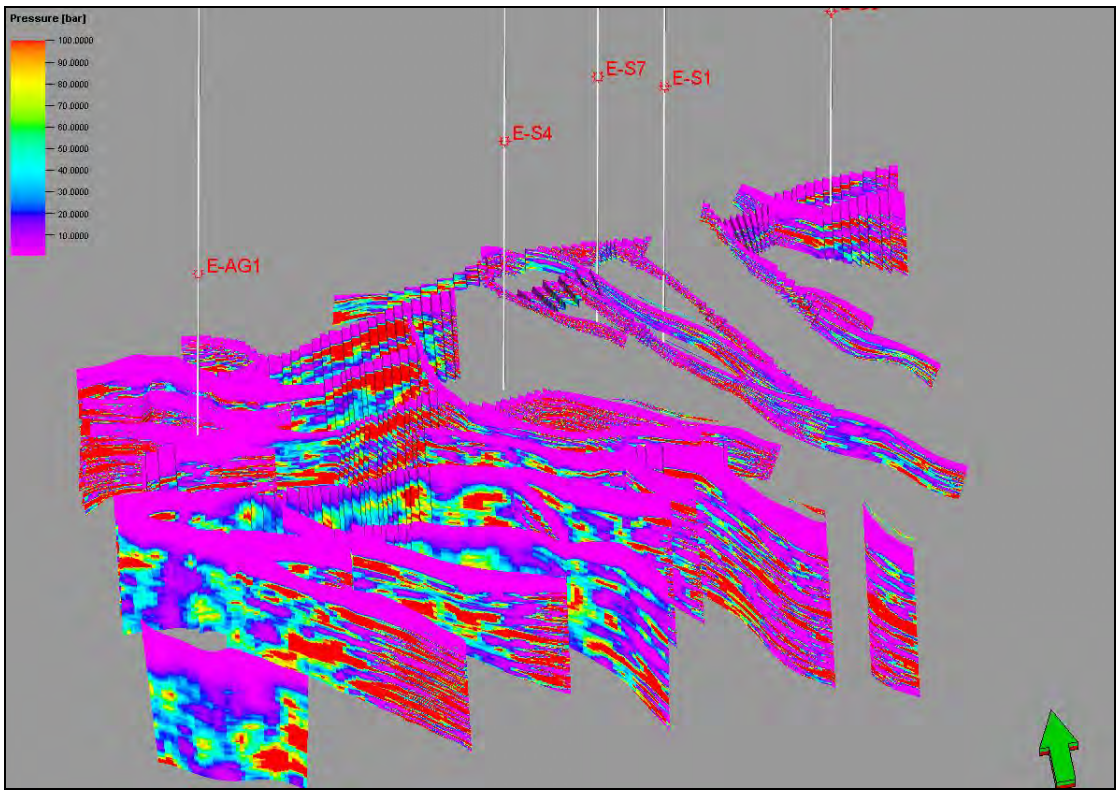

Figure 6.4 Threshold Pressure property distributed along all fault planes.

The other property which is a product of this process is contact depth. Contact depth refers to the theoretical height of the hydrocarbon column at

every cell along the fault plane. Bretan et al. (2003) have shown how the hydrocarbon column can be calculated using density data for the related fluids (at reservoir conditions) together with the across-fault pressure difference (derived from the Shale Gouge Ratio relationship). The contact depth property highlights leak points along each (Figure 6.6).

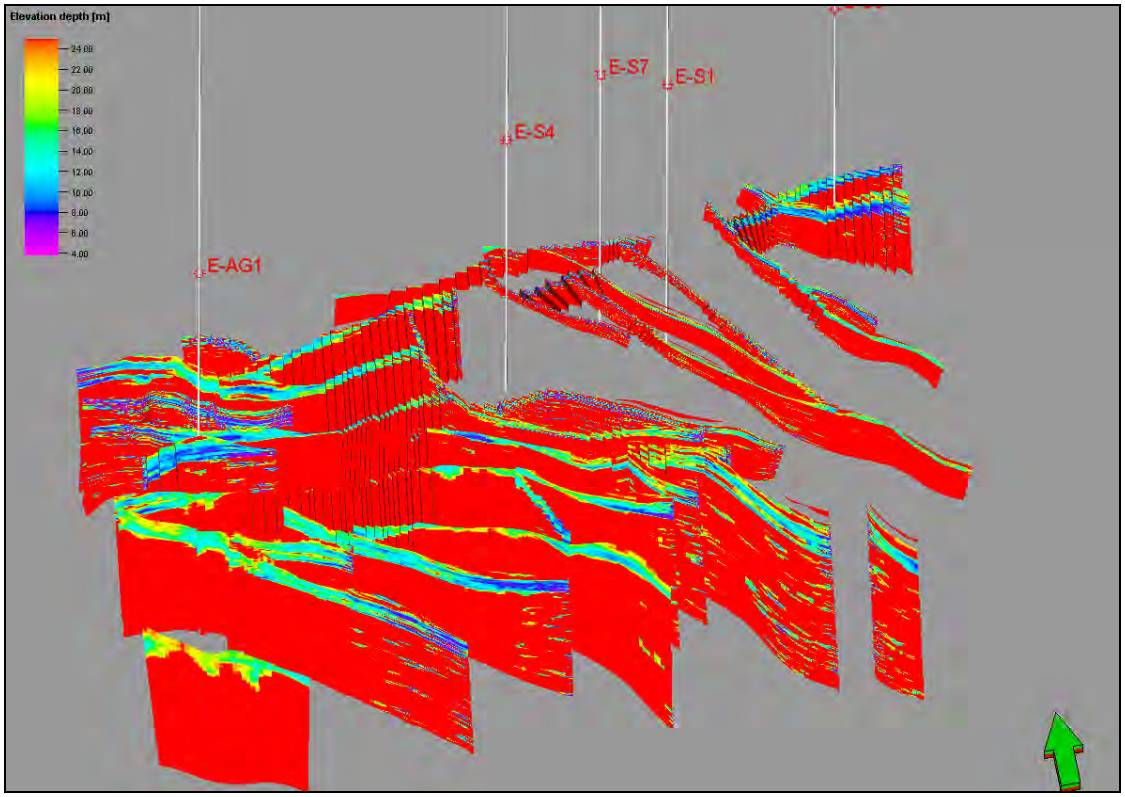

Figure 6.5 Column height property distributed along all fault planes.

As mentioned above, densities of fluid, both hydrocarbon and water, are needed to carry out the calculation. The density of water in this reservoir was calculated to be 0.98 g/cc (using a salinity of 25000ppm; Davies, 1997). From the PVT (pressure, volume and temperature) analysis, the gas specific gravity value relative to air was measured to be 0.654 (Flopetrol Johnston, 1984). This was converted to 0.13 g/cc at reservoir conditions using a bottom hole temperature of 100°C, a reservoir pressure of 3200 psia and a molecular weight of gas of 19.2 g/mol (Flopetrol Johnston, 1984).

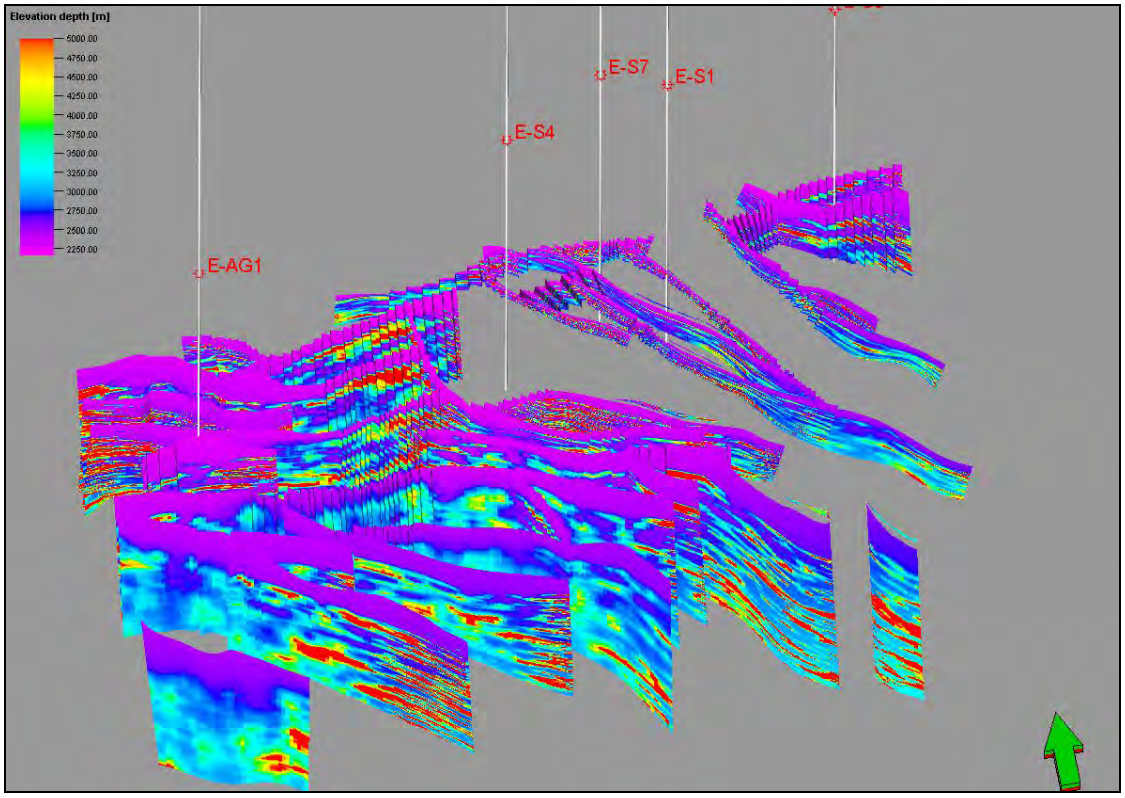

Figure 6.6 Contact depth property distributed along all fault planes.

6.3 Fault-Seal Results and Discussion

Analysing the results of the fault properties generated through the fault seal analysis, reveals that the faults separating the E-S1 and E-S4 compartments (Fault 8 & 10) are not completely sealing. A closer look at all the calculated fault properties suggests that hydrocarbons will leak through “open” areas along the fault plane.

The Volume of Clay (VCL; maximum cross fault calculation) property (Figure 6.7) displays a high density of sand-sand juxtapositions above the hydrocarbon-water contact and close to the crest of the structure or the top of the faults (the crest of the structure corresponds to the top of the faults). This is not a direct indicator of whether faults seal or not, but in this case it provides early signs for possible non-sealing properties.

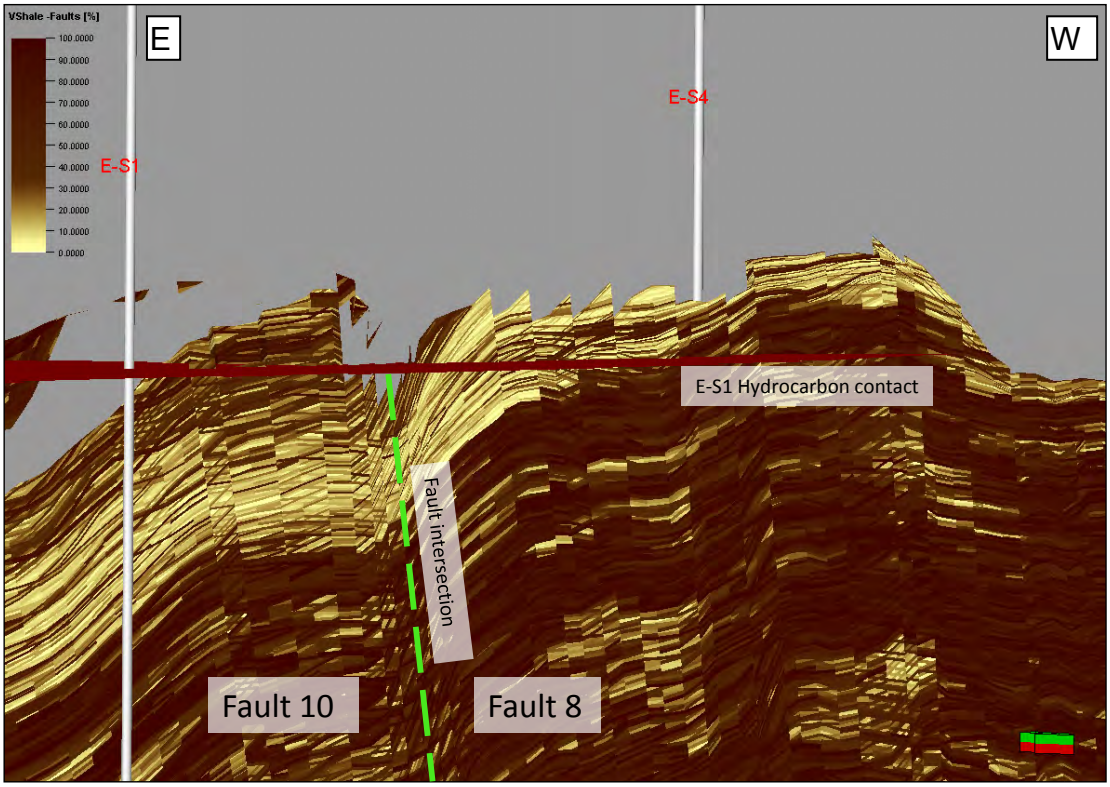

Figure 6.7 Volume of Clay property distributed along fault 8 and 10.

The Shale Gouge Ratio property (Figure 6.8) further supports a high sand presence near the crest, either side of the fault. Values of very low Shale Gouge Ratio; 0.1-0.2; are noted in this zone, further highlighting possible

points for hydrocarbon leakage. Like the VCL property, this is not a direct indicator of fault-seal, but with such low Shale Gouge Ratio values, very low threshold pressures (less than 1 bar) will still cause the faults to leak.

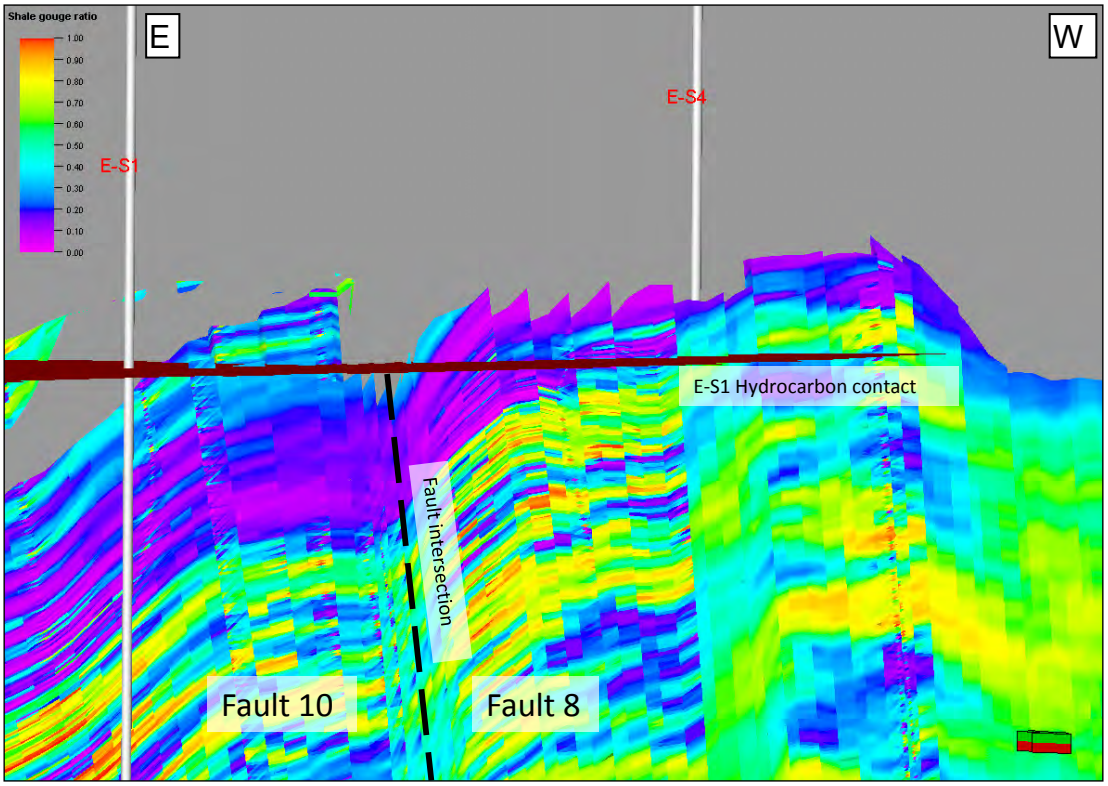

Figure 6.8 Shale Gouge Ratio property distributed along fault 8 and 10.

Threshold pressures above the hydrocarbon contact are seen to be low. The threshold pressure property shows that the majority of data values are greater than 1 bar (Figure 6.9). Furthermore, in Figure 6.10, all pressure values above 0.1 bar are represented by colours ranging from dark blue towards the warmer spectrum. At the top of the faults threshold pressures reach 9-10 bar. Threshold pressures of this magnitude coupled with low Shale Gouge Ratio values of 10-20% show that these faults have a high potential to leak (Figure 6.11; Bretan et al., 2003).

Both column height and contact depth properties further support the view that the studied faults are not completely sealing from a perspective of fault rock clay content, and both highlight the top of the faults as being the likely leak point. Potential column heights are seen to be as low as 5m (dark blue cells in Figure 6.12) and contact depths have values that are less than the existing

hydrocarbon contact (i.e. less than 2205m, indicated by dark blue to purple colours in Figure 6.13). In other words, these cells or positions on the fault plane are unable to hold the column of hydrocarbon controlled by the existing E-S1 contact. Having highlighted the most-likely leak points along the fault plane, it must be noted that parts of the fault below these leak points can be said to be sealing. In terms of contact depth, the cells are able to hold a hydrocarbon column greater than that controlled by the E-S1 contact.

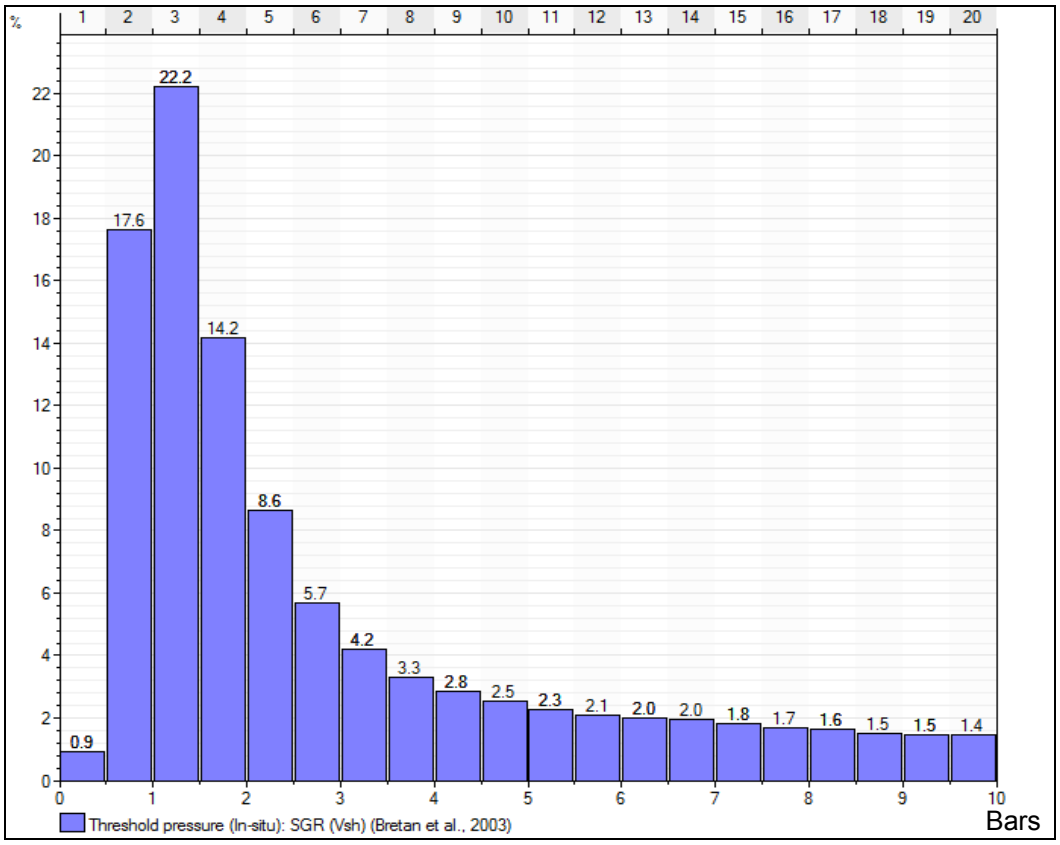

Figure 6.9 Histogram of threshold pressure.

A shortcoming of this method is that it does not cater for a hydrocarbon against hydrocarbon system; the fault-seal scenario evaluated in the software was a gas against water system. In order to cater for gas against oil, an additional case was run substituting the density of water with the density of oil from E-S4 i.e. 0.848 g/cc (35 API, Willis et. al., 1987). This may not provide an ideal solution but may serve to at least provide a qualitative solution. In this case the system variables are not very different as the oil density is

similar to the water density. As expected, the faults are still seen to be non-sealing (Figures 6.14, 6.15 and 6.16).

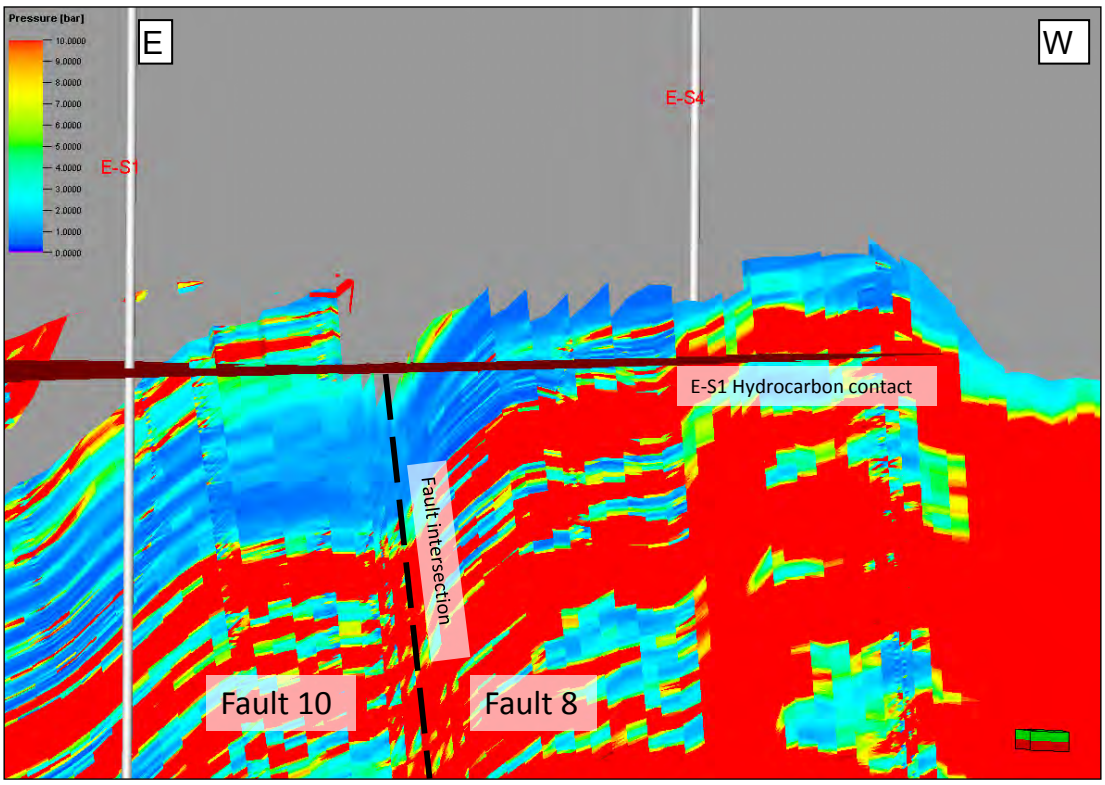

Figure 6.10 Threshold pressure property distributed along fault 8 and 10.

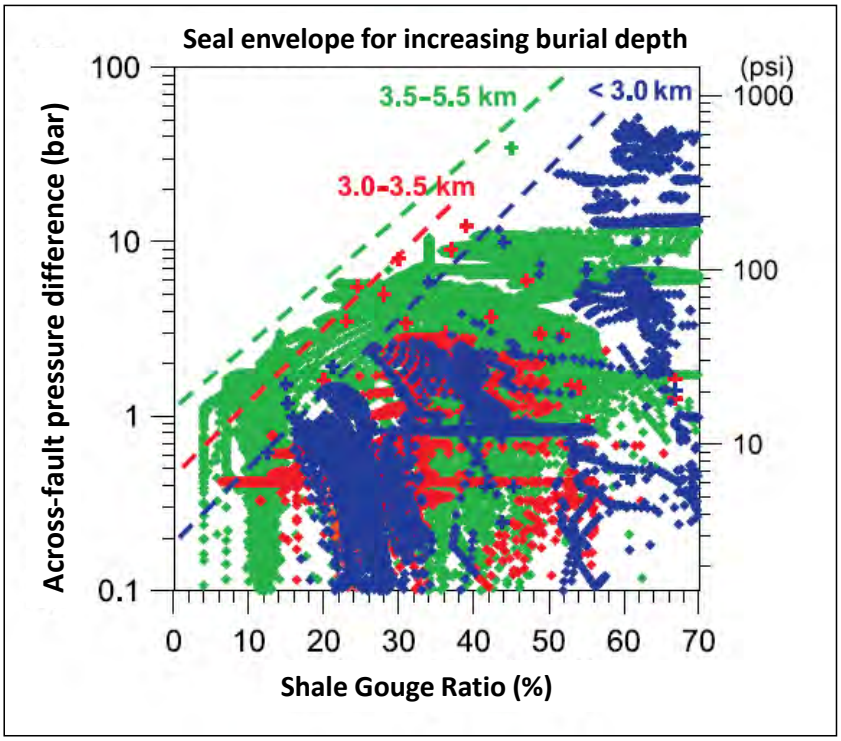

Figure 6.11 Plot of SGR vs buoyancy/threshold pressure (after Bretan et al., 2003).

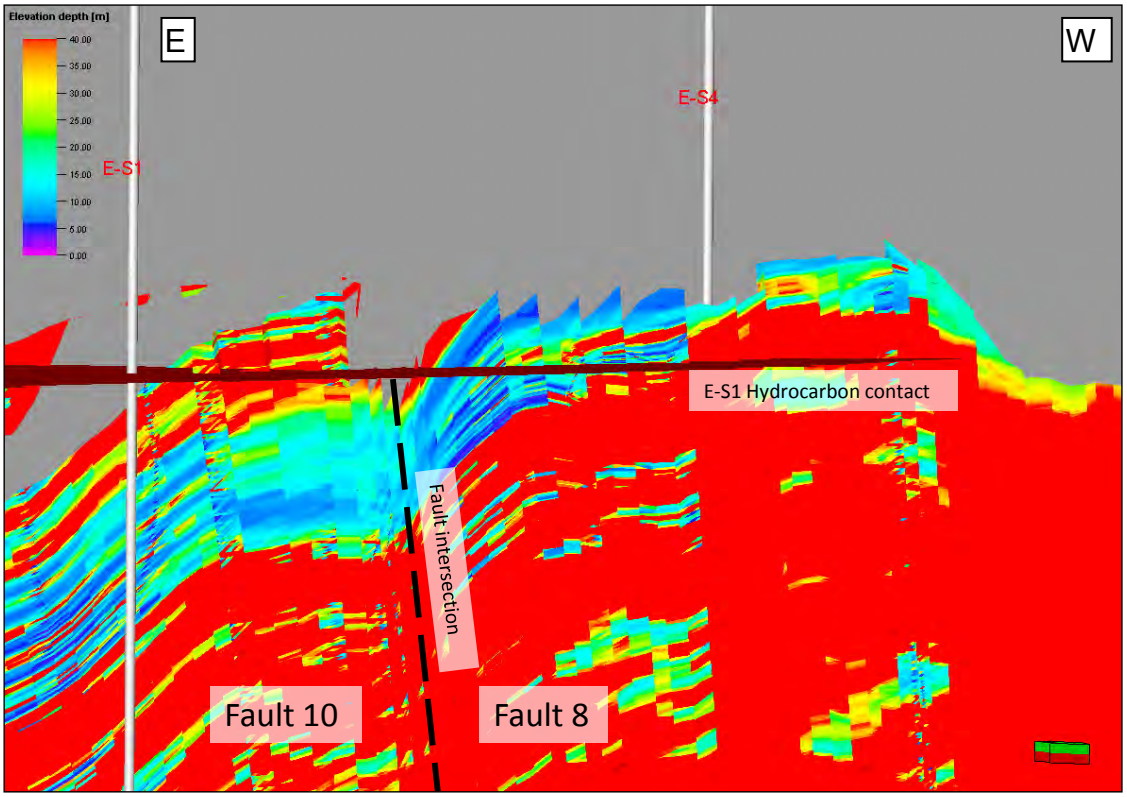

Figure 6.12 Column height property distributed along fault 8 and 10.

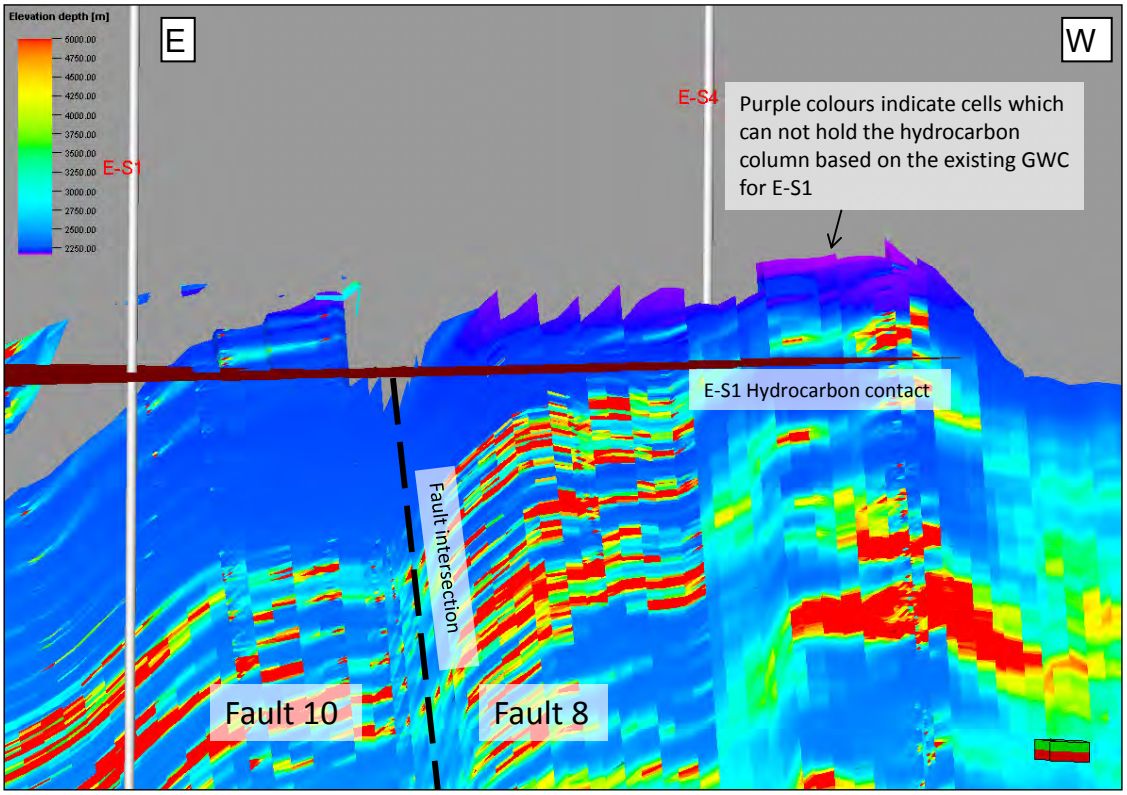

Figure 6.13 Contact depth property distributed along fault 8 and 10.

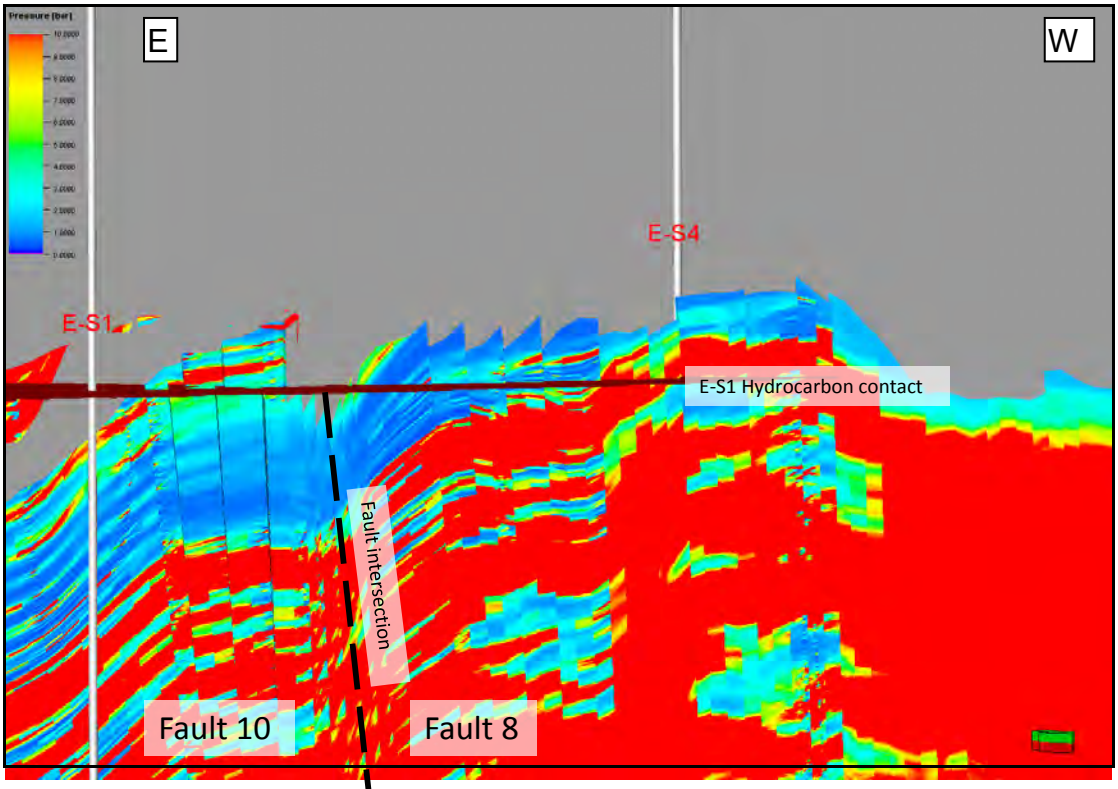

Figure 6.14 Threshold pressure property distributed along fault 8 and 10 in the case where oil density was substituted for water density.

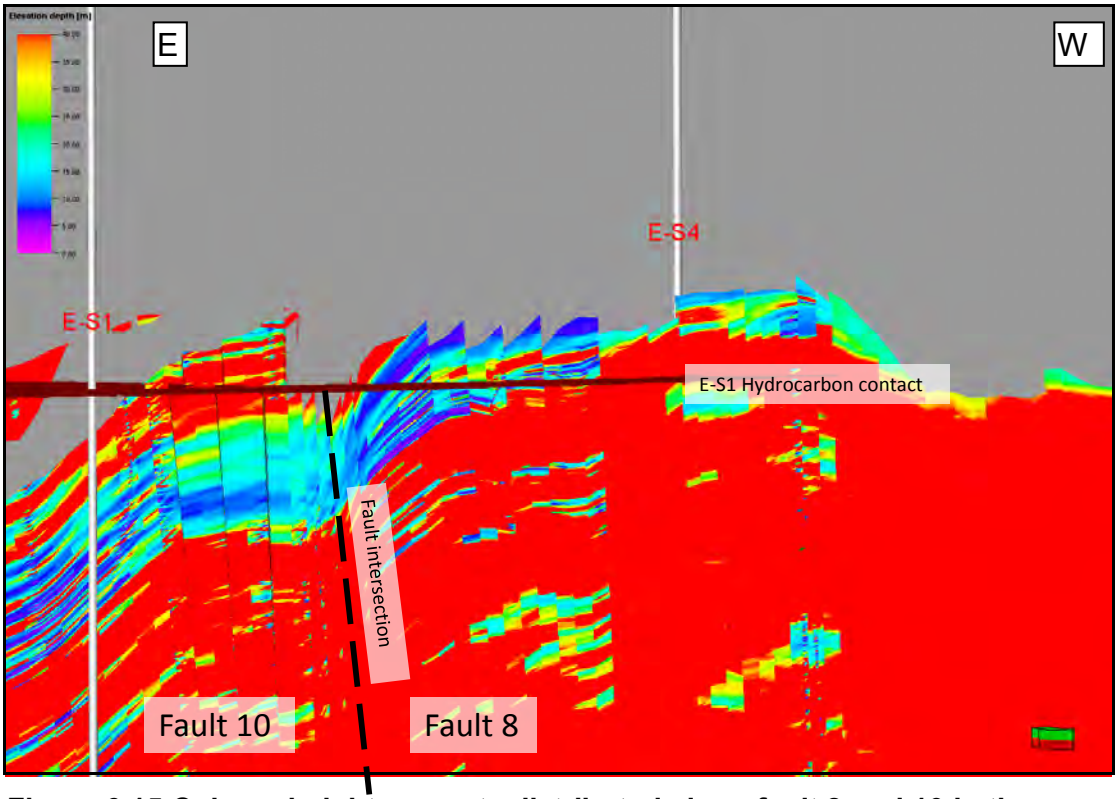

Figure 6.15 Column height property distributed along fault 8 and 10 in the case where oil density was substituted for water density.

To further test this solution, Shale Gouge Ratio and buoyancy pressure data were evaluated independently using the calibration plot from Bretan et al. (2003). Using the calibration plot of Shale Gouge Ratio against threshold pressure for sand-sand reservoir juxtapositions created using global data (Figure 6.11) together with the failure envelope for reservoirs with a burial depth of less than three kilometres, and superimposing the Shale Gouge Ratio vs. threshold data for the studied faults, the bulk of the fault data falls beyond the defined failure envelope (Figure 6.17), indicating that parts of the faults will not seal (This plot does not consider the depth of the data).

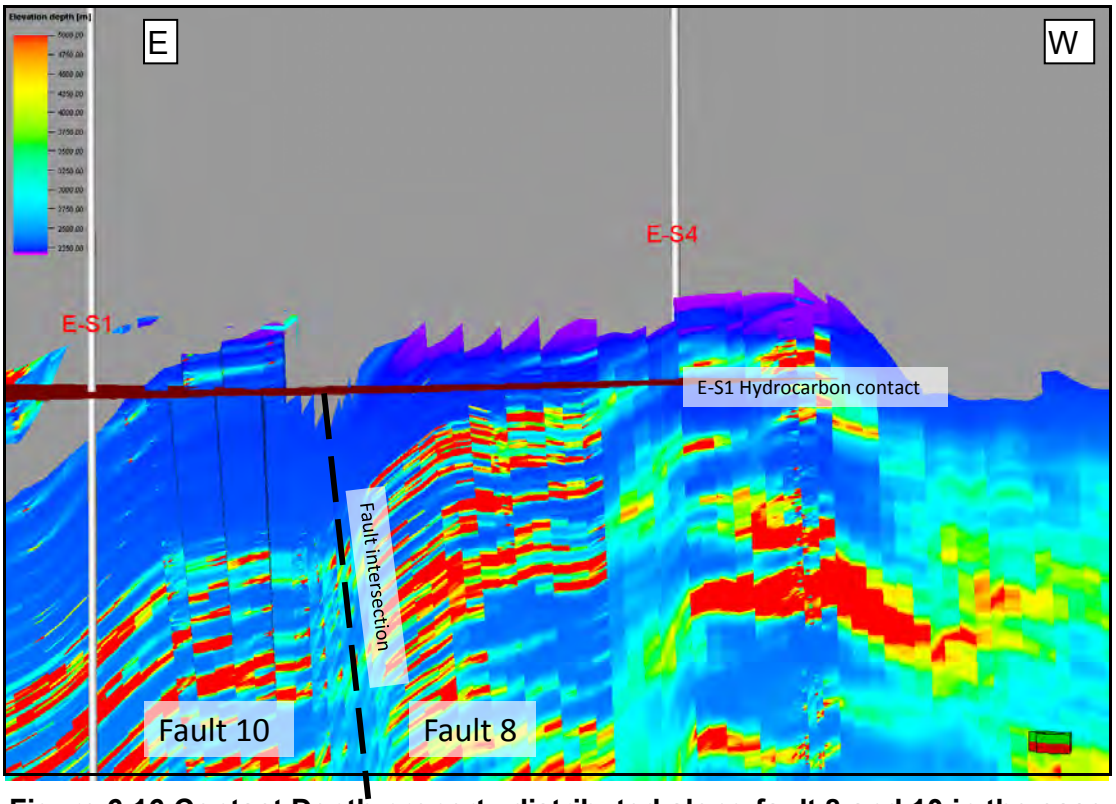

Figure 6.16 Contact Depth property distributed along fault 8 and 10 in the case where oil density was substituted for water density.

Global data supports the view that faults with low Shale Gouge Ratio values (less than 20%) occurring at depths less than 3km generally have a high propensity to leak. Bretan et al. (2003) explains this phenomenon as being due to clean sand on sand juxtapositions which are too shallow to be affected by diagenetic overprinting and cataclasis. They do take into account the plausibility of gas columns being supported by Shale Gouge Ratio with

values of 10%, but attribute this to pore-throat reduction rather than a phyllosilicate filled fault zone.

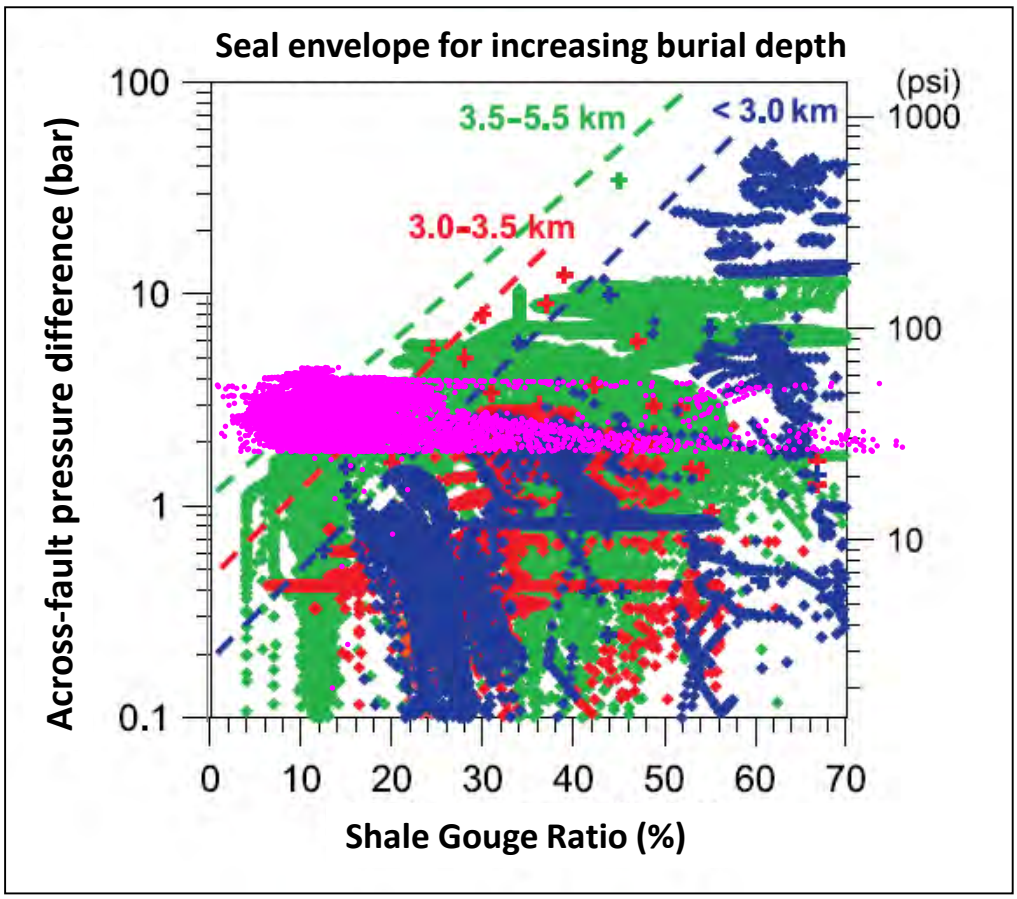

Figure 6.17 SGR vs threshold pressure points for the faults in the model (pink) superimposed on the plot using global data (after Bretan et al., 2003).

Although the fault seal analysis results has shown the faults to be leaking in some places, the question regarding the existence of different hydrocarbon contacts in adjacent fault blocks has not been answered. This was investigated by analysing RFT (Repeat Formation Test) data from the E-S1 and E-S4 wells (Figure 6.18). The aquifer can be interpreted to be common in both fault blocks owing to similar pressures in the water leg. However, the pressure data taken in the reservoir indicates the occurrence of two discrete fault blocks isolated from each other. This piece of data doesn't allow for an unequivocal conclusion to be made.

The pressure difference across the fault separating the two fault blocks, at the highest point where reservoir sands overlap, is approximately 29 psi (2 bar). If this data is plotted on Figure 6.17 (SGR vs threshold pressure

calibration plot), using the average Shale Gouge Ratio of 18%, measured along the fault plane, it can be seen that in theory fluids would leak through the fault therefore supporting the presence of a gas cap in the E-S4 fault block. It is possible that the calculated Shale Gouge Ratio values are lower than what they are in reality. If this is the case, a Shale Gouge Ratio of 25% would be enough to make an effective fault seal considering the 2 bar differential pressure measured on the RFT plot.

This may be a point of further study and investigation, in order to better resolve this relationship and to understand the mechanisms controlling the separation of oil and gas across the faults. This result will affect the choice of development plan for the field, and will probably lead to a more conservative plan assuming a "worst-case scenario", which is that the faults are sealing

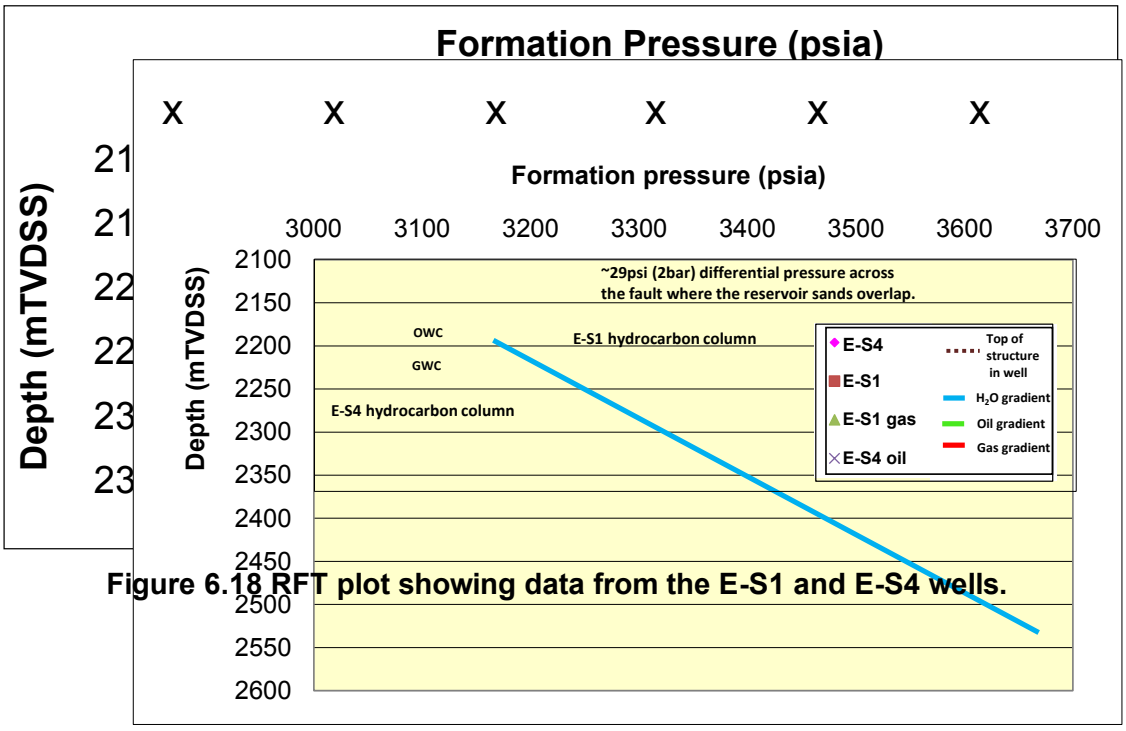

Figure 6.18 RFT plot showing data from the E-S1 and E-S4 wells.

7 RECOMMENDATION

In the light of contradicting evidence; the fault seal analysis indicating no fault seal while the pressure data shows two isolated fault blocks; it would be safest to assume that the faults are sealing when planning the development of the field. The economics of the project may not support drilling two separate wells, one in each of the fault blocks, owing to the relatively small size of the hydrocarbon accumulations. A highly deviated or short horizontal well is recommended, which will access both the E-S4 and E-S1 fault blocks. The well should be drilled from the E-S4 block to the E-S1 block (west to east; Figure 7.1), and the plan should be to intersect the E-S4 block higher up-structure in order to test for the presence of a gas cap (reservoir pressure in E-S4 is at the same pressure as the bubble point pressure of 3096 psig; Willis et al., 1987).

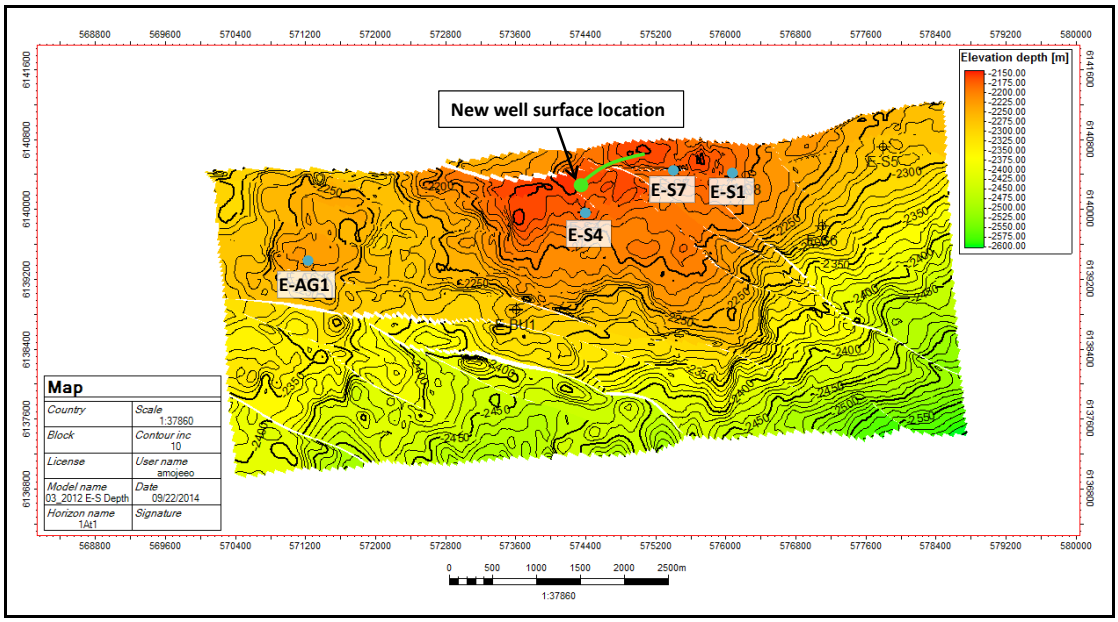

Figure 7.1 1At1 structure map showing the proposed location for a hydrocarbon producer.

Regarding the completion strategy, it is recommended that the well be completed using a sliding sleeve (John Egan, Pers. Comm.). Both the oil and gas zones should be perforated and flow from these zones should be controlled using the sliding sleeve mechanism. The sliding sleeve can shut-

off either one of the zones while keeping the other open or it can be adjusted to allow both zones to flow or remain shut-in simultaneously. The oil should be produced first keeping the gas zone shut-in, as it is likely to deplete quicker than the gas. When oil production drops below economic levels, the gas zone can be opened. The benefits of this are two-fold; it will initiate the production of gas and the interaction of gas with the oil in the borehole (or the formation in the near bore) would cause the oil become “lighter”, prolonging the production and increasing the recovery of the oil. In this way, the well will be producing with commingled flow. An additional advantage of using a sliding sleeve is that, if any production problems are experienced owing to the commingled flow, either zone can be shut-off to allow single-phase flow. The method provides a degree of flexibility with the ability to change strategy based on real time production behaviour and data.

8 CONCLUSION

The general 3D geo-cellular modelling workflow followed in this study can be considered as being relatively standard. However, the methodology used to create the contact region property can be considered to be an example of attempting to model many different and seemingly “meaningless” properties to reach a simplified and integrated outcome. By undertaking this mini workflow, it was possible to finally have a single hydrocarbon map representing different hydrocarbon accumulations with different hydrocarbon phases and contacts (Figure 5.37 and 5.38).

The hydrocarbon volumes calculated during this study can be considered to be similar to those calculated in previous studies. The new structural interpretation together with the choice to implement a J function water saturation could account for the differences in volume. The oil accumulation in the E-S4 region was slightly larger than previously thought and was calculated to be 11.26 MMbbl STOIIP. The oil in the E-AG1 structure was considered to be insufficient to justify further development at 27 Mbbl STOIIP. For the E-S1 and E-S7 fault blocks, the gas volumes were calculated to be 12.5 and 4.3 Bscf GIIP respectively. Using recovery factors of 75% and 11% for gas and oil respectively, based on existing data and reports, the recoverable hydrocarbons are 12.6 Bscf and 1.3 MMbbl. It is recommended that the recovery factor for the oil in the E-S4 area be reviewed as it seems very low for a typical oil of this density.

The fault-seal analysis has shown the faults, and more specifically the faults separating the E-S4 oil from the E-S1 gas accumulations (faults 8 and 10), to be not completely sealing. This is based on the juxtaposition pattern across the faults and the relationship of Shale Gouge Ratio and threshold pressure for data points along the fault planes. All the fault properties calculated suggest that leakage will occur at the crest of the fault planes while the lower part of the faults (up to the hydrocarbon-water contact) have the ability to seal.

Plotting the Shale Gouge Ratio vs threshold pressure data against global data supports this view. Most of the data falls in the range of low Shale Gouge Ratio (10-20%) and threshold pressures of greater than 1 bar. This, interpreted together with the burial depth envelope (the blue line representing less than 3km in Figure 6.14) shows that the faults have a high propensity to leak hydrocarbons but does not give any direct indication regarding the depth at which leakage may occur.

Contrary to the result achieved from the fault seal analysis, Repeat Formation Test pressure data indicates that E-S4 and E-S1 have intersected different hydrocarbons in two isolated fault blocks. Differences in pressure coupled with different hydrocarbon contacts in the two blocks support the idea of discrete accumulations. In is an interesting observation that the results obtained using the Shale Gouge Ratio do not agree with the observations from the pressure data and there remains a potential for future studies. It is difficult to solve this discrepancy with the data currently available and it would be prudent to plan a development plan capable of handling the scenario assuming the faults are sealing. If a production well is drilled, it may well provide the data needed in order to better understand this complex phenomenon.

Incorporating all the results from the study, it is recommended that a single highly deviated or short horizontal well be drilled from the E-S4 fault block, targeting a part of the reservoir which is up-structure from the current well, towards the E-S1 fault block. This would provide drainage points for fluids in both the compartments. It is recommended that the well be completed with a sliding sleeve, which would provide the flexibility needed to manage multi-phase fluid production.

9 BIBLIOGRAPHY

Bretan, P., Yielding, G., Mathiassen, O. M. and Thorsnes, T., 2011, Fault-seal analysis for CO_2 storage: An example from the Troll area, Norwegian Continental shelf: Petroleum Geoscience, V. 17, p. 181-192.

Fouché, J., Brown, D. M. and Goodwin, N. V., 1997, Reservoir appraisal of the E-S/E-AG oil fields in the upper shallow marine sequence incorporating the E-S 3D survey: Doc. No. SOE-EXP-RPT-0436, Soekor E and P (PTY) LTD.

Higgs, R., 2008, Sedimentology of F-O gas field, Bredasdorp Basin, offshore South Africa: Interpreted depositional environments, sequence stratigraphy and diagenetic history, and their bearing on poro-perm prediction: Prepared for PetroSA by RPS Energy.

Petroleum Engineering, 1992, Reservoir appraisal of the E-S/E-AG oil and gas field: OF. 821, Soekor (PTY) LTD.

Yielding, G., 2012, Using probabilistic shale smear modelling to relate SGR predictions of column height to fault zone heterogeneity: Petroleum Geoscience, V. 18, p. 33-42.

Yielding, G., Roberts, A. and Bretan, P., 2005, Best practice in structural geological analysis: First Break (EAGE), V. 23.

10 REFERENCES

Amaefule, J. O., Altunbay, M., Tiab, D., Kersey, D. G. and Keelan, D. K., 1993, Enhanced Reservoir Description: Using core and log data to identify hydraulic (flow) units and predict permeability in uncored Intervals/Wells, 68th Annual Tech. Conf. And Exhibit. Houston, TX Paper SPE26435.

Bohling, G., 2005, Stochastic simulation and reservoir modelling workflow, Kansas Geological Survey: C&PE 940,http://people.ku.edu/~gbohling/cpe940.

Bretan, P., Yielding, G. and Jones, H., 2003, Using calibrated shale gouge ratio to estimate hydrocarbon column heights: AAPG Bulletin, V. 87, No. 3, p. 397-413.

Broad, D.S., Jungslager, E.H.A., McLachlan, I.R. and Roux, J., 1996, Geology of offshore Mesozoic basins: Contribution to a text book on the geology of Africa published by the Geological Society of South Africa, p. 6-10, 15-19.

Brown, L.F., Benson Jr, J.M., Brink, G.J., Doherty, S., Jollands, A., Jungslager, E.H.A., Keenan, J.H.G., Muntingh, A. and van Wyk, N.J.S., 1995, Sequence stratigraphy in offshore South African divergent basins: An atlas on exploration for Cretaceous lowstand traps, Soekor (PTY) LTD: AAPG.

Caers, J., 2005, Petroleum Geostatistics: Society of Petroleum Engineers.

Cerveny, K., Davies, R., Dudley, G., Kaufman, P., Knipe, R. and Krantz, B., 2004, Reducing uncertainty with fault-seal analysis: Oilfield Review: Winter 2004/2005.

Crane, R. C., 1982, A Computer Model for the Architecture of Avulsion-controlled Alluvial Suites: Unpublished PhD dissertation, University of Reading.

Dalrymple, R.W., Zaitlin, B.A. and Boyd, R., 1992, Estuarine facies models: conceptual basis and stratigraphic implications: Journal of Sedimentary Petrology, V. 62, No. 6., p. 1130-1146.

Davies, C.P.N., 1995, Log-derived salinity data: An investigation of sands in the Bredasdorp Basin (Upgraded April 1997): Doc. No. SOE-GCH-RPT-249, Soekor E and P (PTY) LTD.

Dubost, F., Corbett, C., Kirkham, T. and Navarro, R., 2009, E-M field integrated subsurface study: Report prepared for PetroSA by Schlumberger Data and Consulting Services.

Dubrule, O., 1998, Geostatistics in petroleum geology: AAPG Continuing education course note series #38.

Dubrule, O., 2014, Petroleum geostatistics: Course notes, course held at University of Western Cape.

El Saadi, O., 2010, E-W core report, PetroSA: unpublished report.

Fedderson, J., Poquioma, F., Phadziri, R. and Frewin, J., 2007, Geophysical review of the E-S area: Technical Note No. 276, Project 196, PetroSA.

Field Appraisal Team, 1984, Geological and geophysical appraisal of the E-M gas field: OF. 3964 Soekor (PTY) LTD.

Fielding, C. R., 1986, Fluvial channel and overbank deposits from the Westphalian of the Durham coalfield, NE England: Journal of Sedimentology, V. 33, No. 1, p. 119-140.

Fielding, C.R. and Crane, R.C., 1987, An application of statistical modelling to the prediction of hydrocarbon recovery factors in fluvial sequences. In: Ethridge, R.M., and Harvey, M.D., (eds)., Recent developments in fluvial sedimentology: Society for Sedimentary Geology (SEPM) Special Publication 39, p. 321-327.

Flopetrol Johnston, 1984, PVT Study Report for E-S1: OF. 6179, Soekor (PTY) LTD.

Frewin, J., 2005, South coast gas development project: Geological modelling of the E-S gas discovery of the central Bredasdorp Basin, offshore South Africa: Doc. No. PETSA-TEC-RPT-0607, PetroSA.

Frewin, J., Fouché, D., Mudaly, K., Padayachee, P., Turner, J. and Xabendlini, Z., 2001, Review of volumetrics of the upper shallow marine and fluvial intervals for the E-S4 and E-AG1 boreholes: Doc. No. SOE-EXP-RPT-0557, Soekor E and P (PTY) LTD.

Fox, R. J. and Bowman, M. B. J., 2010, The challenges and impact of compartmentalization in reservoir appraisal and development. In: Jolley, S. J., Fisher, Q. J., Ainsworth, R. B., Vrolijk, P. J., and Delisle, S., (eds) Reservoir Compartmentalization. Geological Society, London, Special Publications, 347, p. 9-23.

Goodwin, N. and Brown, D., 1998, Stochastic modelling of the E-S/E-AG synrift fluvial reservoirs: Doc. No. SOE-EXP-RPT-0447, Soekor (PTY) LTD.

Ingram, G.M., Urai, J.L. and Naylor, M.A., 1997, Sealing processes and top seal assessment, in P. Møller-Pederson and A.G. Koestler, eds., Hydrocarbon seals: Importance for exploration and production: Singapore, Elsevier, Norwegian Petroleum Society (NPF) Special publication 7, p.165-174.

Jolley, S. J., Fisher, Q. J. and Ainsworth, R.B., 2010, Reservoir Compartmentalization: an introduction. In: Jolley, S. J., Fisher, Q. J., Ainsworth, R. B., Vrolijk, P. J., and Delisle, S., (eds) Reservoir Compartmentalization. Geological Society, London, Special Publications, 347, p. 1-8.

Jungslager, E.H.A., 1996, Geological Evaluation of the Remaining Prospectivity for Oil and Gas of the Pre-1At1 “Synrift” Succession in Block 9, Republic of South Africa: Soekor (PTY) LTD.

McMillan, I.K., Brink, G.J., Broad, D.S. and Maier, J.J., 1997, Late Mesozoic sedimentary basins off the Coast of South Africa: Sedimentary basins of the world, African basins, 3rd ed. edited by R.C. Selley. p 319-376.

Meilianda, E., Huhn, K., Alfian, D. and Bartholoma A., 2012, Application of multivariate geostatistics to investigate the surface sediment distribution of the high-energy and shallow sandy Spiekeroog shelf at the German bight, southern north sea: Open Journal of Marine Science, V. 2, No. 4.

Mudaly, K., Gralla, D., Frewin, J. and Cairncross, M., 2002, Evaluation of the E-S/E-AG reservoir: Technical Note No. 163, Project 56 and 29, PetroSA.

Petrel, 2014, Documentation accessed via Help Centre from Petrel 2014 software.

Petroleum Agency SA, 2000, Petroleum Exploration Opportunities: Petroleum Agency SA, Published report.

Petrowiki, 2013, Geostatistical Conditional Simulation, http://petrowiki.org/, published by SPE, August 2014.

PGS, 2000, An evaluation of the E-S field: PGS Reservoir (UK) Limited: Bredasdorp Alliance.

Pyrcz, M. J. and Deutsch, C. V., 2014, Geostatistical reservoir modelling (2nd edition): Oxford University Press.

RDR, 2013, Fault and fault sealing in exploration and production: Course notes delivered by R.K. Davies.

Selley, R. C., 1985, Report on consulting visit 24 June – 5 July 1985: OF. 3938 Soekor (PTY) LTD.

Selley, R. C., 1986, Report on consulting visit 30 June – 11 July 1986: OF. 4987 Soekor (PTY) LTD.

Timetrax, 1999, A biostratigraphic study through the syn-rift section of six wells in the F-O and F-S areas and the F-A field, Breadsdorp Basin, offshore South Africa: Private report for PGS Reservoir (UK) LTD: project No. B0991.

Wickens, H. DeV., 1989, The sedimentology of the C to D sequences in the E-M/E-S/E-W area, Northern Bredasdorp Basin, Soekor (PTY) LTD.

Willis, R., Auret, S., Strauss, P. and Holmes, L., 1987, The appraisal of the E-S oil field: OF. 6040, Soekor (PTY) LTD.

Yielding, G., 2002, Shale gouge ratio – Calibration by geohistory, in A. G. Koestler and R. Hunsdale, Hydrocarbon seal quantification: Amsterdam, Elsevier, Norwegian Petroleum Society (NPF) Special Publication 11, p. 1-15.

Yielding, G., Bretan, P. and Freeman, B., 2010, Fault seal calibration: a brief overview. In: Jolley, S. J., Fisher, Q. J., Ainsworth, R. B., Vrolijk, P. J., and Delisle, S., (eds) Reservoir Compartmentalization. Geological Society, London, Special Publications, 347, p. 243-255.

Yielding, G., Freeman, B. and Needham, D.T., 1997, Quantitative fault seal prediction: AAPG Bulletin, V.81, No. 6, p. 897-917.

Zakrevsky, K. E., 2011, Geological 3D modelling, EAGE Publication.

11 Appendix A – Equations using Petrel Syntaxes

From Section **5.4.5 Water Saturation (Sw and J_Sw)**:

Equation 7

FZ I= (0.0314*(Sqrt(K/ Φe)))/(Φe /(1- Φe))

Where:

K = Permeability

Φe = Effective Porosity

Equation 10

ContactRegions= If(ES1_GWC_2205<>U,2,If(ES4_OWC_2192<>U,3
If(ES7_GWC_2212<>U,4, If(EAG1_OWC_2229<>U,1,0))))

Where:

U = Undefined,

ES1_GWC_2205,

ES4_OWC_2192,

ES7_GWC_2212 &

EAG1_OWC_2229

are the mock volume maps for each specified region;

And, numbers 0 to 4 are contact region codes (Table 9).

Equation 11

Ht= If (ContactRegions=1, OWC_2229_E_AG1,
If (ContactRegions=3, OWC_2192_E_S4,
If ContactRegions=2, GWC_2205_E_S1,
If (ContactRegions=4, GWC_2212_E_S7, 0))))

Where:

OWC_2229_E_AG1,

OWC_2192_E_S4,

GWC_2205_E_S1 &

GWC_2212_E_S7

are the individual Ht property maps modelled geometrically using the “Above Contact” method.

Equation 12

J_Sw=If(ContactRegions = 0,1 ,If (ContactRegions =1 Or ContactRegions=3,
If (FZI>=.5,Pow(((0.005845*Sqrt(K/PHI) *Ht)/0.019), (1/-3.9)) ,
Pow(((0.005845*Sqrt(K/PHI) *Ht)/0.16), (1/-1.3))) ,
If (FZI>=.5,Pow(((0.005845*Sqrt(K/PHI) *Ht)/0.07), (1/-2.3)) ,
Pow(((0.005845*Sqrt(K/PHI) *Ht)/0.16), (1/-1.3)))))

Where:

K = permeability from the model

PHI = porosity from the model

FZI = Flow Zone Indicator

Ht = Height Above Contact property.

From Section **6.2.1.1 Volume of Clay (VCL)**:

Due to the calculation algorithm in the software, the VCL property needed to be changed to a Vsh property before computing the clay content prediction. The VCL property was converted to a Vsh property using the following equation:

Vsh = VCL × 100

Where:

Vsh = the volume of shale (%)

And VCL = the Volume of Clay (fraction).